UC Berkeley
UC Berkeley Electronic Theses and Dissertations

Title

Characterizing the role of bacterial actin proteins, MamK and MamK-like, in the organization of magnetosome organelles in Magnetospirillum magneticum AMB-1

Permalink

https://escholarship.org/uc/item/83j2x1r2

Author

Abreu, Nicole Angelina

Publication Date

2015

Peer reviewed|Thesis/dissertation

Characterizing the role of bacterial actin proteins, MamK and MamK-like, in the organization of magnetosome organelles in *Magnetospirillum magneticum* AMB-1

By

Nicole Angelina Abreu

A dissertation submitted in partial satisfaction of the requirements for the degree of
Doctor of Philosophy

in
Microbiology in the
Graduate Division
of the
University of California, Berkeley

Committee in charge:

Professor Arash Komeili, Chair
Professor Kathleen R. Ryan
Professor Matthew D. Welch
Professor David G. Drubin

Spring 2015

ABSTRACT

Characterizing the role of bacterial actin proteins, MamK and MamK-like, in the organization of magnetosome organelles in *Magnetospirillum magneticum* AMB-1

by

Nicole Angelina Abreu

Doctor of Philosophy in Microbiology

University of California, Berkeley

Professor Arash Komeili, Chair

Cellular organization is critical for life to flourish. Historically, this area of research has focused on eukaryotic systems, but recent advances have resulted in bacteria as model organisms to study cell biology. This research is aimed to elucidate how bacteria organize their internal structures. To address this question, the bacterial model organism, *Magnetospirillum magneticum* AMB-1 (AMB-1) was used and the role of two bacterial actin proteins, MamK and MamK-like, were studied.

The first chapter of this dissertation, a published review article (Cornejo-Warner *et al.*, Current Opinion in Cell Biology 2014) written in collaboration with fellow Komeili lab member Elias Cornejo-Warner, introduces the topic of bacterial cell compartmentalization, highlighting examples from *Bacillus subtilis* and *Caulobacter crescentus*. Additionally, the organization of bacterial organelles is discussed with examples of two model systems, the magnetosomes of magnetotactic bacteria and the carboxysomes of cyanobacteria.

The second chapter of this dissertation, a combination of a published primary research article (Abreu *et al.*, Journal of Bacteriology 2014) and unpublished supporting data, focuses on a bacterial actin protein, MamK-like. MamK-like is encoded in the magnetosome islet, a region of DNA distinct from the more heavily studied magnetosome island in AMB-1. The work described in this chapter, with assistance in molecular biology from Ertan Ozyamak and *in vitro* work from Soumaya Mannoubi, resulted in determining that this protein does indeed play a role in AMB-1 organelle alignment.

The third chapter of this dissertation (unpublished work) focuses on the efforts that were taken to further understand the mechanism of MamK turnover by Flourescence Recovery After Photobleaching (FRAP) studies, a continuation of previous work published by Olga Draper (Draper *et al*. Molecular Microbiology 2011).

The fourth chapter of this dissertation (unpublished work) focuses on the experiments developed (*ex vivo*: Bacterial two hybrid and *in vitro*: MamK affinity tagged pulldowns and Mass Spectrometry) to identify MamK and MamJ interacting proteins.

The fifth chapter of this dissertation is a conclusion of the work as it stands and proposals for future directions that could lead to a more comprehensive understanding of the organelle organization phenotype and bacterial actin behavior.

CHAPTER 1

Compartmentalization and organelle formation in bacteria

Elias Cornejo, Nicole Abreu and Arash Komeili

Department of Plant and Microbial Biology, University of California Berkeley, California, USA

ABSTRACT

A number of bacterial species rely on compartmentalization to gain specific functionalities that will provide them with a selective advantage. Here, we will highlight several of these modes of bacterial compartmentalization with an eye toward describing the mechanisms of their formation and their evolutionary origins. Spore formation in *Bacillus subtilis*, outer membrane biogenesis in Gram-negative bacteria and protein diffusion barriers of *Caulobacter crescentus* will be used to demonstrate the physical, chemical, and compositional remodeling events that lead to compartmentalization. In addition, magnetosomes and carboxysomes will serve as models to examine the interplay between cytoskeletal systems and the subcellular positioning of organelles.

INTRODUCTION

The cell is a crowded place and subcellular organization is vital to regulating its many metabolic processes (*1*). In eukaryotes, such organization is prominently achieved through the compartmentalization of biochemical reactions in various intracellular organelles. By limiting diffusion to a confined space, concentrations of enzymes and substrates can be optimized to promote specific enzymatic reactions. In turn, sequestration of activities within compartments protects the cell from toxic byproducts of such reactions. While historically considered to be simple cells with a low degree of subcellular differentiation, compartmentalization in the form of organelles is also a widespread phenomenon among bacterial cells (*2*). Unlike the eukaryotic endomembrane system, bacterial species are not equipped with a standard set of organelles. Instead, varying combinations of organelles provide unique capabilities to individual bacterial species. One notable class is the protein-bounded bacterial microcompartments, exemplified by the carbon-fixing carboxysomes of cyanobacteria (*3*). Lipid-bounded organelles, including the dazzling varieties of photosynthetic membranes found in heterotrophic bacteria and cyanobacteria, constitute another set of bacterial compartments (*4, 5*). In addition to organelles, other modes of compartmentalization, such as the creation of spores and protein diffusion barriers to subdivide the cytoplasmic space, have also been described in bacterial cells (*6, 7*). Despite the impressive list of bacterial compartments and their cytological characterization, the molecular mechanisms that govern their formation, function, and segregation are still a major question in bacterial cell biology. Here, we will focus on recent discoveries on the physical, chemical, and compositional remodeling of membranes during compartmentalization as well as the mechanisms leading to the spacing and positioning of organelles within the cell. Those interested in acquiring a more in depth knowledge of this fascinating topic, are encouraged to read several recent review articles on the function, diversity, and evolution of bacterial organelles (*2, 8*).

MEMBRANE REMODELING

A fundamental aspect of organelle formation in any organism is the remodeling of cellular membranes during the compartmentalization process. Remodeling can be physical in nature such as the bending, migration, and fusion of lipid bilayers to produce and stabilize organelles. Chemical remodeling of lipids can also produce distinct compartments within the cell. Additionally, compositional remodeling of membrane domains, through protein targeting and/or exclusion, can subdivide a continuous structure into distinct compartments. These types of membrane remodeling have been described in numerous eukaryotic systems. In contrast, almost nothing is known about the methods and molecules used by bacteria to remodel their lipids into a compartment. Here we highlight three cases where mechanisms and evolution of bacterial membrane remodeling events have been recently elucidated.

PHYSICAL REMODELING: SPORE FORMATION

Perhaps the most thoroughly studied example of membrane remodeling in bacteria is the engulfment of forespore during the sporulation process of *Bacillus subtilis*. When growth is challenged by harsh conditions, *B. subtilis* cells undergo a unique developmental program to form a highly durable and dormant endospore. During the early stages of sporulation, an asymmetric division event creates a larger 'mother' cell that proceeds to engulf the smaller 'forespore' cell to form an internal, double-membraned compartment (Figure 1a). A number of mechanisms have been implicated to drive the mother cell membrane around the forespore and have been recently reviewed (*9*). These include cell wall synthesis, cell wall degradation and specific protein interactions between SpoIIQ and SpoIIIAH that bridge across the mother and forespore membrane to prevent membrane retraction (Figure 1a) (*9-12*).

The final step of the engulfment process is the joining of the two ends of the migrating membranes to create a completely internalized endospore. Genetic analysis had implicated one protein, SpoIIIE, in membrane fission. However, *spoIIIE* null mutants also have defects in DNA translocation and septum morphology at earlier stages of sporulation raising the possibility that impaired membrane fission may be an indirect effect (*13-15*). By examining a set of mother cell genes that are expressed at the early stages of engulfment that when mutated, fail to release the forespore into the mother cell cytoplasm, Doan and colleagues recently identified fission protein B (FisB) as a direct catalyst of membrane fission in *B. subtilis* (*15*) (Figure 1a). Fluorescent protein fusions to FisB localize primarily to the edges of the migrating mother cell membrane that serve as the sites of membrane fission. Furthermore, purified FisB promotes membrane fusion *in vitro* via a specific interaction involving the extracellular domain of FisB and cardiolipin, an anionic phospholipid that is enriched in highly curved membranes including the forespore of *B. subtilis* (*15-17*). The authors propose that FisB may concentrate cardiolipin and create localized defects in the lipid bilayer that would favor the fission reaction. While these results highlight the importance of FisB in membrane fission, a small percentage of *fisB* mutants eventually complete engulfment, suggesting that alternative mechanisms may function at a slower rate to complete engulfment (*15*). A recent report identified core set of genes shared among sporulating bacteria, including three novel genes involved in endospore formation (*18*). This genomic signature may be a useful tool to identify additional mechanisms for membrane remodeling.

CHEMICAL REMODELING: GRAM-NEGATIVE OUTER MEMBRANE

Membrane remodeling is not limited to the physical movement and bending of lipid bilayers. Often, extensive modification of the chemical composition of cellular membranes is required for compartment formation and function. In bacteria, the construction of the Gram-negative outer membrane (OM) provides a model for understanding the mechanisms of chemical remodeling in biological membranes. As should be familiar to most students of biology, the Gram stain, developed by Hans Christian Gram in 1884, is a histological method for identifying and classifying bacterial

species. Gram-positive bacteria have a single cell membrane that is surrounded by a thick, multi-layered cell wall. Gram-negative bacteria have two membranes separated by a thin cell wall (*19*) (Figure 1b). The OM displays a number of characteristics that define it as a bacterial compartment. It is an asymmetric lipid bilayer with lipopolysaccharide (LPS), a glycolipid, on its outer leaflet and phospholipids on its inner leaflet. Beta-barrel proteins in the OM form pores that allow for non-specific exchange of small molecules with the extracellular environment while limiting diffusion of many cytoplasmically secreted proteins. Furthermore, the tight packing of LPS on the outer leaflet provides an impermeable barrier to small hydrophobic and hydrophilic molecules that can be harmful to the cell (*20*). The OM does not just function as barrier but also creates a chemically distinct periplasmic compartment where important processes, such as certain types of respiration, can occur.

While tremendous progress has been made in defining the chemical nature of the OM and uncovering the molecular mechanisms of its biogenesis (*21*, *22*), the evolutionary origins of this structure have remained mysterious. A recent study has searched for the answer to this question by examining the curious mode by which some bacterial cells produce and germinate spores (*23*). Phylogenetically, most endospore forming bacteria fall under the Bacilli and Clostridia classes of the Gram-positive Firmicutes phylum (*24*). Interestingly, some members of the Clostridia, such as *Acetonema longum*, can form spores but are decidedly Gram-negative in their vegetative state, as they possess an inner membrane and an OM that contains LPS. Through high-resolution electron cryotomographic (ECT) imaging of *A. longum* and *B. subtilis* cells at different stages of sporulation and spore germination, Tocheva and colleagues were able to show that the inner membrane of the mother cell engulfs the forespore and forms the outer spore membrane (*23*, *25*). During germination in *A. longum*, however, this membrane acquires the morphological and chemical signatures of an OM, including LPS (Figure 1b). Sequencing of the *A. longum* genome revealed the presence of homologs of genes known to encode for OM proteins in Gram-negative bacteria as well as those involved in sporulation in Gram-positives. Phylogenetic analysis showed that the OM proteins of *A. longum* do not cluster with those of other Gram-negatives whereas its sporulation proteins group with those of other Gram-positives. A parsimonious explanation for these results is that *A. longum* did not acquire the ability to produce an OM due to a recent horizontal gene transfer event, in which case its OM proteins would have been in tighter phylogenetic groups with homologs from Gram-negative organisms. Similarly, sporulation also seems to be an ancient characteristic of this organism. These findings lead to the tantalizing hypothesis that ancestors of Gram-positive and Gram- negative bacteria were able to link spore germination to construction of an OM. Subsequently, the majority of Gram-positives lost the ability to form an OM while the loss of sporulation genes gave rise to present-day Gram-negative organisms.

COMPOSITIONAL REMODELING: PROTEIN DIFFUSION BARRIERS

Diffusion gradients are used by cells to control the timing and location of essential cellular processes (*26*). Protein diffusion barriers had only been described as a feature of eukaryotic cells until their recent discovery by Schlimpert and colleagues in the Gram-negative bacterium, *Caulobacter crescentus* (*7, 27*). At a specific point during its cell cycle, *C. crescentus* physically remodels its cell envelope to form a polar stalk that functions as a holdfast for attachment to surfaces. During phosphorus limiting growth periods the stalk undergoes a dramatic elongation leading to the hypothesis that it may have a role in phosphorus uptake from the environment. Even though the stalk is a protrusion of the cell envelope, Schlimpert and colleagues found that periplasmic proteins do not move between the stalk and the cell body. Furthermore, they found that the stalk itself was compartmentalized into several segments that restricted protein movement. Early electron microscopic examination had found that curious cross band structures were spread through out the *C. crescentus* stalk. Using a combination of genetic and biochemical approaches, the authors identified a protein complex consisting of four proteins (StpA, StpB, StpC, and StpD) that localize to these conspicuous crossband structures. Deletions of the genes encoding the Stp factors result in a loss of cross band structures visualized by ECT and absence of compartmentalization within the stalk (Figure 2a). By preventing the accumulation of newly synthesized proteins into the stalk, these cross band structures essentially lead to a compositional remodeling of the compartment. One consequence of the loss of stalk compartmentalization is that proteins synthesized after stalk formation are no longer restricted to the cell body and are less concentrated in locales where their activity might be needed. This is especially of concern in phosphate starvation conditions in which the stalk elongates to the point that its surface area exceeds that of the cell body. In agreement with this model, the authors demonstrate that mutants missing the *stp* genes, take longer to accumulate proteins within their cell body and are outcompeted by wild-type cells in co-culturing experiments. Thus, in the case of the *C. crescentus* stalk, compositional remodeling partially acts to prevent the dilution of important cellular proteins (Figure 2b). Additionally, the authors hypothesize that the compositional remodeling of the stalk may also allow for localized activities that may be used to shuttle phosphate into the cell.

ORGANELLE POSITIONING

The subcellular positioning of compartments plays a key role in the function of many bacterial organelles. Recent studies have uncovered some of the molecular mechanisms that lead to the organization and positioning of two unique bacterial organelles, the magnetosome compartments of magnetotactic bacteria and the carboxysomes of cyanobacteria (*28*).

Compartmentalized through an invagination of the inner cell membrane, the magnetosome creates a controlled chemical environment optimal for formation and maturation of magnetite or greigite both of which are iron-based magnetic crystals. Magnetosome formation requires multiple steps utilizing genes that form membrane

invaginations, localize proteins, nucleate crystals and align structures into a chain (*29-34*). The end product of these processes is a well-aligned magnetosome chain (Figure 3a), which is thought to provide navigational capability toward preferred oxygen concentrations in a stratified water column, a process termed magnetoaerotaxis (*35*). Subcellular organization of magnetosomes into a chain is dependent on MamK, a bacterial actin homolog that is present in all magnetotactic bacteria. High resolution imaging of *Magnetospirillum magneticum* AMB-1 by ECT revealed that organized chains of magnetosomes are flanked by filaments that disappear in a *mamK* deletion mutant (Figure 3a) (*33*). Much like other actin-like proteins, MamK forms filaments that are dynamic *in vivo* (*36*)and *in vitro* (*37, 38*)in a manner that is dependent on the ATPase activity of the protein. The dynamic behavior of MamK *in vivo* also relies on the redundant action of acidic proteins MamJ and LimJ (Figure 3a) (*36*). In their absence, MamK filaments are static as seen in a fluorescence recovery after photobleaching assay. In addition, the loss of *mamJ* and *limJ* results in multiple gaps within the magnetosome chain and a clustering of putative MamK filaments within these spaces. One interpretation of these results is that MamK dynamics may be acting to pull magnetosomes together. Alternatively, the loss of MamJ and LimJ could change the localization of MamK in the cell leading to altered dynamics and an inability to form a coherent chain.

Despite the clear advances in understanding the behavior and properties of MamK as an actin-like protein, the specific mechanism by which it acts on the magnetosome chain remains unknown. The phenotypes of the *mamK* deletion strains are consistent with its action in either establishing or maintaining the magnetosome chain. Furthermore, in a related species, *Magnetospirillum gryphiswaldense* MSR-1, deletion of *mamK* results in ectopic chain localization and failure of partitioning the chain between daughter cells (*39, 40*). It has even been suggested that MamK acts to link physical forces on the magnetosome chain into changes in cell motility (*41*). Regardless of the specific mechanism of its action, MamK is clearly important for proper navigation in magnetic fields (*42*). A recent study using an agar plate magnetoaerotaxis assay found that *mamK* mutants had a significantly wider path around a magnetic field as compared to the wild type strain. In the environment, such a difference could translate into a longer travel period, and subsequently higher energy expenditure, for reaching a desired locale.

Similar to magnetosomes, the carboxysome organelles of cyanobacteria are also arranged linearly within a cell with a consistent spacing pattern. This arrangement relies on the action of the cytoskeletal protein, ParA, without which carboxysomes are unequally distributed among daughter cells (Figure 3b) (*43*). ParA filaments are also highly dynamic within the cell and undergo pole-to-pole oscillations that may be important in carboxysome positioning (Figure 3b). Given its crucial role in carbon fixation, the failure to acquire carboxysomes results in a significantly longer doubling time. ParA and its homologs belong to the Walker type family of ATPases and are often associated with segregation of plasmid or chromosomal DNA in diverse bacterial species. However, recent work has shown that a ParA homolog, PpfA, can also be used to segregate chemotaxis protein clusters during cell division in *Rhodobacter sphaeroides* (*44*). In this case, non-specific interactions of PpfA with DNA as well as specific interactions with its

chemotaxis protein cargo provide the means for separating the protein complexes (*45*). These findings leave open the possibility that in cyanobacteria, carboxysomes interact with chromosomes and that ParA is primarily directing the localization and segregation of DNA. However, deletion of *parA* does not affect the spacing of chromosomal DNA in cyanobacteria while disrupting the organization of carboxysomes (*46*). Thus, while DNA–ParA interactions may be important, specific interactions of this cytoskeletal protein with the carboxysome are likely needed for the proper positioning of this bacterial organelle.

CONCLUSION

The discoveries of cytoskeletal elements, organelles and means of sophisticated spatio-temporal regulation in bacteria have transformed the simplistic views of this complex and metabolically diverse domain of life. The most fundamental roadblock in understanding compartmentalization comprehensively in bacteria is the scarcity of reliable model systems that can help to illuminate specific facets of the organelle formation process. As such, isolated examples of compartmentalization in genetically tractable organisms have carried the bulk of the weight in defining the mechanistic basis of membrane remodeling, protein localization, and organelle segregation in bacteria. The diversity of these organelles and the specifications in their morphology and function makes it unlikely that a universal mechanism for compartmentalization exists among all bacteria. For instance, membrane remodeling in sporulation relies in part on the use of peptidoglycan as a guide while no such cues will be available during magnetosome formation. Likewise, while magnetosomes and carboxysomes rely on cytoskeletal elements for their subcellular positioning, the proteins involved are not related hinting at distinct molecular activities in these two systems. Clearly, an expansion of available model organisms and a more thorough cataloging of bacterial organelles are needed to truly revolutionize this field. If successful, such endeavors will open new avenues of research in microbiology and uncover novel mechanisms of cell organization and compartmentalization.
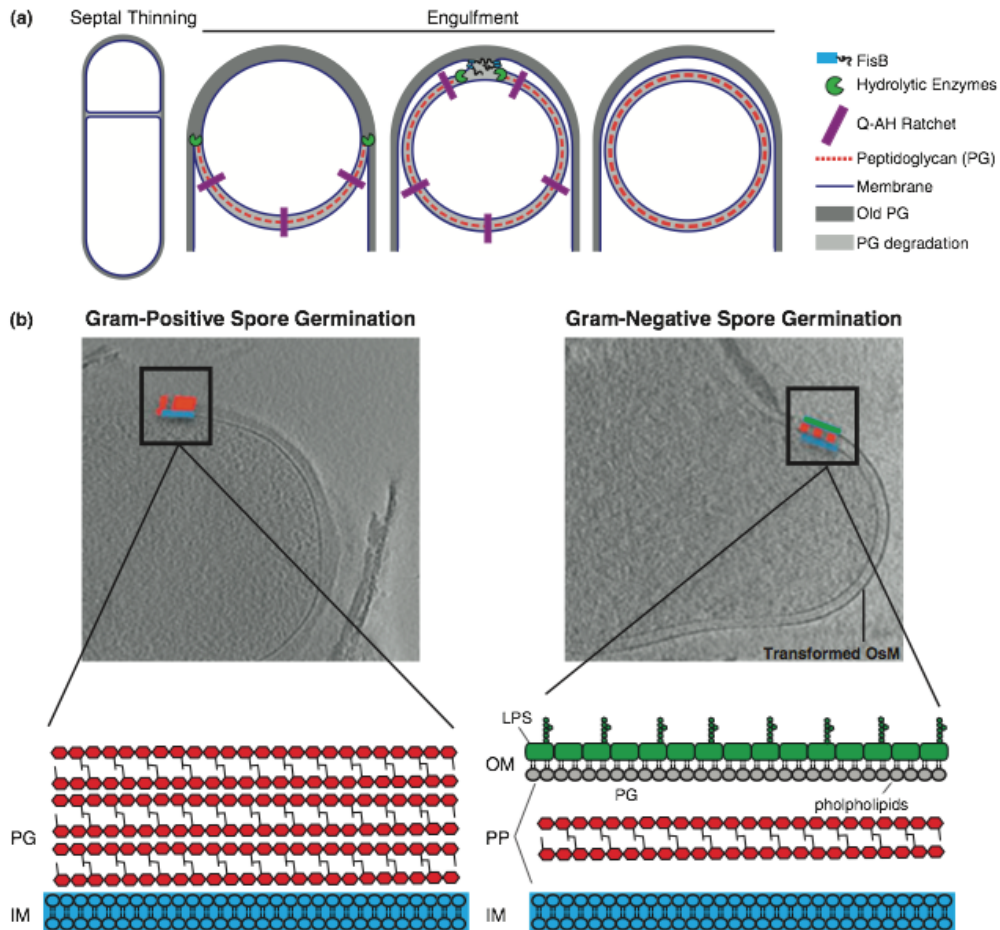
**Figure 1**. (a) Mechanisms of membrane remodeling during the different stages of engulfment. Engulfment initiates with degradation of septal peptidoglycan, commonly referred to as septal thinning. Peptidoglycan synthesis, peptidoglycan degradation and a specific 'ratchet-like' mechanism that is mediated by proteins SpoIIQ and SpoIIIAH (Q-AH) are all factors that have been shown to be important for driving the mother cell membrane around the forespore. To be released into the mother cell, migrating membranes meet at the cell pole and undergo a fission event that is mediated by FisB. Note that the outer spore membrane (OsM) is derived from the cytoplasmic membrane of the mother cell. (b) Spore germination of Gram-positive *Bacillus subtilis* (left) as compared to Gram-negative *Acetonema longum* (right). Upon germination, Gram-positive *Bacillus subtilis* (left) sheds its OsM whereas Gram-negative *Acetonema longum* (right) retains its OsM. Furthermore, *A. longum* transforms its OsM into a canonical Gram-negative outer membrane (OM). The cell envelope of Gram-negative versus Gram-positive bacteria are very different. Gram-positive bacteria have a thick cell wall that is made up of multiple layers of peptidoglycan (PG) that surrounds an inner membrane (IM). On the other hand, Gram-negative bacteria maintain a thin layer of cell wall in-between two membranes. The OM of Gram-negative bacteria is compositionally different from the IM and creates a compartment, the periplasm (PP), that chemically distinct from the cytoplasm. The OM is an asymmetric bilayer with lipopolysaccharide (LPS) distributed in the outer leaflet and phospholipids distributed in the inner leaflet. Copyright (2013) Wiley. Used with permission from Ref (*25*)

9
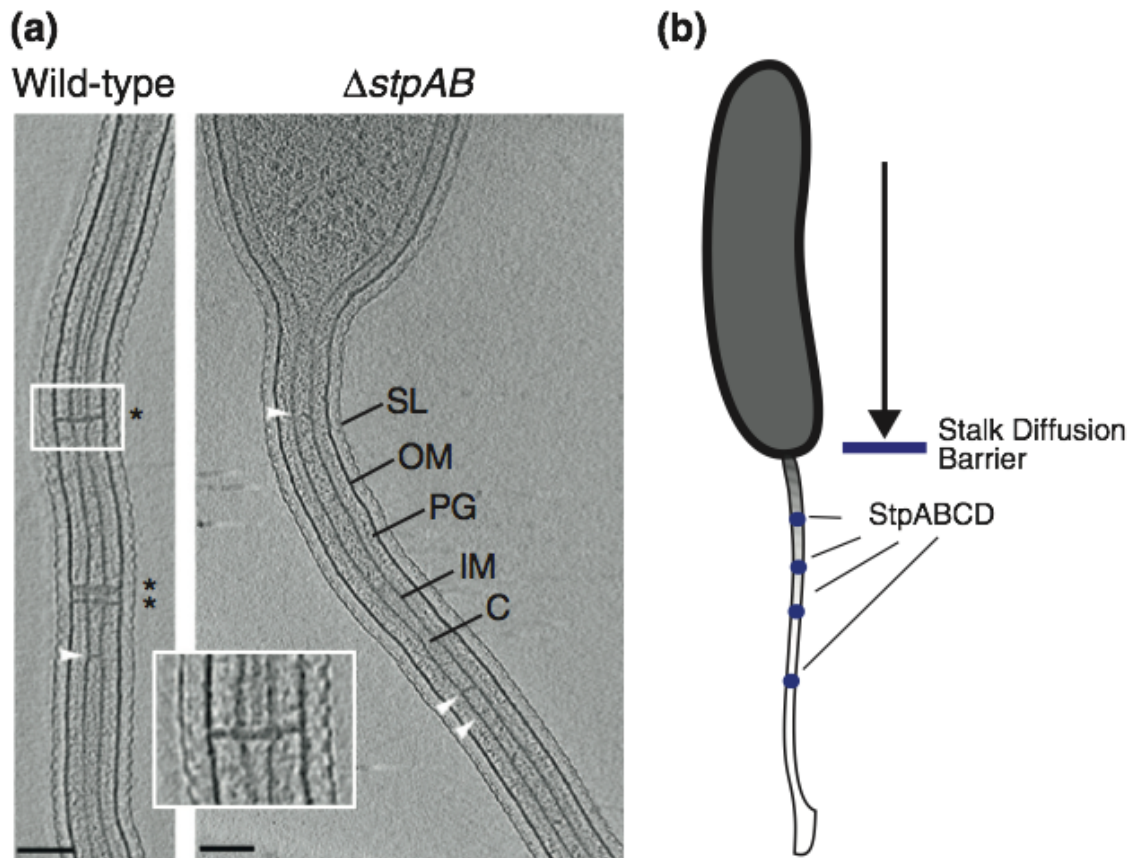
Figure 2. (a) Electron cryotomography images of wild-type *Caulobacter crescentus* cells containing stalk diffusion barriers (* and inset). Δ*stpAB* cells lack these structures. White arrows indicate unidentified structures that span the interior of the stalk (SL = S layer, OM = outer membrane, PG = peptidoglycan, IM = inner membrane, C = cytoplasm). Scale bar 100 nm. Reprinted from Ref. (*7*) with permission from Elsevier. (b) Stalk diffusion barriers: comprising a protein complex of StpA, StpB, StpC, and StpD (blue circles), diffusion barriers limit soluble and membrane protein diffusion into the stalk of *C. crescentus*.
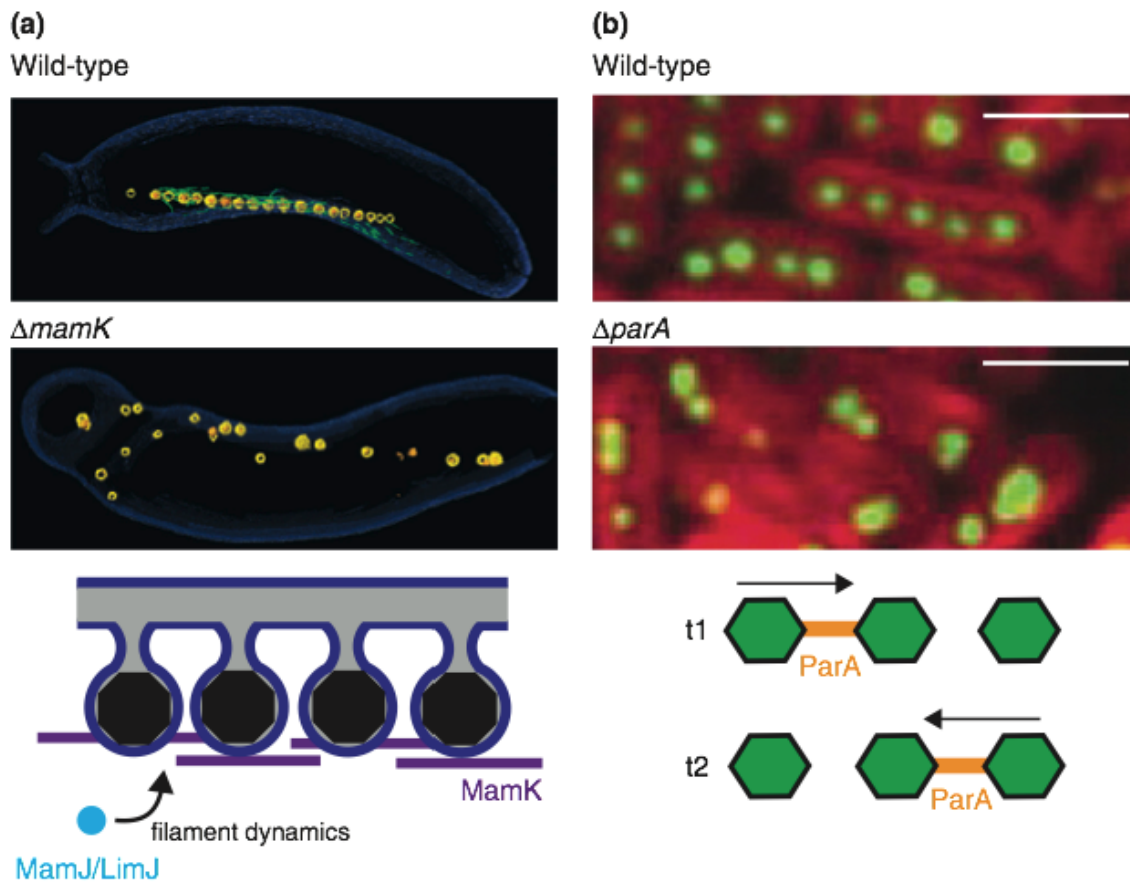
Figure 3. Organization of bacterial organelles by cytoskeletal filaments. (a) The bacterial actin protein MamK is responsible for alignment of magnetosomes into a chain in magnetotactic bacteria. Reconstructed electron cryotomography images of wild-type *Magnetospirillum magneticum* AMB-1 with an aligned magnetosome chain (top panel) and Δ*mamK* cells with disorganized magnetosomes (middle panel). The magnetosome (yellow) chain contains iron- based crystals (orange) and is flanked by filamentous structures (green) that disappear in the Δ*mamK* mutant. MamK dynamic filament behavior is influenced by the presence of MamJ and LimJ (bottom panel). The precise mechanisms that govern this process remain elusive. From Ref. (*36*). Reprinted with permission from AAAS. (b) Alignment and segregation of carboxysomes in cyanobacteria is dependent on ParA, another bacterial cytoskeletal protein. Carboxysomes are evenly distributed throughout the cell in wild-type *Synechococcus elongatus* PCC 7942 (top panel), but not in a mutant lacking *parA* (middle panel). Rubisco protein (RbcL) fused to YFP indicates the localization of carboxysomes (green) and thylakoid membrane fluorescence is shown in red. ParA oscillates from pole to pole and is found distributed in between carboxysomes (bottom panel). T1 and T2 represent time points that are roughly 30 min apart. From Ref. (*43*). Reprinted with permission from AAAS. Scale bar 2 mm.

CHAPTER 2

The interplay between two bacterial actin homologs, MamK and MamK-like, is required for the alignment of magnetosome organelles in *Magnetospirillum magneticum* AMB-1

Nicole Abreu[a], Soumaya Mannoubi[b,c,d], Ertan Ozyamak[a], David Pignol[b,c,d], Nicolas Ginet[b,c,d] and Arash Komeili[a#]

Department of Plant and Microbial Biology, University of California Berkeley, California, USA[a]; CEA, IBEB, Lab Bioenerget Cellulaire, Saint-Paul-lez-Durance, France[b]; CNRS, UMR Biol Veget & Microbiol Environ, Saint-Paul-lez-Durance, France[c]; Aix-Marseille Université, Saint-Paul-lez-Durance, France[d]

ABSTRACT

Many bacterial species contain multiple actin-like proteins tasked with the execution of crucial cell biological functions. MamK, an actin-like protein found in magnetotactic bacteria, is important in organizing magnetosome organelles into chains that are used for navigation along geomagnetic fields. MamK and numerous other magnetosome formation factors are encoded by a genetic island termed the magnetosome island. Unlike most magnetotactic bacteria, *Magnetospirillum magneticum* AMB-1 (AMB-1) contains a second island of magnetosome related genes that was named the magnetosome islet. A homologous copy of *mamK*, *mamK-like*, resides within this islet and encodes a protein capable of filament formation *in vitro*. Previous work had shown that *mamK-like* is expressed *in vivo* but its function, if any, had remained unknown. Though MamK-like is highly similar to MamK, it contains a mutation that in MamK and other actins blocks ATPase activity *in vitro* and filament dynamics *in vivo.* Here, using genetic analysis, we demonstrate that *mamK-like* has an *in vivo* role in assisting organelle alignment. In addition, MamK-like forms filaments *in vivo* in a manner that is dependent on the presence of MamK and the two proteins interact in a yeast two-hybrid assay. Surprisingly, despite the ATPase active site mutation, MamK-like is capable of ATP hydrolysis *in vitro* and promotes MamK filament turnover *in vivo*. Taken together, these experiments suggest that direct interactions between MamK and MamK-like contribute to magnetosome alignment in AMB-1.

INTRODUCTION

Despite their small size, bacterial cells are remarkably organized and can display a stunning degree of control over the production and positioning of highly ordered subcellular structures (*2, 43, 47*). Magnetotactic bacteria (MTB) are recognized for their ability to form organelles called magnetosomes (*48*). These compartments are derived from the inner cell membrane and, with the aid of specialized proteins, synthesize magnetic iron-based crystals. MTB align these individual magnetosomes into an ordered chain within the cell that provides navigational capability towards preferred oxygen concentrations in stratified water columns (*35*). One such bacterium, *Magnetospirillum magneticum* AMB-1 (AMB-1) serves as an excellent model organism for these cellular processes.

In most MTB, the genes required for magnetosome formation are encoded on a genomic region called the magnetosome island (MAI). One of the magnetosome genes conserved in all MTB studied to date is *mamK*, which encodes a bacterial actin protein. The bacterial actin superfamily contains numerous phylogenetically distinct subgroups (*49, 50*) each of which participate in specialized functions such as cell shape determination (*51-53*), motility (*54*), DNA segregation (*55-57*) and cytokinesis (*58, 59*). High resolution imaging of AMB-1 cells by electron cryotomography (ECT) shows that magnetosomes are flanked by filamentous structures (*33*). In AMB-1, the deletion of *mamK* results in a disorganized magnetosome chain and loss of magnetosome-associated filaments (*33*). *Magnetospirillum gryphiswaldense* MSR-1 (MSR-1), a close relative of AMB-1, appears to utilize MamK in a distinct manner to position its magnetosome chains within the cell (*40*). In stark contrast to AMB-1, MSR-1 magnetosome chains do not span the cell length and require magnetic interactions as well as MamK for their assembly. Furthermore, after cell division in MSR-1, magnetosome chains rapidly relocalize to the midcell of daughter cells in a process that seems to require MamK (*40*). However, since the magnetosome chain of AMB-1 spans the entire length of the cell, the cell division coupled relocalization of the magnetosome chain is not likely to occur. Additionally, MamK has been hypothesized to interact with signaling proteins in order to translate relative orientation in magnetic fields into changes in cell motility (*41*). Thus, while MamK is a central player in magnetosome chain organization, the specific mode of its action, its species-specific activities and the full range of its cellular functions remain unknown.

Much like other actin-like proteins, MamK is able to polymerize and depolymerize in a manner that is dependent on its ATPase activity. ATP-bound MamK monomers assemble into filaments and ATP hydrolysis is required for filament depolymerization *in vitro* (*37*). MamK filaments also require an intact ATPase active site and the action of other magnetosome proteins to exhibit dynamics *in vivo*. In particular, a highly acidic protein, MamJ, and its homolog LimJ are necessary for the dynamic behavior of MamK in AMB-1 (*36*). MamJ also participates in magnetosome chain formation since its deletion in MSR-1 results in a dramatic aggregation of magnetosomes within the cell (*60*). In AMB-1 the deletion of *mamJ* and *limJ* leads to a completely different phenotype with the appearance of a few gaps in the magnetosome chain (*36*). The differences between the chain organization phenotypes of *mamJ* and *mamK* mutants of AMB-1 and MSR-1 have

led to speculation that additional players may participate in chain formation in a species-specific manner.

AMB-1 contains a homologous copy of *mamK*, called *mamK-like*, within a genomic region termed the magnetosome islet (MIS) (*61*). The MIS resides outside of the MAI and is likely to have been acquired through a secondary horizontal gene transfer event as its genes have differing GC content and codon usage compared to the MAI (*61*). The presence of the islet brings up the question of whether these two different genomic islands, both encoding for potential magnetosome proteins, are active in AMB-1. Many of the genes within the MIS are pseudogenes or encode truncated proteins. The only genetic analysis of an MIS gene, *mamE-like*, found that it is not redundant with its MAI homologs and does not play a discernible role in magnetosome formation (*31*). Additionally, several residues conserved amongst bacterial actins are absent in MamK-like. In particular, the conserved glutamate residue in its ATPase active site is substituted by an alanine (Figure 4). In MamK and other actins, the mutation of this glutamate (e.g., E143A in MamK) blocks ATPase activity and filament dynamics both *in vivo* and *in vitro* (*36*, *37*, *49*, *62*). Previous work has shown that *mamK-like* is expressed *in vivo* (*61*). Thus, if MamK-like interacts with MamK, it is possible that it would interfere with the dynamics of the chain formation process. These observations raise important questions regarding functionality of the MIS and the potential involvement of MamK-like in magnetosome chain formation.

While members of different bacterial actin subgroups often co-exist in the same organism and carry out their individualized functions without interference from other actin-like proteins, in rare cases, multiple isoforms of the same bacterial actin can also exist in a single organism. *Bacillus subtilis* for example, has three forms of MreB: MreB, Mbl (MreB-like) and MreBH (MreB homolog), that promote cell shape by performing related yet distinct functions in the cell (*63-66*). Thus, we sought to explore the functionality and potential activity of MamK-like as a partner to MamK in AMB-1. Here, we demonstrate that *mamK-like* has a function in chain alignment in AMB-1. We show that MamK-like interacts with MamK and depends on it for *in vivo* filament formation. Surprisingly, the A141 residue of MamK-like does not block its ATPase activity allowing for the protein to positively participate in MamK filament dynamics *in vivo*. Collectively, we show a unique facet to the process of magnetosome formation and provide evidence that MamK-like modulates MamK activity in AMB-1. Additionally, these findings highlight the diverse manner in which bacteria organize their cellular architectures.

15

MATERIALS & METHODS

Growth Conditions.
AMB-1 mutant strains and those bearing plasmids were grown in a modified MG medium as described previously (*29, 33*). Cells and culture growth conditions for Fluorescence Recovery After Photobleaching (FRAP) were prepared as described previously (*36*). Optical densities and coefficient of magnetism (C_{mag}) measurements of strains (measuring the ability of the cells to turn in a magnetic field) in this study are listed in Table 1. Media for the yeast two-hybrid strains were prepared according to the TRAFO Yeast Transformation protocols and previous work (*67, 68*).

Molecular Biology.
Plasmids used in this paper are listed in Table 2. Polymerase chain reactions (PCRs) were performed with primers listed in Table 3 (Integrated DNA Technologies) and Accuprime^{TM} *Pfx* DNA polymerase (Invitrogen) on a MyCycler thermocycler (Biorad). Restriction enzymes, Calf Intestinal Phosphatase, and T4 DNA ligase were purchased from New England Biolabs.

Plasmid Construction.
The marker-less Δ*mamK-like* deletion construct was created by PCR of genomic wild-type AMB-1 DNA (AMB-1 gDNA) with primers: *NA01* and *NA02* for the upstream recombination site, *NA03* and *NA04* for the downstream recombination site. A fusion PCR using the upstream and downstream fragments as templates was executed using *NA01* and *NA04* primers to generate the deletion insert. The pAK31 plasmid backbone was digested with SpeI enzyme and ligated with the deletion insert resulting in plasmid pAK576. The pAK576 construct confers resistance to Kanamycin and contains the counter-selectable marker *sacB*. AMB-1 cells are first selected for Kanamycin resistance (the first recombination event). These cells are then counter-selected on MG agar with 2% sucrose (the second recombination event). These resulting cells are then screened for the loss of the gene of interest by PCR. The *mamK-like-gfp* plasmid (pAK699) was created by PCR of AMB-1 gDNA with *NA33* and *NA19* primers. The pAK22 plasmid backbone was digested with EcoRI and BamHI enzymes and ligated with the *mamK-like* insert digested with MfeI and BamHI. The complementation constructs were created first by digesting *mamK-gfp* out of the pAK22 backbone with EcoRI and SpeI. Untagged *mamK* (with stop codon) was amplified from AMB-1 gDNA with *NA79* and *NA56* to create pAK742. This construct was then digested with SpeI and SacI and ligated with the *gfp-mamI* insert amplified from pAK266 with *NA80* and *NA81* to generate pAK726. The pAK726 plasmid was digested with EcoRI and SpeI enzymes, then ligated with the *mamK-like* insert generated by amplifying AMB-1 gDNA with *NA33* and *NA35* to generate pAK706. To generate the pET-SUMO plasmids for protein expression, the *mamK* and *mamK-like* genes were amplified from AMB-1 gDNA and cloned into a pET-SUMO vector (InvitrogenTM) as following the supplier's protocol. Primers are listed in Table 3.

Site direct mutagenesis.
pET-SUMO-*mamK* and pET-SUMO-*mamK-like* plasmids were used as templates for
site-directed mutagenesis to create mutants *mamK*[E143A], *mamK*[D17N], *mamK-like*[A141E] and
mamK-like[D15N] using the QuickChange kit II XL Site Directed Mutagenesis (Stratagene).
Primers are listed in Table 3.

Strain Construction.
The nonpolar *mamK-like* deletion was constructed in wild-type and Δ*mamK* backgrounds
as described previously (*29*, *33*). Primers used to create the deletion plasmid are listed in
Table 3. The *mamK, mamK-like* double deletion strain was created by deleting *mamK-
like* in a Δ*mamK* background.

Sequence alignment.
Accession numbers for bacterial actin-like proteins (Figure 4) are: *Magnetospirillum
magneticum* AMB-1 MamK-like: ACU87671.1; *Magnetospirillum magneticum* AMB-1
MamK: YP_420328.1; *Magnetospirillum gryphiswaldense* MSR-1 MamK:
CAM78025.1; *Thermotoga maritima* MreB: 2WUS_B; *Escherichia coli* MreB:
EDV65518.1. Alignment was generated with MUSCLE (*69*).

Western Blot of AMB-1.
AMB-1 colonies were transferred into 1.5 ml microcentrifuge tubes containing 1.5 ml
MG media with 10 μg/ml Kanamycin (for plasmid expressing strains) or MG media
alone (for untransformed cells). A 1:100 dilution of AMB-1 cells from 1.5 ml cultures
were inoculated into 10 ml of MG media with or without Kanamycin. Cultures were
grown in 10% O_2 for two days, then passaged 1:100 into 10 ml of fresh MG medium.
These cultures were then grown for an additional two days, then cells harvested by
centrifugation at 15,000 x *g* for 15 minutes at room temperature (Sorvall Mach 1.6R).
Pelleted cells were resuspended in 2X SDS Laemmli buffer (with 5% β-
Mercaptoethanol). Cells were heated at 70° C for 10 minutes with mixing at the 5 minute
mark and loaded onto a 12% Laemmli gel which was run at 150 V for 1 hour. Each
sample contained roughly an equal amount of cells per volume of 2X SDS Laemmli
buffer. Adjustments were based on cell density (OD_{400}, Ultrospec 2100 pro, Amersham
Biosciences). Proteins were transferred onto a PVDF membrane at 100 mA for 1 hour.
After blocking the membrane for 1 hour at room temperature with 5% milk in TBST,
primary antibody was applied (1:5000 Chicken α-GFP, Aves # GFP-1020) for 1 hour at
room temperature. After washing with TBST multiples times, secondary antibody
(1:20,000 Goat α Chicken conjugated to HRP, Aves # H-1004) was applied for 1 hour at
room temperature. The Western lightning Plus ECL (Perkin Elmer) system was used to
visualize bands.

Fluorescence and Differential Interference Contrast microscopy.
Light microscopy was carried out using a Zeiss AxioImager M2 equipped with Qimaging
QiClick camera. GFP-tagged proteins were excited by the Lamda LS Illumination System
(Sutter Instruments). Images were analyzed with iVision software (Biovision).

Fluorescence Recovery After Photobleaching (FRAP).
Agarose pads and slides were prepared as described previously (*36*), with additional changes highlighted in Chapter 3 of this dissertation. FRAP experiments were carried out on a Zeiss 710 UV/Vis laser scanning confocal microscope. MamK-GFP filaments were imaged using 488 nm excitation wavelength at 0.5-3.0 % laser power. The filaments were bleached using 488 nm laser light at 100 % laser power for 7-10 iterations. Images were captured every 50 seconds for up to 30 minutes through the 100 X oil objective with the LSM710 Imaging Software 3.2 (Zeiss). Due to the lack of an auto-focus feature, each frame was monitored and manual focusing was performed if necessary. Images were analyzed using Fiji (*70*). For each FRAP run, regions of interest (ROIs) were drawn in three areas: 1) background 2) whole filament and 3) bleached segment. Each whole filament and bleached ROIs had the background intensity value (arbitrary units) from that time point subtracted. Images that had a steep decrease in fluorescence intensity (generally due to loss of focus rather than photobleaching) were dropped from downstream analysis. To generate the percent recovery graphs, runs were normalized by calculating the ratio of bleached ROI intensity over the whole filament ROI intensity for each timepoint. The run was considered recovered under the following criteria: 1) Fluorescence intensity of the bleach region returned to 50 percent of the whole filament at the same time point and 2) whole filament fluorescence intensity values did not dip drastically due to photobleaching. For $T_{1/2}$ comparisons: a comparison between genetic backgrounds was analyzed by a two-tailed T-test analysis to determine statistically significant ($p \leq 0.05$) differences in $T_{1/2}$. This analysis takes into account only the cells that resulted in recovery.

Gene Transcription Analysis.
Cultures were sampled at the same growth stage and ran in technical replicates. Cells were cultivated in 250 ml Schott flasks closed with a septum. Growth medium (200 ml) was supplemented with Wolfe's vitamin solution and 30 µM $FeSO_4$ and flushed with 4% O_2. Cultures were sampled at 24 hours (during the exponential growth phase) and 41 hours (the end of the exponential growth phase). At both time points 90 ml of each culture was centrifuged (7500 x g, 10 minutes, 4 °C) and cell pellet was resuspended by vortexing in 1 ml of a mix of RNA protect solution and fresh culture medium (2:1). After 5 minute incubation at room temperature the cells were pelleted at maximum speed and flash-frozen in liquid nitrogen for storage at -80 °C. Total RNA was extracted from cellular pellets with the RNAeasy Minikit (Qiagen). Contaminant DNA was removed from the RNA samples by digestion with DNAse. RNA polymerase sigma factor *rpoD* (amb0697), a housekeeping gene, was selected as a reference to normalize the data. The reverse transcriptase reaction was performed on 400 ng of total RNA using the SuperScript® VILO cDNA synthesis kit (Invitrogen). cDNA was quantified by spectrophotometry (Nanodrop) and stored at -80 °C (mean value was 2158 ± 100 ng/µl). Primers for *mamK*, *mamK-like* and *rpoD* amplification were chosen using Primer3, a free online tool to design and analyze primers for PCR and real time PCR experiments (http://simgene.com/Primer3). Primers are listed in Table S3. Optimization of the primers was conducted with SYBR® Green Real-Time PCR in the qRT PCR machine on dilutions of AMB-1 gDNA. The AMB-1 gDNA stock (50 ng/µl) was prepared into 8 dilutions (from 10^{-2} to 10^{-9}) in DNAse/RNAse-free water. With the help of TECAN robot

dispenser, we deposited on a 384 wells plate 2 μl of AMB-1 gDNA for each dilution (in technical triplicates). A mix of SYBR® Green Real-Time PCR master mix, primers solution at 10 μM and water (respectively 10:12, 1:12, 1:12) was prepared for each gene to be tested and 3 μl deposited in each well. Negative controls with DNAse/RNAse-free water replacing the genomic DNA were also included. The protocol in the qRT PCR machine was performed as follows: 1) 1 cycle 10 minutes at 95 °C to activate the polymerase. 2) 45 cycles with 10 seconds at 95 °C, 10 seconds at 60 °C for hybridization and 10 seconds at 72 °C. The SYBR® Green fluorescence was measured after each cycle and the data was interpreted with Light cycler 480 software (Roche). A standard curve for each gene was computed using the crossing-point values. For the DNA quantities we used arbitrary units resulting in relative expression values, which is sufficient for the purpose we set to this study.

To the best of our knowledge, *rpoD* was never validated as reference gene in *M. magneticum* AMB-1. Nevertheless this gene is frequently cited in the literature for bacterial expression normalization in RT-qPCR experiments. To compare the different strains at a given time of the growth curve, we used *rpoD* to normalize our data as we observed that for a given time, *rpoD* expression levels are comparable for the wild-type and mutant strains. In this context, *rpoD* is used as an internal reference to normalize the data between the strains.

The standard curves were generated with serial dilutions of AMB-1 genomic DNA (1/1, 1/10, 1/100 and 1/1000, in triplicates); the parameters of the resulting standard curves computed with the Light Cycler® software are summarized in Table 4.

Dual color labeling experiment.
The MamK-GFP, MamK-like-RFP dual-label plasmid pAK705 was generated by amplifying *mamK-like* from AMB-1 gDNA with *NA50* and *NA44* and RFP from a plasmid (gifted from Zambryski lab) with *NA43* and *NA45*. Fragments were digested with NheI and cleaned before ligated. Resulting fragments were then digested with SpeI and XbaI and ligated into pAK22 (MamK-GFP plasmid) that was digested with the same enzymes. Images were acquired as described in "Fluorescence and Differential Interference Contrast microscopy" section of methods.

Yeast Two-Hybrid Assays.
Yeast two-hybrid (Y2H) assays were conducted employing a previously established plasmid and yeast strain system (*68*, *71*). A set of Y2H plasmids enable the fusion of proteins of interest via polylinkers to the Gal4 DNA binding (pCD plasmids) or the Gal4 activation domain (pC-ACT plasmids). Gene sequences for *mamK*, *mamK-like* and *mreB* were amplified from AMB-1 gDNA using primer sets specified in Table S3 and ligated into pCD and pC-ACT plasmids through NdeI and BamHI restriction sites. The gene *mamK* was fused to Gal4 domains in pCD.3 and pC-ACT.3 resulting in plasmids pAK140 and pAK141, respectively. The genes *mamK-like* and *mreB* were fused to Gal4 domains in pCD.1 and pC-ACT.1 (*mamK-like*: pAK485 and pAK483 respectively; *mreB*: pAK479 and pAK489 respectively). Plasmids were individually transformed into either

19

the yeast strain YD116 (mating type a) or the strain YD119 (mating type α). Cells harboring the pCD and pC-ACT plasmids were created by mating and cells were selected on media plates lacking tryptophan and leucine as genes for their synthesis are encoded on the respective plasmid. Mated yeast strains carrying both plasmids were grown in 5 ml of media lacking tryptophan and leucine before adjusting volumes to plate equal numbers of cells (OD_{600} of 0.3), then serial 1:10 dilutions were made and plated on plates lacking tryptophan and leucine or tryptophan, leucine and uracil. Yeast strains YD116 and YD119 utilize the GAL1–URA3 reporter for assessment of Gal4 transcription factor reconstitution upon protein-protein interaction. Hence, the interaction of MamK, MamK-like and MreB was assessed on media plated lacking tryptophan, leucine and uracil. Images were taken on an iPad (Apple).

Expression and purification of MamK and MamK-like.
N-terminal tagging of MamK and MamK-like with the SUMO tag allows affinity purification of the proteins and a seamless removal of the tag by the action of the SUMO protease. The pET-SUMO plasmids were co-transformed into One Shot® *BL21 Star™* (*DE3*) chemically competent *Escherichia coli* cells along with the pRARE plasmid encoding several rare tRNAs (*72*). Transformants were selected on LB medium in the presence of both kanamycin (50 µg/ml) and chloramphenicol (25 µg/ml). For protein expression of either MamK or MamK-like, cells were grown overnight in Terrific Broth (TB) medium in the presence of both antibiotics at 30°C under shaking. Overnight cultures were diluted into fresh medium and grown to $OD_{600} \pm 0.6$ at 37°C; isopropyl β-D-1thiogalactopyranoside was then added to a final concentration of 0.1 mM to induce protein expression and cultures were incubated shaking at 16°C overnight. Cells were harvested by centrifugation (7500 x *g*, 15 minutes) and the cell pellet was resuspended in 20 mM HEPES (pH 8), 250 mM NaCl. A protease inhibitor cocktail and DNase I are added to the suspension to prevent protein degradation and reduce the viscosity of the lysate, respectively. Cells were disrupted with a French Press (1000 psi, three passages). The lysate was centrifuged at low speed (10,000 x *g*, 10 minutes) to remove large debris and the supernatant was ultracentrifuged (150,000 x *g*, 1 hour) to separate membranes and polymerized protein from soluble MamK or MamK-like. The supernatant was then loaded onto a Ni-NTA resin (pre-packed 1 ml His-Trap HP column, (GE Healthcare) using an Äkta Fast Protein Liquid Chromatography system (GE Healthcare). Three washing steps were carried out with increasing concentrations of imidazole (20 mM, 50 mM and 100 mM) and elution was performed at 300 mM imidazole. Eluted proteins are immediately desalted and the buffer exchanged using a size exclusion chromatography column PD-10 (stabilization buffer 100 mM Bis Tris Propane, pH 8.5). The seamless removal of the SUMO tag was performed by incubation of the SUMO-tagged proteins with the SUMO protease (the *sumo* gene amplified from *Saccharomyces cerevisiae* and cloned into a pET28b was kindly provided by Dr. Christopher D. Lima (*73*)). The incubation mix contained 1 U SUMO protease for 20 µg protein and proteolysis lasted for 3 hours at 30 °C or overnight at 4 °C. The proteolysis mixture was loaded onto the nickel affinity column: a successful cleavage of the SUMO tag will leave the untagged protein in the flow-through. The Bradford assay was used for protein quantification.

<u>ATPase activities</u>. The inorganic phosphate release resulting from ATPase activity was measured spectrophotometrically using the Malachite Green test (adapted from (*74*)). A 500 µl reaction mixture was prepared in 100 mM Bis-Tris propane buffer (pH 8.5) with known quantities of protein and incubated at room temperature to determine initial velocities. Typically we used 2 µM of protein for ATP concentrations above 1 mM, 4 µM of protein between 250 µM and 1 mM ATP and 8 µM under 250 µM ATP. The reaction was triggered by addition of ATP and $MgCl_2$ in concentrations ranging from 25 µM to 4 mM. 50 µl aliquots were sampled every 5 minutes and the reaction stopped by adding 20 µl of 0.6 M perchloric acid. The colorimetric reaction was made by adding 100 µl of malachite green reagent and 14 µl of a stabilizing solution of 34% sodium. After incubation at room temperature for 10 minutes under soft stirring the absorbance was measured at 645 nm in a microplate reader (TECAN, infinite M200). The data are normalized to a standard curve made with phosphate standards prepared in the 100 mM Bis-Tris propane buffer (pH 8.5) and protein-free controls were performed.

RESULTS

MamK-like participates in magnetosome chain alignment.
In order to investigate the function of MamK-like *in vivo*, we created in-frame deletions
of the *mamK-like* gene in wild-type and Δ*mamK* strains. Previous work using RT-PCR
had found that *mamK-like* is expressed in wild-type AMB-1 and Δ*mamK* backgrounds
(*61*). Here, using qRT-PCR we determined that *mamK-like* was expressed at
approximately half of the levels of *mamK* (Figure 5). Furthermore, the deletion of *mamK-like* or *mamK* did not result in a change in the expression levels of the other gene (Figure
5). Additionally, the deletion of *mamK-like*, alone or in combination with *mamK*, did not
result in gross cell morphological changes as assessed by transmission electron
microscopy (TEM) (Figure 6).

We next investigated if MamK-like is important for the chain-like organization of
magnetosomes in AMB-1 cells. To visualize the misalignment of the magnetosome chain
we use a fluorescent fusion to a magnetosome membrane marker (GFP-MamI). In several
strains, such as the Δ*mamK*, Δ*mamJ*, Δ*limJ* and Δ*mamJ* Δ*limJ* mutants, GFP-MamI has
been successful in revealing a large range of magnetosome chain organization defects
that are congruent with high resolution imaging via ECT (*29, 31, 36*). Since it depends on
fluorescence microscopy rather than ECT, imaging of GFP-MamI is a rapid and high
throughput method of determining the integrity of the magnetosome chain across a large
number of cells in a population. Furthermore, this visualization technique can detect
mineral-loaded magnetosomes as well as empty membranes that could only be detected
by ECT otherwise. Linear localization patterns of GFP-MamI correlate to aligned
magnetosomes (both full and empty) and cells with unaligned magnetosomes have
multiple unaligned foci, cell membrane localization or diffuse staining (Figure 7B).
Compared to wild-type cells that have a high proportion of aligned magnetosomes (77.3
percent, n=1870), Δ*mamK* cells display a less organized localization pattern with only
33.3 percent of cells showing alignment (n=1161, Figure 7A). The Δ*mamK-like* cells
also display a higher degree of disorganization compared to wild-type (45.8 percent of
cells with aligned magnetosomes, n=1276, Figure 7A). The deletion of both *mamK* and
mamK-like results in the most severe disorganization phenotype (25.8 percent of cells
with aligned magnetosomes, n=807, Figure 7A). Complementation experiments were
performed to confirm that these results were due solely to the loss of the targeted gene
products. The Δ*mamK* and Δ*mamK-like*, as well as the double deletion cells, were
complemented with a copy of the deleted gene on a plasmid. Cells lacking *mamK* were
complemented at about 63 percent of wild-type, and cells lacking *mamK-like* were
complemented to wild-type levels (Figure 7A). The differences in complementation
levels suggest that protein expression from the plasmid may not be sufficient to
completely rescue the Δ*mamK* phenotype. Complementation of the double deletion strain
with either *mamK* or *mamK-like* indicates that the phenotype of this strain is due to gene
loss and demonstrates that both MamK and MamK-like participate in chain alignment.

MamK and MamK-like proteins interact in a yeast two-hybrid assay and form colocalizing filaments *in vivo.*

MamK-like shares 56% sequence identity with MamK from AMB-1. Given that both proteins are part of the same family, have a high degree of conservation and participate in the same cellular process, we reasoned that they could potentially interact with each other. Utilizing a yeast two-hybrid assay, MamK and MamK-like proteins displayed interactions with themselves and with each other (Figure 8). This interaction was specific in that neither MamK nor MamK-like interacted with the more distantly related bacterial actin protein, MreB, from AMB-1, which can interact with itself in the yeast-two hybrid assay (Figure 8). As a negative control, pairings between empty vector constructs did not result in interaction and growth (Figure 8). To investigate the potential interactions between these two proteins *in vivo,* we co-expressed MamK-GFP and MamK-like-RFP and found that they form colocalizing filaments in AMB-1 (Figure 9). Taken together, these results suggest that MamK and MamK-like proteins interact in their filamentous form.

MamK influences MamK-like's ability to form filaments *in vivo*.

The results above indicate that an interaction exists between MamK and MamK-like. We reasoned that formation of filaments of one protein *in vivo* might require the presence of the other. MamK-GFP filaments formed with similar frequency in wild-type and Δ*mamK-like* strains (data not shown). In contrast, MamK-like-GFP filaments depended on the presence of MamK for efficient filament formation. In the wild-type background, 52 percent of cells had MamK-like-GFP filaments, 38 percent of cells had diffuse patterns and 10 percent of cells had foci (n=345, Figure 10A). The Δ*mamK-like* background had a similar proportion of MamK-like-GFP filaments, with 54 percent of cells with filaments, 38 percent with a diffuse pattern and 8 percent of cells with foci (n=441, Figure 10A). In contrast, very few cells in the Δ*mamK* (9 percent) or Δ*mamK*Δ*mamK-like* (6 percent) backgrounds displayed MamK-like-GFP filaments (n=540 for Δ*mamK* and n=426 for Δ*mamK*Δ*mamK-like*, Figure 10A). To confirm expression of fusion proteins, western blotting using an anti-GFP antibody was performed on wild-type cells expressing MamK-like-GFP. In contrast to cells expressing MamK-GFP, a distinct signal for the GFP fusion fragment was detected suggesting that the MamK-like-GFP fusion is less stable than MamK-GFP (Figure 10C). This may also account for some of the diffuse localization patterns observed in cells expressing MamK-like-GFP (Figure 10B and 10C).

MamK-like can affect MamK turnover *in vivo*.

Thus far, our data indicate that MamK and MamK-like are capable of physical and functional interactions within the cell. We previously hypothesized that MamK-like could affect MamK dynamics if the two proteins formed mixed polymers (*36*) (Figure 11A). This was based on the observation that nucleotide hydrolysis is required for MamK dynamics *in vivo* and that MamK-like carries a mutation that should render it a non-active ATPase (A141 in MamK-like corresponding to E143A in MamK, Figure 4). The *in vivo* dynamics of MamK have been characterized in previous work with Fluorescence Recovery After Photobleaching (FRAP) assays (*36*). MamK-GFP filaments localize as thin lines in AMB-1 cells although, occasionally, curved lines or doubled filaments are

also observed (Figure 11B). During FRAP experiments, sections of GFP-tagged MamK filaments are irreversibly photobleached and the recovery of fluorescence in the bleached segment is tracked over time (Figure 11C). Recovery in FRAP is most likely the result of monomer turnover (depolymerization/polymerization), filament sliding, or new filament formation events. The $T_{1/2}$ of recovery denotes the time point at which 50 percent of the fluorescence intensity returns to the bleached region relative to the whole filament at that same time point. The fluorescence recovery frequency of MamK-GFP has previously been observed in approximately 50 percent of wild-type cells with a $T_{1/2}$ of 11 ± 6 minutes (*36*). In this study MamK-GFP in the wild-type background had similar recovery frequency and slightly slower average $T_{1/2}$ (50 percent of cells recovered, at $T_{1/2}$ of 14.3 ± 5.5 minutes, n=32, Figure 11F). The longer recovery times in this set of experiments could be due to the difference in imaging equipment, as less photobleaching occurs with the confocal microscope used in this study allowing for more frequent and longer imaging of cells than in previous work.

Since the two proteins appear to form mixed filaments, we hypothesized that the putative mutations in the ATPase active site of MamK-like could account for the relatively slow dynamics of MamK-GFP filaments and the large proportion of cells in which no recovery is observed. However, the deletion of *mamK-like* did not affect turnover frequency (50 percent, n=22) or rates ($T_{1/2}$: 15.5 ± 7.7 minutes) of recovery of MamK-GFP filaments in FRAP experiments (Figure 11F). In contrast, the total amount of MamK in the cells had an impact on the FRAP experimental results. Loss of endogenous MamK (in the $\Delta mamK$ background) lowered recovery frequency (23 percent of cells recovered compared to 50 percent in wild-type) but did not significantly affect the $T_{1/2}$ of recovering cells (13.2 ± 8.0 minutes, n=44, Figure 11F). However, the $T_{1/2}$ of MamK-GFP filaments in the strain deleted for *mamK* and *mamK-like* were significantly ($p \leq 0.02$, Figure 12A) slower than in $\Delta mamK$ cells alone (21.2 ± 6.6 minutes, n=45, Figure 12A). Thus, the dynamics of the MamK-GFP filament is most severely impacted when both native MamK and MamK-like are absent. These results show that MamK-like does not have a negative impact on the turnover of MamK filaments *in vivo*. Instead, MamK-like appears to promote the turnover of MamK filaments, either by supplying a source of monomers in the cytoplasmic pool that are incorporated into MamK filaments, new filament growth, or by lateral filament sliding. The importance of these potential interactions is most evident when endogenous MamK and MamK-like are absent in the cell.

MamK-like displays ATPase activity despite the E141A mutation.
The above results lead to the surprising conclusion that the interaction of MamK-like with MamK has a positive affect on filament turnover despite the presence of a mutation that should inhibit ATP hydrolysis and as a result impede the depolymerization of filaments. Thus, we investigated whether MamK-like has ATPase activity despite the E141A mutation. Recombinant MamK-like was purified and analyzed in a phosphate release assay. Compared to MamK which has a K_m of 143 μM and V_{max} of 0.2 μM $P_i \bullet$ $min^{-1} \bullet uM^{-1}$, MamK-like has a K_m of 127 μM and V_{max} of 0.32 μM $P_i \bullet min^{-1} \bullet \mu M^{-1}$ in our experiments (Figure 13). This is surprising, as the substitution of this residue in MamK (Figure 13) and other actins abolishes ATPase activity. When the residue is changed back to a glutamate (A141E), MamK-like displays a higher level of phosphate

release to both MamK and MamK-like with a K_m of 151 μM and V_{max} of 0.52 μM P_i • min^{-1} • uM^{-1} (Figure 13). Additionally, ATPase activity of MamK-like is abolished when a highly conserved aspartate residue (D15, Figure 13) in its Phosphate 1 loop, predicted to participate in ATP binding, is mutated (*75*). Combined with the *in vivo* FRAP experiments, these results show that MamK-like is an ATPase that can influence the behavior and function of MamK filaments.

DISCUSSION

The MAI has been the focal point of research on magnetosome formation in recent years. In a scenario that is unusual amongst MTB, AMB-1 contains a second subset of magnetosome formation genes in the MIS whose function and potential participation in magnetosome formation have been debated. Here, we demonstrate that one gene from the MIS, *mamK-like*, is transcribed and its product interacts with MamK to regulate MamK dynamics and align magnetosomes in the cell.

Magnetosome alignment can be assessed through more than one method. In our research we used a magnetosome marker for this purpose. It is important to note that, at first glance, whole cell TEM images (such as those in Figure 6) appear to show no obvious distinctions in magnetosome alignment between wild-type and mutant cells. This assumption is misleading, however, since conventional TEM can only image the electron-dense magnetic particles and fails to visualize empty magnetosome membranes. Cells with fragmented chains, for instance, cannot be distinguished from those containing continuous stretches of empty and filled magnetosome membranes. In other words, "gaps" in a wild-type cell are often still filled with empty magnetosomes (as visualized by ECT) whereas gaps in *mamK* deletion cells are truly devoid of any magnetosomes, empty or filled (*33*). Additionally, in Δ*mamK* mutants, isolated empty magnetosomes have been seen on the side of the cell opposite the magnetosome chain using ECT but not in TEM images (*33*). This observation could imply that subcellular positioning of an empty magnetosome influences its ability to transport iron or initiate crystal formation. For these reasons, we have developed GFP-MamI as a robust fluorescent marker for magnetosome membranes. By examining various mutants, we have found that this reporter can mark empty and filled magnetosomes and provide a view of chain organization that is consistent with ECT imaging (*29, 36*).

Using GFP-MamI as a reporter, we find that both MamK and MamK-like are needed to align magnetosomes in AMB-1. Since a higher proportion of Δ*mamK* cells have misaligned chains compared to Δ*mamK-like* cells, we hypothesize that MamK may be a dominant player in magnetosome chain formation in AMB-1. Consistent with this view, the loss of MamK correlates with the decreased capability of MamK-like-GFP to form filaments while MamK-like has no influence on the ability of MamK-GFP to form filaments in AMB-1 (Table 5, unpublished data). Previously, expression of MamK-like, fused to a fluorescent protein, in *E. coli* allowed for the formation of filaments that resemble those seen in AMB-1 (*61*). Since MamK was not present in these *E. coli* strains it is possible that overexpression of MamK-like can over-ride the requirement of MamK for robust filament formation. Unfortunately, to date we have been unable to generate antibodies that unambiguously distinguish between MamK and MamK-like, thus making it difficult to directly measure the endogenous protein levels.

Perhaps, the most surprising of our results is that MamK-like can hydrolyze ATP. The substitution at residue 141 of MamK-like (A141 in MamK-like and E143 in MamK) should abolish ATP hydrolysis since this site coordinates ATP through a Mg^{2+} ion in both eukaryotic and bacterial actins (*75*). The absence of the glutamate residue is not the only

26

feature that distinguishes MamK-like from other actins. The so-called "Phosphate 1" (DLGT) and "Adenosine" glycine rich loop (GGG) regions, highly conserved in the actin-like family and involved in ATP phosphates binding, are also modified in MamK-like (with DFGY and GAG respectively, Figure 4) (*75*). Despite these changes, MamK-like is still capable of hydrolyzing ATP *in vitro*, a finding that is consistent with its positive role in promoting MamK filament dynamics *in vivo*. This suggests that several modifications of the ATPase active site are compensating for the loss of the glutamate at position 141. Determining the mechanistic basis of MamK-like's ATPase activity will be an important addition to our knowledge of the structural diversity and evolution of bacterial actins.

Given the data in this study, some potential scenarios can be envisioned for how MamK and MamK-like behave in AMB-1. Because MamK influences MamK-like-GFP filament formation *in vivo* (Figure 10), the two proteins colocalize (Figure 9) and are able to interact with each other (Figure 8), we would hypothesize that they either form a mixed copolymer (Figure 14A) or are interacting laterally as pure filaments (Figure 14B). In the copolymer mode of interaction, MamK and MamK-like proteins would form an interchangeable monomer pool whose total concentration is the most important determinant of efficient filament dynamics. Thus, the most severe phenotypes are observed when both proteins are absent from the cell. If monomers cannot mix, pure MamK filaments would then serve as nucleating sites for MamK-like to form filaments via lateral association. In this case, the dynamics seen in FRAP can be due to sliding of filaments against each other. In the double deletion strain the total number of filaments falls below a threshold required for efficient filament sliding and recovery in FRAP.

While our current experimental techniques do not provide sufficient resolution to unequivocally distinguish between these two modes of interaction, we believe that the simplest scenario to explain all of the data is the formation of mixed filaments between MamK and MamK-like. This view is partly influenced by the observation that recovery in FRAP experiments is dependent on the ATPase activity of MamK. Since ATPase activity is required for the *in vitro* depolymerization of MamK filaments (20), and those of all actin-like proteins examined to date (*36, 37, 49, 62*), it is likely that recovery in FRAP is due to polymerization/depolymerization events rather than filament sliding. Furthermore, an examination of a structural model of MamK and its homology to MamK-like indicate that individual monomers of these two proteins could interact at critical points of contact. Previous structural analysis of MreB from *Thermotoga maritima* identified potential contact points that link monomers to one another in a protofilament (Figure 4, marked pink) (*76*). A model of MamK monomers, based on this *Thermotoga maritima* MreB structure, fit within the filament structure of MamK, obtained by electron microscopy, with high confidence (*37*). In a multiple sequence alignment, many of the residues in these points of contact are conserved between diverse MreB proteins (Figure 4, marked blue). Similarly, these regions are conserved between MamK and MamK-like (Figure 4, marked green) but distinct from MreB. MamK and MamK-like also share a 5 residue region, unique to the MamK family, that is predicted to be important for protofilaments to form double stranded filaments (Figure 4, red box) (*37*). These comparisons indicate that MamK and MamK-like have the necessary sequence

conservation to form a mixed copolymer. Additionally, the variations in these putative contact sites between MamK and MreB may prevent unwanted cross-talk between functionally distinct families of bacterial actins that have to coexist in the same cell.
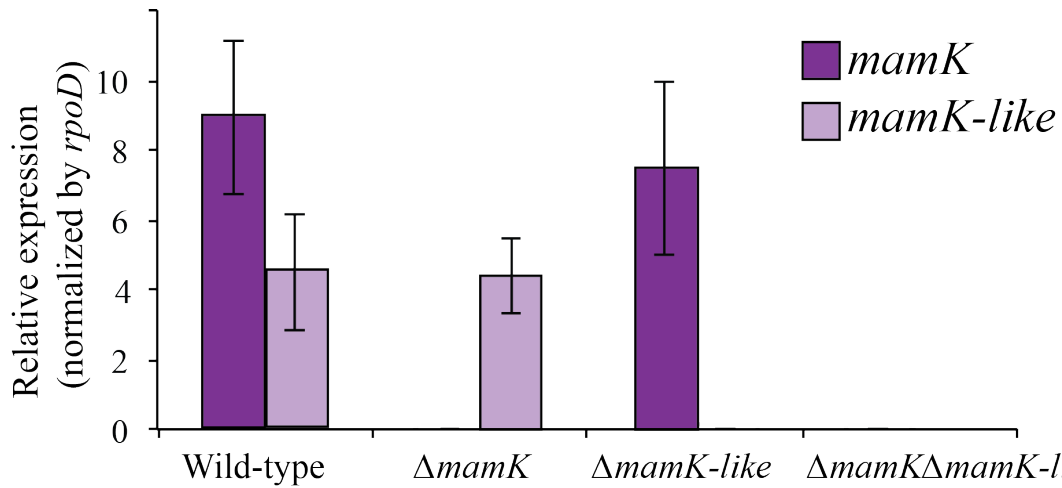
The co-existence and cooperation between MamK and MamK-like are reminiscent of presence of multiple MreB isoforms in *B. subtilis*, which partner in cell shape determination (*64, 65, 77*). The existence of multiple MamK isoforms within the same cell is not limited to AMB-1, however. The alpha-proteobacterium, *Magnetovibrio blakemorei* MV-1 and gamma-proteobacterium strain SS-5 each contain two MamK homologs within their MAIs (*78*). In contrast to MamK-like, however, these MamKs have normal ATPase active sites (Abreu and Komeili, unpublished data). Additionally, the magnetotactic delta-proteobacteria, such as *Desulfovibrio magneticus* RS-1 and *Desulfamplus magnetomortis* BW-1, contain MamK as well as another potential bacterial actin-like protein, Mad28, within their MAIs (*79*). While Mad28 is not part of the MamK subfamily, it is possible that it participates in chain alignment through interactions with MamK. As more magnetotactic bacterial genomes are sequenced, we may find that participation between multiple MamK family members is a rather common mode of magnetosome chain organization.

Finally, studies on the interactions and dynamics of MamK and its homologs can have broader implications in the understanding of the evolution and diversity of the vastly understudied superfamily of bacterial actins. In most eukaryotes, actin is highly conserved and its function and dynamics are impacted by a standard set of actin binding proteins. Interestingly, the intestinal parasite *Giardia intestinalis*, contains one of the most divergent eukaryotic actins and also lacks many of the canonical actin binding proteins (*80*). This fascinating "exception to the rule" supports a hypothesis that preservation of essential interactions between actin and its conserved regulatory partners are a key evolutionary constrained that limits the protein's sequence divergence amongst eukaryotes. In contrast, the various families of bacterial actins are highly divergent at the sequence level indicating the absence of a common set of binding proteins and regulators for these proteins. In such a system, isoforms of a bacterial actin-like protein with variations in ATPase activity or binding capacity can provide a rapid path for incorporation of regulatory modules within the cell.

```
                                  Phosphate 1
AMB-1 MamK-like  ---MIVNDNQNILYVGIDFGYSKTVIMTSRGKSLSLK--SLVGYPKDFVGLARLGRPYLV
    MSR-1 MamK   -MSEGEGQAKNRLFLGIDLGTSHTAVMTSRGKKFLLK--SVVGYPKDVIGLKLLGRPYVV
    AMB-1 MamK   -MSEGEGQAKNRLFLGIDLGTSHTAVMSSRGKKFLLK--SVVGYPKDVIGLKLLGRPYVV
       Tm MreB   -------MLRKD--IGIDLGTANTLVFL-RGKGIVVNEPSVIAIDST----T--GEILKV
       Ec MreB   MLKKFRGMFSND--LSIDLGTANTLIYV-KGQGIVLNEPSVVAIRQDRAGSP--KSVAAV
    AMB-1 MreB   MFSKLTGWMSAD--MAIDLGTANTLVYV-KGRGIVLNEPSVVAIAEE--KGK--KKVLAV

AMB-1 MamK-like  GDEAFEM----RSYLHLRNPLLDGLLNPISEQDIDVTRHFISHIIKCAEPAAG---EKVF
    MSR-1 MamK   GDEAFEM----RSYLDLRYPLQDGVLSEISDRDIEVARHLLTHVVKSAEPGAN---DEIC
    AMB-1 MamK   GDEAFEM----RSYLDIRYPLQDGVLSEISDRDIEVARHLLTHVVKSAEPGPN---DEIC
       Tm MreB   GLEAKNMIGKTPATIKAIRPMRDGVIA----DYTVALVMLRYFINKAKGGMNL--FKPR
       Ec MreB   GHDAKQMLGRTPGNIAAIRPMKDGVIA----DFFVTEKMLQHFIKQVHSNSFMR-PSPR
    AMB-1 MreB   GDEAKMMLGRTPGYIQAIRPLRDGVIA----DFEVAEEMIKHFIRKVHNRRSF--ASPL

                                  Connect 1              Phosphate 2
AMB-1 MamK-like  AVIGVTPRFTAANKKLLLKLAQEY-CQNVLLMSAPFLAGNS----IGKASGSIIIDIGAW
    MSR-1 MamK   AVIGVPARASGANKALLLKMAQEV-VHTALVVSEPFMVGYG----LDKLNNTIIVDIGAG
    AMB-1 MamK   AVIGVPARASAANKALLLKMAQEV-VHTALVVSEPFMVGYG----LDKLINTIIVDIGAG
       Tm MreB   VVIGVPIGITDVERRAILDAGLEAGASKVFLIEEPMAAAIGSNLNVEEPSGNMVVDIGGG
       Ec MreB   VLVCVPVGATQVERRAIRESAQGAGAREVFLIEEPMAAAIGAGLPVSEATGSMVVDIGGG
    AMB-1 MreB   VIVCVPSGSTAVERRAIQESAESAGARRVFLIEEPMAAAIGAGLPVTEPTGSMVVDIGGG

                 Phosphate 2
AMB-1 MamK-like  TTDICAMKGRIPRPEDQSSIAKAGSYIDERLKNSILERYPALQINANIARMVKEQFAFVG
    MSR-1 MamK   TTDICALKGTVPGPEDQVTLTKAGNYIDERLQNAILERHPELQMNTNVACAVKEQFSFVG
    AMB-1 MamK   TTDICALKGTVPGPEDQVTLTKAGNYVDERLQNAILERHPELQMNVNVACAVKEQFSFVG
       Tm MreB   TTEVAVI--SLGSIVTWESIRIAGDEMDEAIVQYVRETY-RVAIGERTAERVKIEIGNVF
       Ec MreB   TTEVAVI--SLNGVVYSSSVRIGGDRFDEAIINYVRRNY-GSLIGEATAERIKHEIGSAY
    AMB-1 MreB   TTEVAVL--SLGGIVYSRSVRVGGDKMDEAIIAYIRRNH-NLLVGEGSAERIKKEIGSAC

AMB-1 MamK-like  RPQ--LVAACEFRSAGKAVRCDVTEQVRA-------ACESPFAEIAERIGAVLCVVPPED
    MSR-1 MamK   ARG--EAATFEFRAAGKPVRCDVTESVKI-------ACEALMPDIIESIEILLRSFQPEY
    AMB-1 MamK   TPT--EVASFEFRAAGKPVRADVTEPVKI-------ACEALMPDIIESIETLLRSFQPEY
       Tm MreB   PSK--ENDELETTVSGIDLSTGLPRKLTLKGGEVREALRSVVVAIVESVRTTLEKTPPEL
       Ec MreB   PGD--EVREIEVR--GRNLAEGVPRGFTLNSNEILEALQEPLTGIVSAVMVALEQCPPEL
    AMB-1 MreB   PPEDGEGRTMEIK--GRDLMNGVPKELIISERQIAESLAEPVGAIIEAVKVALEHTAPEL

                                  Adenosine              Connect 2
AMB-1 MamK-like  QALVL-KNIVITGAGAQIRGLPEYVKSMLAPYGDARVSIANEPLMEACKGALSMAQEIPP
    MSR-1 MamK   QATVL-QNIVFAGGGSRIRGLAAYVKDKLRPFGNADVTCVKDPTFDGCRGALRLAEELPP
    AMB-1 MamK   QATVL-QNIVFAGGGSRIRGLAAYVKEKLRPFGNANVTCVKDPTFDGCRGALRLAEELPP
       Tm MreB   VSDIIERGIFLTGGGSLLRGLDTLLQKETG----ISVIRSEEPLTAVAKGA-GMVLDKVN
       Ec MreB   ASDISERGMVLTGGGALLRNLDRLLMEETG----IPVVVAEDPLTCVARGG-GKALEMID
    AMB-1 MreB   AADIVDKGIVLTGGGALLSNLDYVLRHATG----LPVSIADDPLSCVALGT-GRALEEMP

AMB-1 MamK-like  HFWGQL------
    MSR-1 MamK   QYWCQLGDVSGQ
    AMB-1 MamK   QYWRQLGDVSGS
       Tm MreB   ILKKLQGAG---
       Ec MreB   MHGGDLFSEE--
    AMB-1 MreB   KLKNVLTSMY--
```

Figure 4. Alignment of MamK-like, MamK and MreB proteins. Highly conserved ATPase residues are boxed. MamK-like's A141 residue is marked red. Based on Löwe *et al.* 2001, monomer-monomer interaction residues within the MreB protofilament are marked pink (*76*). Conserved residues between MamK and MamK-like in these regions are marked green. Conserved residues between MreB proteins in these regions are marked blue. Alignment was generated with MUSCLE. (AMB-1: *Magnetospirillum magneticum* AMB-1, MSR-1: *Magnetospirillum gryphiswaldense* MSR-1, Tm: *Thermotoga maritima*, Ec: *Escherichia coli*)

Figure 5. Transcription of *mamK-like* occurs in AMB-1. qRT-PCR expression analysis of wild-type, Δ*mamK*, Δ*mamK-like*, and Δ*mamK*Δ*mamK-like* strains in late exponential growth. The levels of *mamK* and *mamK-like* transcription were calculated relative to the housekeeping gene *rpoD*. (Results are shown as mean ± SD)
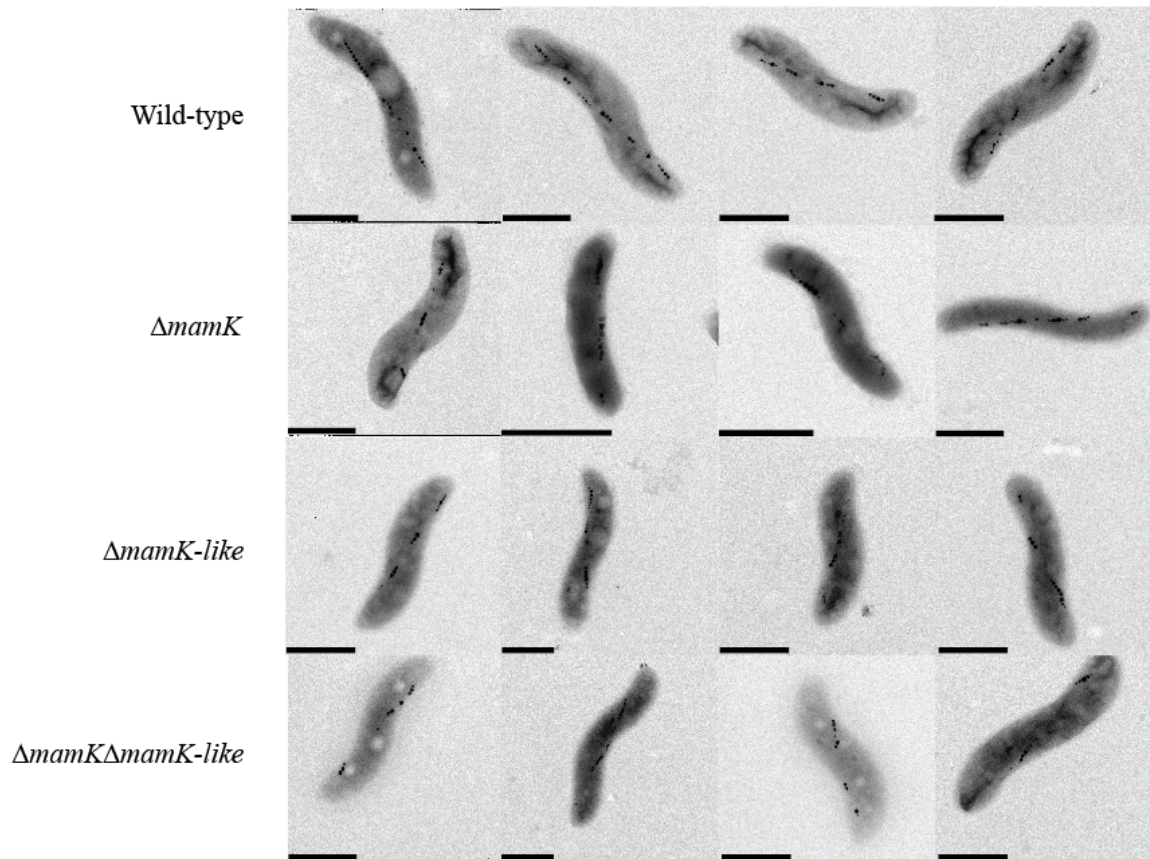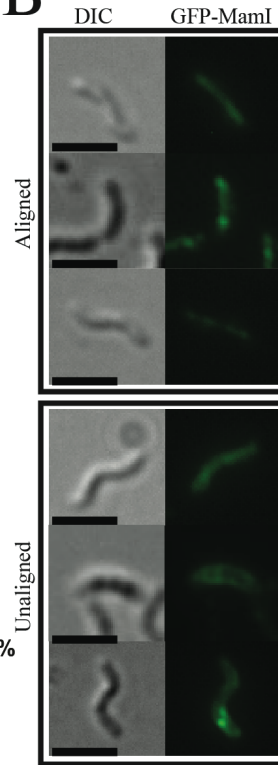
Figure 6. Transmission Electron Microscope images of wild-type, Δ*mamK*, Δ*mamK-like*, Δ*mamK*Δ*mamK-like* cells. Cell morphologies appeared similar in all four strains imaged. Due to the inability to visualize empty magnetosome membranes, this technique does not enable accurate assessments of chain alignment. (Scale bar for each image = 1 μm)
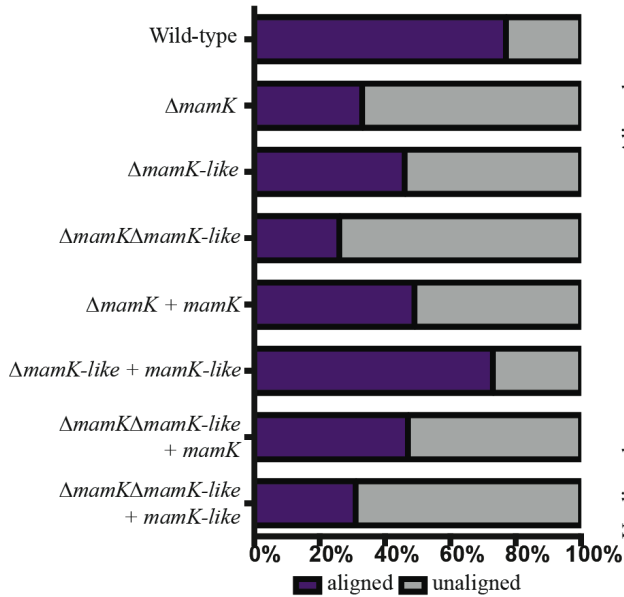
Figure 7. GFP-MamI localization patterns indicate magnetosome alignment. A) GFP-MamI alone in wild-type (n=1870), Δ*mamK* (n=1161), Δ*mamK-like* (n=1276), and Δ*mamK*Δ*mamK-like* (n=807) cells. Complementation experiments: GFP-MamI and MamK in Δ*mamK* (n=685) and Δ*mamK*Δ*mamK-like* (n=759) cells. GFP-MamI and MamK-like in Δ*mamK-like* (n=1063) and Δ*mamK*Δ*mamK-like* (n=964) cells B) Representative images of aligned localization patterns (linear and linear with puncta) and unaligned localization patterns (diffuse, membrane and unaligned puncta) are shown. (Scale bar = 2 μm)

Bait	Prey		Cell Number	Cell Number
Empty	Empty	-		
Empty	MamK-like	-		
MamK-like	Empty	-		
MamK	Empty	-		
Empty	MamK	-		
MamK	MamK	+		
MamK-like	MamK-like	+		
MamK	MamK-like	+		
MamK-like	MamK	+		
MreB	Empty	-		
Empty	MreB	-		
MreB	MreB	+		
MamK	MreB	-		
MreB	MamK	-		
MamK-like	MreB	-		
MreB	MamK-like	-		

- Tryptophan
- Leucine

- Tryptophan
- Leucine
- Uracil

Figure 8. Yeast two-hybrid assays demonstrate interaction between bacterial actin proteins. Bait and prey fusions to MamK, MamK-like, and MreB from AMB-1. Interactions are observed and noted with plus (+) signs, non-interacting protein pairs are noted with minus (-) signs.
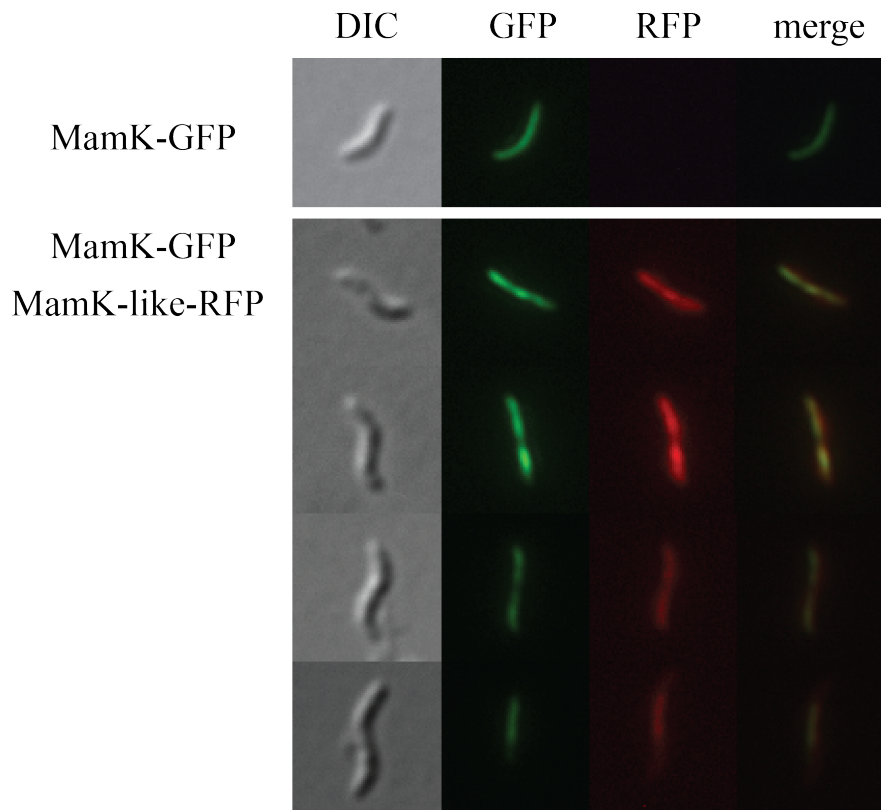
Figure 9. Co-localization of MamK-GFP and MamK-like-RFP in wild-type AMB-1 cells. Top panel shows MamK-GFP only expressing cells for comparison.
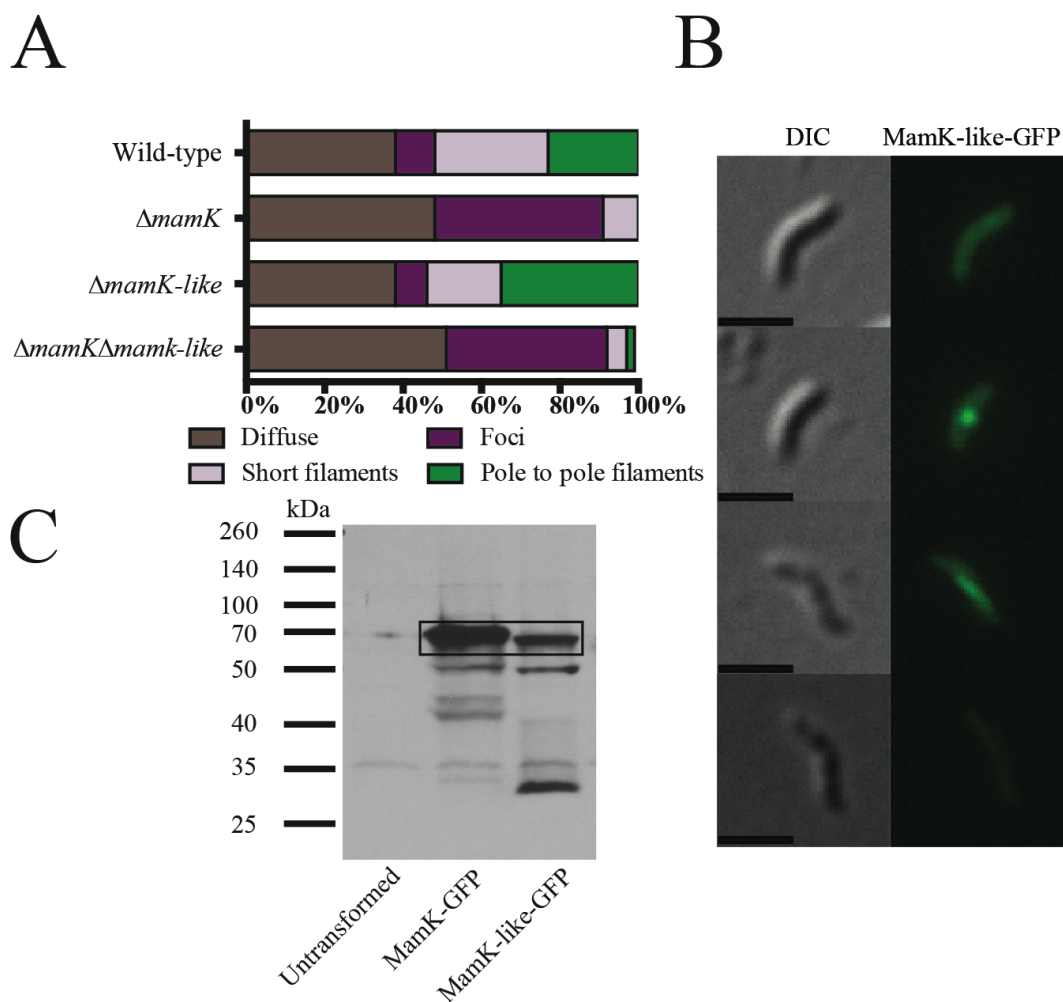
Figure 10. Filament assessment through fluorescent protein fusions. A) Distribution of MamK-like-GFP localization patterns in AMB-1 cells (Wild-type n=345, Δ*mamK* n=540, Δ*mamK-like* n=441, Δ*mamK*Δ*mamK-like* n=426). B) Representative images of MamK-like-GFP localization patterns AMB-1 cells with diffuse, foci, short filaments, and full-length filaments shown. (Scale bar = 2 μm) C) Western blot using anti-GFP antibody detects GFP fusions to MamK (column 2) and MamK-like (column 3) (box indicates full length), and reveal significant levels of unfused GFP in the MamK-like-GFP expressing cells (column 3).
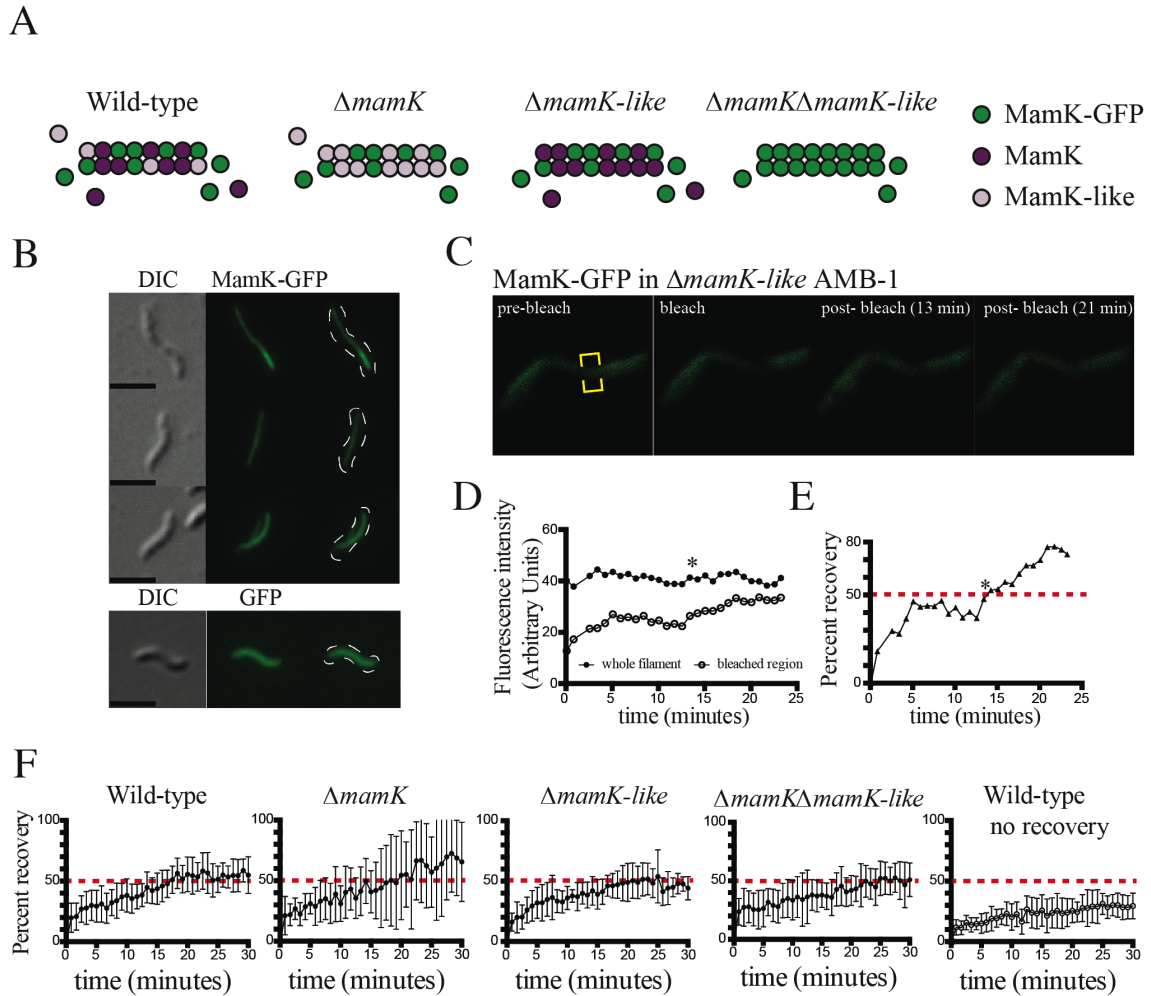
Figure 11. Analysis of MamK-GFP dynamics by Fluorescence Recovery After Photobleaching (FRAP). A) Schematics representing the types of MamK proteins present in FRAP experiments (Green circles: MamK-GFP, dark purple circles: endogenous MamK, light purple circles: endogenous MamK-like). B) DIC and fluorescence images of wild-type AMB-1 cells illustrate MamK-GFP filaments. A cell is shown with cytoplasmic GFP for comparison (bottom panel). (Scale bar = 2 μm) C) A FRAP experiment time course (images are from MamK-GFP in the Δ*mamK-like* background). This is a 9X zoom of a confocal image, hence the blurred appearance of the filament. D) Fluorescence intensity of whole filament (filled circles) and bleached region (open circles) of the run shown in C. ($T_{1/2}$ is noted by the asterisk @ 13 minutes.) E) Percent recovery for the same run. F) Normalized (average ± SD) percent recovery of each strain's recovering cells. The 50 percent mark is noted with a dashed red line. Non-recovery cells (in wild-type background) are shown for comparison in the last panel.

A

B

MamK-GFP in Wild-type AMB-1

pre-bleach   bleach   post- bleach (14 min) post- bleach (26 min)

C

MamK-GFP in ΔmamK

pre-bleach   bleach   post- bleach (13 min) post- bleach (30 min)
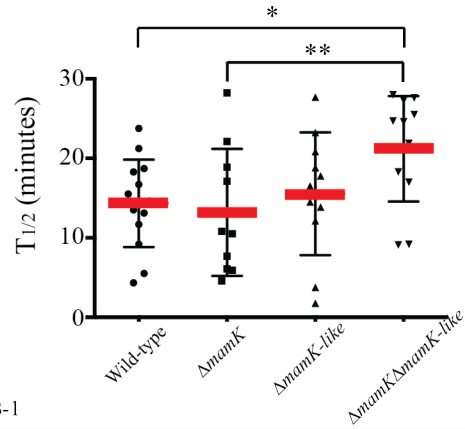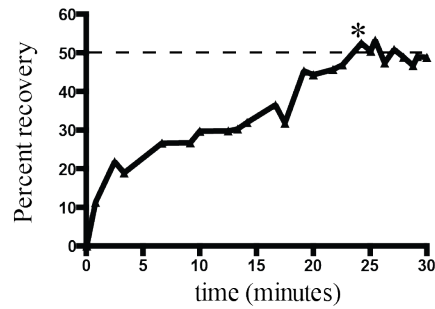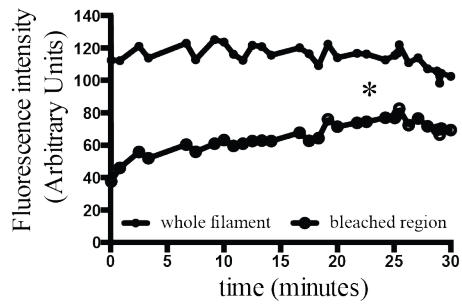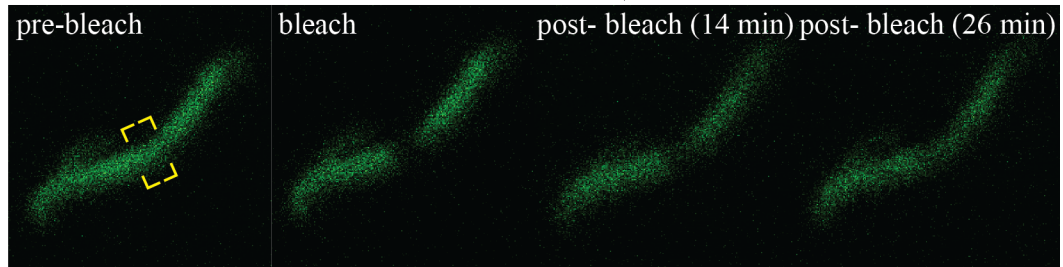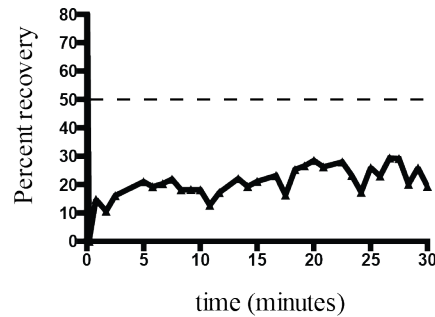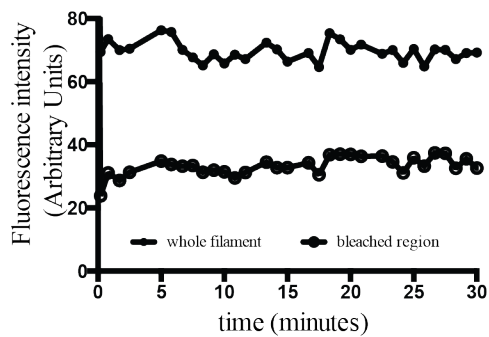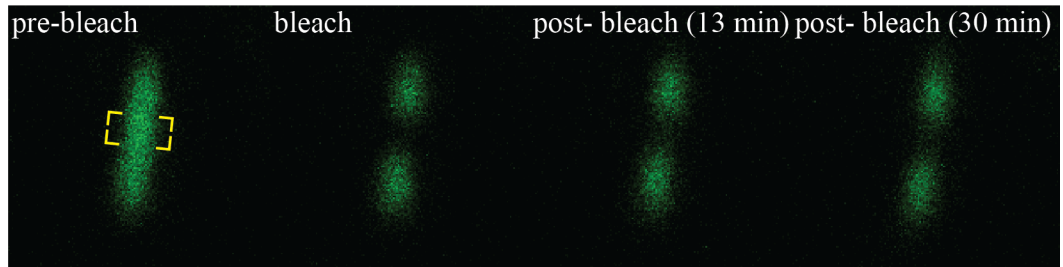
Figure 12. Representative FRAP images and $T_{1/2}$ analysis. A) Dot plots illustrating the $T_{1/2}$ of each individual cell experiencing recovery. Data is shown as average (red lines) ± SD. Significantly different comparisons between wild-type and Δ*mamK*Δ*mamK-like* strains (*); Δ*mamK and* Δ*mamK*Δ*mamK-like* strains (**) are noted. A two-tailed T-test was used to determine p values and considered all data points of recovering cells. B) In the wild-type background, approximately 50% of cells experience recovery. This is a representative run of a cell with a slower than average $T_{1/2}$: 23 minutes (asterisk) (MamK-GFP in wild-type AMB-1). The fluorescence intensity units over time and normalized percent recovery graphs are also shown. C) In the Δ*mamK* background, approximately 23% of cells experience recovery. This is a representative run that shows a cell lacking recovery in a 30-minute timeframe (MamK-GFP in Δ*mamK* AMB-1). The fluorescence intensity units over time and normalized percent recovery graphs are also shown.
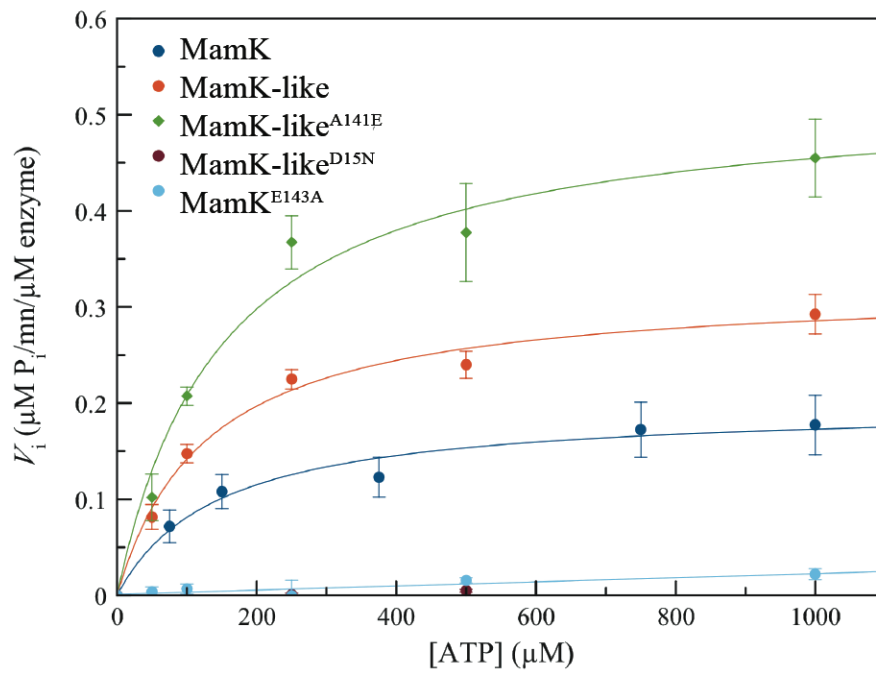
Figure 13. Phosphate release assays indicate an ATPase activity for MamK-like. MamK (dark blue), MamK-like (red), MamK-like^{A141E} (green), MamK-like^{D15N} (brown), and MamK^{E143A} (light blue) were assayed for phosphate release.
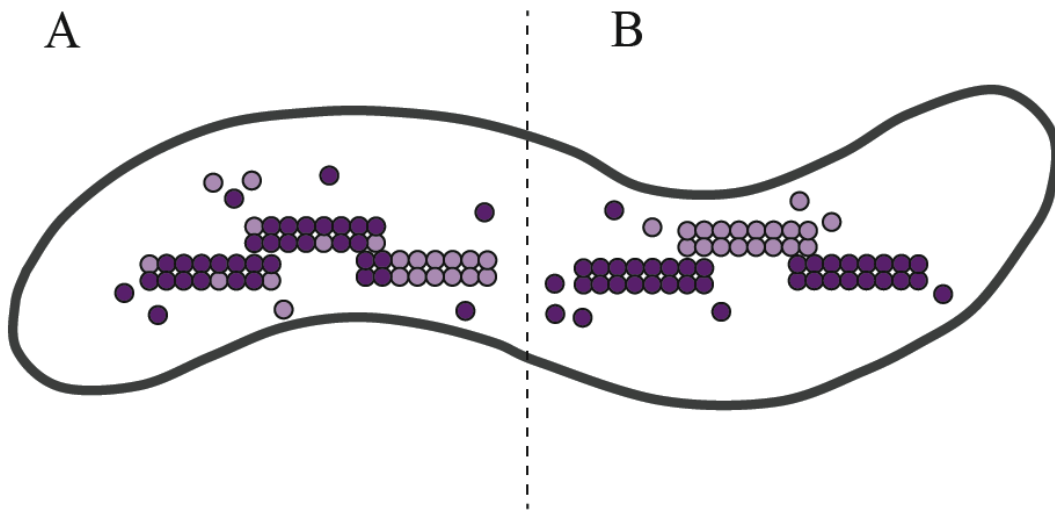
Figure 14. Possible modes for MamK/MamK-like interaction. A) Interchangeable monomers of MamK (dark purple circles) and MamK-like (light purple circles) are incorporated into a copolymer filament. Additionally, MamK may serve as a nucleating protein for MamK-like. B) MamK filaments serve as nucleating sites for MamK-like filaments to form via lateral association.

Table 1. Optical density (OD$_{400}$) and Coefficient of magnetism (C$_{mag}$) measurements

Strain	OD$_{400}$	C$_{mag}$
Wild-type	0.25 ± 0.03	1.88 ± 0.06
$\Delta mamK$	0.23 ± 0.03	1.86 ± 0.02
$\Delta mamK$-like	0.22 ± 0.01	1.85 ± 0.05
$\Delta mamK \Delta mamK$-like	0.24 ± 0.03	1.79 ± 0.12

Note: results are shown as average ± S.D at 48 hour time point.

Table 2. Plasmids

Plasmid name	Product(s)	Parental Plasmid	Source
pAK22	MamK-GFP		Komeili, 2006
pAK100	Y2H Bait (Empty)		Durfee, 1999
pAK102	Y2H Bait (Empty)		Durfee, 1999
pAK103	Y2H Prey (Empty)		Durfee, 1999
pAK105	Y2H Prey (Empty)		Durfee, 1999
pAK140	Y2H Bait-MamK	pAK102	this work
pAK141	Y2H Prey-MamK	pAK105	this work
pAK483	Y2H Prey-MamK-like	pAK103	this work
pAK485	Y2H Bait-MamK-like	pAK100	this work
pAK479	Y2H Bait-MreB	pAK100	this work
pAK489	Y2H Prey-MreB	pAK103	this work
pAK576	deletion vector (Δ*mamK-like*)	pAK31	this work
pAK699	MamK-like-GFP	pAK22	this work
pAK266	GFP-MamI	pAK22	Murat, 2010
pAK742	MamK	pAK22	this work
pAK726	MamK, GFP-MamI	pAK742	this work
pAK706	MamK-like, GFP-MamI	pAK726	this work
pAK705	MamK-GFP, MamK-like-RFP	pAK22	this work
	pET-SUMO-*mamK*		this work
	pET-SUMO-*mamK-like*		this work
	pET-SUMO-*mamK*^{E143A}	pET-SUMO-*mamK*	this work
	pET-SUMO-*mamK*^{D17N}	pET-SUMO-*mamK*	this work
	pET-SUMO-*mamK-like*^{A141E}	pET-SUMO-*mamK-like*	this work
	pET-SUMO-*mamK-like*^{D15N}	pET-SUMO-*mamK-like*	this work

Table 3. Primers

Primer name	Sequence	Purpose
NA01-*mamK-like*-US-F	ggggggACTAGTtttatctcccgagatccgttg	Δ*mamK-like*
NA02-*mamK-like*-US-R	<u>cccatccactaaatttaaatattggttatcgttcacaatcat</u>	Δ*mamK-like*
NA03-*mamK-like*-DS-F	<u>tatttaaatttagtggatgggcactttgggggcagctttag</u>	Δ*mamK-like*
NA04-*mamK-like*-DSR	ggggggACTAGTgagtttgtcagccctgaagc	Δ*mamK-like*
NA33-MfeI-*mamK-like*-F	acacacaCAATTGatgattgtgaacgataaccaa	MamK-like-GFP/comp
NA19-BamHI-*mamK-like*-R	tgtgtgtGGATCCaagctgcccccaaaagtg	MamK-like-GFP
NA79-EcoRI-*mamK*-F	acacacaGAATTCatgagtgaaggt	MamK comp
NA56-SpeI-*mamK*-R	tgtgtACTAGTtcacgagccg	MamK comp
NA35-SpeI-*mamK-like*-R	acacacaACTAGTctaaagctgcccccaaaagtg	MamK-like comp
NA80-Spe-rbs-*GFP*-F	acacacaACTAGTggaggtgacggatgagtaaag	GFP-MamI in comp
NA81-SacI-*mamI*-R	acacacaGAGCTCtcaaccatcgat	GFP-MamI in comp
NA43-NheI-RFP-F	acacacaGCTAGCatggcctcctccgaggacgtc	dual color
NA44-NheI-mamK-like-R	acacacaGCTAGCaagctgcccccaaaagtgagg	dual color
NA45-XbaI-RFP-R	acacacaTCTAGActaggcgccggtggagtggcg	dual color
NA50-SpeI-rbs-mamK-like-F	acacacaACTAGTggggacagcatgattgtgaac	dual color
mamK-Ndel-F	acacacaCATATGatgagtgaaggtgaaggccag	Y2H Bait/Prey
mamK-BamHI-R	tgtgtgtGGATCCcgagccggagacgtctccaag	Y2H Bait/Prey
mamK-like-NdeI-F	acacacaCATATGattgtgaacgataaccaaaac	Y2H Bait/Prey
mamK-like-BamHI-R	tgtgtgtGGATCCtaaagctgcccccaaaag	Y2H Bait/Prey
mreB-NdeI-F	acacacaCATATGttttctaagctgacgggttgg	Y2H Bait/Prey
mreB-BamHI-R	tgtgtgtGGATCCtagtacatgctggtcagcacg	Y2H Bait/Prey
mamK-F	ggctcaggaggtggtggttcata	*mamK* qRT-PCR
mamK-R	gagccgctcatccacatagt	*mamK* qRT-PCR
mamK-like-F	gctgtgttgtgtgtggttcc	*mamK-like* qRT-PCR
mamK-like-R	tgcacctttacatgcttcca	*mamK-like* qRT-PCR
rpoD-F	atggcatccacctcaacaac	*rpoD* qRT-PCR
rpoD-R	cgtaataggcgtcgaggaag	*rpoD* qRT-PCR
mamK-SUMO-F	atgagtgaaggtgaaggcca	protein expression
mamK-SUMO-R	tcacgagccggagacgtct	protein expression
mamK-like-SUMO-F	atgattgtgaacgataaccaaaac	protein expression
mamK-like-SUMO-R	ctaaagctgcccccaaaag	protein expression
mamK^{E143A}-F	ctagtggtgtccgcaccgttcatggtc	mutagenesis
mamK^{E143A}-R	gaccatgaacggtgcggacaccactag	mutagenesis
mamK^{D17N}-F	gttccttggcatcaaccttgggacttcc	mutagenesis
mamK^{D17N}-R	ggaagtcccaaggttgatgccaaggaac	mutagenesis
mamK-like^{A141E}-F	gaatgtgcttttaatgtcagaaccttttttggctggaaatagc	mutagenesis
mamK-like^{A141E}-R	gctatttccagccaaaaaaggttctgacattaaaagcacattc	mutagenesis
mamK-like^{D15N}-F	ctctatgtcggtatcaattttggttactcaaagactg	mutagenesis
mamK-like^{D15N}-R	agtctttgagtaaccaaaattgataccgacatagag	mutagenesis

Key: comp: complementation, Y2H: Yeast two-hybrid, UPPERCASE letters: restriction sites, underlined: linker

Table 4. qRT-PCR standard curves

	T = 24h			T = 41h		
	rpoD	*mamK*	*mamK-like*	*rpoD*	*mamK*	*mamK-like*
Error	0.0175	0.0871	0.0124	0.0304	0.0418	0.0331
PCR efficiency	1.937	1.971	1.992	1.940	1.920	1.850

Table 5. MamK-GFP localization patterns

| MamK-GFP | Genetic Background | | | |
	Wild-type	Δ*mamK*	Δ*mamK-like*	Δ*mamK*Δ*mamK-like*
Percent foci	0.4 ± 0.6	19.2 ± 14.6	0.0 ± 0.0	10.6 ± 5.9
Percent filament				
short	3.7 ± 3.8	61.4 ± 22.3	4.3 ± 0.5	58.3 ± 12.5
full length	95.9 ± 4.5	19.5 ± 7.7	95.8 ± 0.5	31.1 ± 10.1
Number of cells analyzed	595	470	491	387

CHAPTER 3

The investigation of MamK dynamics by Fluorescence Recovery After Photobleaching in *Magnetospirillum magneticum* AMB-1 (unpublished data)

INTRODUCTION

Not long ago, scientific dogma described bacteria as simplified cells lacking cytoskeletal organization and or structure. In recent years, the discovery of previously defined eukaryotic characteristics of cytoskeletal components (bacterial homologs of eukaryotic actin, tubulin, and intermediate filaments) and organelles in bacteria has shifted the paradigm.(*55, 81-84*) As a result, the field of bacterial cell biology has emerged and expanded with numerous bacterial systems serving as model organisms. Bacterial actins are very widespread in bacteria and have differing cellular functions, which is reflected in their great sequence diversity. This is in stark contrast to eukaryotic actin, which is highly conserved over evolutionary time (Figure 15). Studies on bacterial actins to date have focused primarily on the ParM and MreB families, where ParM proteins serve to properly partition plasmids and MreB maintains cell shape in many bacteria. A combination of *in vivo* and *in vitro* approaches were crucial to determine the mechanisms of action in these two classes of proteins.

An example of how *in vivo* and *in vitro* approaches have elucidated mechanistic details is evident in the plasmid partitioning systems in bacteria. DNA segregation by bacterial cytoskeletal proteins was first identified in the late 1980's and early 1990's. Plasmid encoded *par* loci in bacteria are widespread and are generally comprised of three elements: 1) an ATPase/GTPase to provide the energy to push or pull DNA, 2) an adaptor protein, and 3) a centromere-like section of DNA on the plasmid where adaptor and NTPase bind. Three classes of NTPases are utilized in different partitioning systems: Walker A type ATPases (i.e. ParA), tubulins (i.e. TubZ), and bacterial actins (i.e. ParM, AlfA) (*85*). Work on ParM began in *E. coli*, where the R1 plasmid was determined to require the ParMR/*parC* complex for proper segregation (*86*). Also, ATPase activity of ParM is required for plasmid segregation (*85, 87*). In addition to filament growth, ParM filaments also exhibit dynamic instability. Studies determined that upon binding to the ParR/*parC* complex, ParM becomes stable and bidirectionally polymerizes to properly segregate plasmids (*55-57, 88, 89*). The bi-phasic mode of ParM behavior lends to its function; the dynamic instability enables filaments to quickly disassemble when a plasmid partner is not found, and binding of plasmid pairs is the signal needed for filament stability and extensive polymerization. This molecular mechanism is not entirely conserved amongst all plasmid-segregating systems, as is evident in AlfA-based plasmid partitioning. In this system, AlfA filaments elongate in a unidirectional manner and are not dynamically unstable (*90*). Antiparallel filament bundles interact and associate into "comet tails" to segregate DNA (*90*). These two examples, ParM and AlfA, highlight the diversity in mechanism present to perform a similar function.

Differences in mechanisms to perform similar functions are not only a characteristic of plasmid segregation systems, as the MreB family of bacterial actins display diverse behaviors as well. Responsible for maintaining cell shape in many bacteria, *mreB* was identified by isolating strains of K-12 *E. coli* that had altered cell morphologies (*91-93*). Interestingly, these initial findings were contradictory to later work that showed that

mreB is an essential gene; depletions of *mreB* led to spherical cells that eventually lysed (*51*). It was later determined that mutants in *mreB* could be viable upon increased expression of FtsZ to compensate for division in cells with an increased surface to volume ratio (*94*), most likely accounting for the original identification of mutants. Additionally, contradictions have occurred over the localization of MreB in cells. Initial research indicated that MreB formed helical filaments, though recent research has concluded that perpendicular circular patterns around the long axis of the cell are more representative (*52, 53*) and helical patterns could be an artifact of fluorescent protein tagging (*95*). Importantly, the dynamic movement of MreB (as well as related Mbl and MreBH proteins) was paired with cell wall machinery as disruptions of component proteins (ex: RodA, RodZ, PBP2A) resulted in static MreB (*52, 53*). *In vitro*, isolated MreB has been reported to form left-handed twisted bundles (*96*), though initial studies of the crystal structure note straight protofilaments (*76*). These reports highlight complexity in filament structure, which can be interpreted as technical variations between groups, but could also implicate the level of diversity in form and behavior even amongst bacterial actins of the same family.

Though ParM and MreB are by far the most characterized, the bacterial actin family tree is much broader, containing more than 35 subgroups (*49*). Our lab and others are working to characterize MamK, a bacterial actin that is distinct from these two families (Figure 15). Previous research determined that MamK affects organization of magnetosomes in *Magnetospirillum magneticum* AMB-1 (AMB-1). Deletion of *mamK* in AMB-1 results in significant disorganization of magnetosome chains (*33*). Also, deletion of *mamK* in a related organism, *Magnetospirillum gryphiswaldense* MSR-1 (MSR-1), results in ectopic and shorter magnetosome chains, and failure of evenly partitioning the chain between dividing daughter cells (*39*).

Due to the phenotype of *mamK* loss, many questions must be answered to understand how the protein aligns the magnetosome chain. What is MamK's intrinsic behavior in isolation? Are there genetic requirements that help facilitate MamK's behavior? To address such questions, previous studies have started to describe the behavior of MamK both *in vitro* and *in vivo*. MamK from MSR-1 was found to have both ATPase and GTPase activity. Additionally, MSR-1 MamK assembled into filaments *in vitro*, as assessed by right angle light scattering (*38*). The ability to scatter light requires the protein to polymerize, which relies on the critical concentration. The critical concentration, or the threshold concentration that supports monomers to associate into filaments, was reported to be 1.4 μM for MSR-1 MamK. These results are similar to work done in AMB-1. Work by Ertan Ozyamak in the Komeili lab demonstrated that MamK is dynamic (also by right angle light scattering) *in vitro*. This behavior requires ATP, though GTP also facilitated polymerization to a lesser extent. Additionally, an intact ATPase site was required for ATPase activity, as MamK proteins with disrupted active sites (E143A) result in filaments that are unable to depolymerize (*37*). Extrinsic conditions such as salt concentration affected MamK's behavior. Potassium levels that more closely mimicked cellular concentrations (>25 μM) resulted in MamK filaments that bundled together, a feature that was not noticeable in the lower concentrations tested. Finally, the critical concentration was reported as ~0.8 μM. Taken together, these

seminal papers demonstrated that MamK is an ATPase that associates into filaments, and depending on buffer conditions, such as nucleotide and potassium concentration, the behavior of the protein can be altered. This behavior modification raises questions as to how the protein behaves *in vivo*.

To assess the *in vivo* behavior of MamK, work by Dr. Olga Draper and Dr. Meghan Byrne of the Komeili lab determined that MamK-GFP is a dynamic protein whose turnover can be recorded by performing Fluorescence Recovery After Photobleaching (FRAP) experiments. In these experiments, two variables are recorded: 1) the percentage of cells that have filaments that experience recovery and 2) the $T_{1/2}$, or time at which 50 percent of the fluorescence returns in the bleached region of interest compared to the whole filament at that same time point. Draper and Byrne determined that wild-type AMB-1 cells expressing MamK-GFP normally experience recovery approximately 50 percent of the time and have a $T_{1/2}$ of 11 ± 6 minutes (Figure 16). MamK-E143A-GFP did not recover by FRAP, indicating the need for ATP hydrolysis for turnover (*36*).

Interestingly, Draper also found that components from the magnetosome island (MAI, Figure 16) were required for MamK-GFP turnover. To find the genetic requirements for MamK-GFP turnover, experiments were initiated in various genetic backgrounds. Research from the Schüler lab postulated that MamJ, a protein from the R5/*mamAB* region of the MAI, could be the protein that connects magnetosomes to MamK (*60, 97*). To investigate whether this was a component that impacted MamK-GFP turnover, FRAP experiments were performed in Δ*mamJ*, Δ*limJ*, and Δ*mamJ*Δ*limJ* double deletion strains. It was determined that each single deletion still resulted in turnover, however, the double deletion of Δ*mamJ*Δ*limJ* resulted in static MamK-GFP filaments (Figure 16) (*36*). Additionally, strains in which the entire *mamAB* region was deleted, or in which the *mamAB* region was the only remaining component of the MAI, turnover still occurred (work by Onur Erbilgin, unpublished). These results could entirely be explained by the requirement of *mamJ* or *limJ*, as complementation experiments with the Δ*mamJ*Δ*limJ* strain was possible with either gene. However, though *mamJ* or *limJ* were necessary for MamK-GFP filament dynamics in FRAP, they were not sufficient. This was shown in an experiment where magnetosome island deletions (ΔMAI) AMB-1 cells expressing MamK-GFP and either MamJ or LimJ did not result in FRAP recovery (Figure 16) (*36*). These finding raised the question as to whether another factor encoded in the *mamAB* region, with redundancy both inside outside of *mamAB*, could also be responsible for MamK-GFP recovery.

To identify whether other turnover requirements exist, two genetic approaches were performed. One approach analyzed double deletions of *mamAB* redundant genes by FRAP. Due to the existence of several redundant gene pairs within the MAI, multiple candidates fit this description (Figure 17A). As an alternative approach, a strain containing only the *mamAB* region of the MAI was further reduced to find a minimal gene set for MamK-GFP turnover (Figure 17B).

It was also important to determine whether intrinsic properties of MamK could impact the FRAP capabilities *in vivo*. Previous work in the lab found that point mutations in

MamK affected FRAP recovery rates (Komeili lab, unpublished data). A particularly interesting mutant variant of MamK (MamK-R85A/D86A) was previously shown to recover much faster than MamK-GFP *in vivo* (Komeili lab, unpublished work). Because of known genetic requirements for MamK-GFP turnover, it was worth testing whether this faster recovering variant also required these necessary components for turnover. To test this hypothesis, MamK-R85A/D86A-GFP was analyzed in the Δ*mamJ*Δ*limJ* background. Results demonstrated no need for these genes in recovery, implicating recovery rate as an ability to bypass genetic requirements. Additionally, as the location of a GFP fusion could impact the behavior of a protein (*95*), additional efforts were employed to study MamK by FRAP. An N-terminal GFP tag was also analyzed, and results indicated that GFP-MamK turns over at a much faster rate than MamK-GFP. Combined with the MamK-GFP results, tagging location of the fluorescent fusions used can impact the behavior of the protein more than originally appreciated.

MATERIALS & METHODS

Cell cultures.
AMB-1 cells were grown in 1.5 ml microcentrifuge tubes with MG liquid media supplemented with Fe Malate (100X: 3 mM, Fe 9 mM Malate), 1X vitamins (100X: Biotin 2 mg/L, Folic acid 2 mg/L, Pyridoxine hydrochloride 10 mg/L, Vitamin B1 hydrochloride 5 mg/L, (-)-Riboflavin 5 mg/L, Nicotinic acid 5 mg/L, Calcium pantothenate 5 mg/L, Vitamin B12 0.1 mg/L, 4-Aminobenzoic acid 5 mg/L, and (±)-α-Lipoic acid 5 mg/L), and Kanamycin [10 ug/ml] (referred to as MG Kan), for 4-5 days at 30° C before inoculating into 10 ml cultures (with MG Kan). The 10 ml cultures were grown overnight in the 10% O_2 incubator at 30° C. The following morning, 1.5 ml of overnight cultures were pelleted (14,000 rpm for 1.5 min on bench-top microcentrifuge) in microcentrifuge tubes before application to slides for FRAP.

Slide preparation.
Agarose pads and slides were prepared by melting agarose in MG media (1% w/v) without Fe Malate or vitamins by microwaving at full power for 1-2 minutes. After the solution was briefly cooled (1-2 minutes), Fe Malate and vitamins were added to concentrations noted above. After brief but vigorous (to incorporate bubbles which help to locate cells in microscopy) swirling, 100 μl of MG/agarose solution was spotted onto a microscope slide and sandwiched between two cover slips and an additional microscope slide. Between 5-10 minutes, slides were peeled apart and pelleted culture (resuspended in 2-4 μl of residual MG Kan) was added onto the pad. A cover slip was then placed on top and vasoline/lanolin/paraffin (VALAP) solution was applied around the edges to seal the slide and protect it from desiccation.

Note: Midway though the experimentation process, addition of pelleted cultures onto agarose pads and subsequent preparation was carried out in ambient air, as opposed to in the 10% O_2 chamber, after experimentation showed no difference in frequency of recovery or $T_{1/2}$ of MamK-GFP in wild-type AMB-1 cells between the two methods.

Fluorescence Recovery After Photobleaching (FRAP) Microscopy.
FRAP experiments were carried out on a Zeiss 710 UV/Vis laser scanning confocal microscope in the Bioimaging Facility. MamK-GFP filaments were imaged using 488 nm excitation wavelength at 0.5-3.0 % laser power. The filaments were bleached using 488 nm laser light at 100 % laser power for 7-10 iterations. Images were captured every 50 seconds for up to 30 minutes through the 100 X oil objective with the LSM710 Imaging Software 3.2 (Zeiss). Due to the lack of an auto-focus feature, each frame was monitored and manual focusing was performed if necessary.

Fluorescence Recovery After Photobleaching (FRAP) Data Analysis.
Images were analyzed using Fiji (*70*). For each FRAP run, regions of interest (ROIs) were drawn in three areas: 1) background 2) whole filament and 3) bleached segment. Each whole filament and bleached ROIs had the background intensity value (arbitrary units) from that time point subtracted. Images that had a steep decrease in fluorescence intensity (generally due to loss of focus rather than photobleaching) were dropped from

51

downstream analysis. To generate the percent recovery graphs, runs were normalized by calculating the ratio of bleached ROI intensity over the whole filament ROI intensity for each timepoint. The run was considered recovered under the following criteria: 1) fluorescence intensity of the bleach region returned to 50 percent of the whole filament at the same time point and 2) whole filament fluorescence intensity values did not dip drastically due to photobleaching. For $T_{1/2}$ comparisons: a comparison between genetic backgrounds was analyzed by a two-tailed T-test analysis to determine statistically significant ($p \leq 0.05$) differences in $T_{1/2}$. This analysis takes into account only the cells that resulted in recovery. See Appendix 1 for detailed protocol/instructions.

RESULTS

MamK-GFP turnover is similar between two different microscope setups.
Upon initiation of the FRAP experiments, it was noted that previous work had been performed on a different microscope (Zeiss 510) than an upgraded system that was less prone to overall photobleaching (Zeiss 710). In lieu of this, necessary work needed to be done to verify whether different microscope setups could affect the results observed. Initial experiments on the new microscope were challenging due to the loss of focal plane when 2 minutes image intervals were taken (2 minute time points were first used because of previously established methodology). To optimize conditions on the new microscope, images were taken at shorter time intervals (every 50 seconds) to allow for more accurate focusing between images. Taking pictures more often did not increase overall photobleaching, an issue that impacted previous capability to take additional time points. After making this adjustment, recovery frequencies in genetic backgrounds were similar to previously published work. Compared to 47 percent of cells recovering (*36*), 50 percent of cells in the wild-type background experienced recovery. The $T_{1/2}$ measurements between the two groups slightly differed; previous work had an average $T_{1/2}$ of 11 ± 6 minutes (*36*), where the current setup found a $T_{1/2}$ of 14 ± 6 minutes (Table 6). This longer $T_{1/2}$ could be accounted for the difference in microscopes used, as the Zeiss 710 is less prone to photobleaching over the course of a FRAP run and can take images over a longer period of time. Similar results were recapitulated in previous work in the Δ*mamJ*Δ*limJ* background, as no cells experienced recovery of MamK-GFP on the Zeiss 710 (Table 6). Overall, these results indicated that slight variability is present depending on the microscope used, however, the increased capability to image without overall photobleaching did not result in drastic differences between strains tested in previous experiments. Because of these reasons, the Zeiss 710 was determined to be the preferred microscope to conduct FRAP experiments.

The Δ*mamH*ΔR12 double deletion has a different phenotype depending on culture condition used.
Because of previous results implicating an additional *mamAB* redundant gene in MamK-GFP FRAP recovery, we sought to complete the creation of double deletions of all potential candidates. The remaining candidate was *mamH*, a protein annotated as a major facilitator superfamily of transporters. This gene has redundancy in R12 of the MAI (Figure 17A). Initial characterizations of the single deletion of *mamH* was classified as indistinguishable from wild-type cells (*29*). However, creation of the double deletion Δ*mamH*ΔR12 resulted in a different phenotype compared to wild-type. Upon measuring C_{mag} for level of cell magnetism, it was also noted that Δ*mamH*ΔR12 cells had reduced magnetism compared to wild-type cells (Figure 18A). Upon visualization of the cells, it was noted that they had elongated cell phenotypes (Figure 18B, 19A).

The Δ*mamH*ΔR12 double deletion has differing FRAP recovery characteristics depending on culture condition.
The FRAP experiments performed in this background also had interesting results, where MamK-GFP turnover was nearly abolished (Table 7, Figure 19B). Initially excited by these results, complementation experiments were carried out by reintroducing *mamH* on a

plasmid. By the time complementation experiments were taking place, the media conditions in the lab had changed; reverting back to the original MG media as opposed to the HEPES buffered media that was used during the period of initial characterization (MG HEPES, pH7.2). In original MG media (MG, pH 6.9), ∆mamH∆R12 cells appeared more like wild-type cells in their cell morphology (Figure 18B) and their ability to turnover MamK-GFP in FRAP (Table 7, Figure 19D). Due to the complexity of this phenotype, I focused on analyzing other potential regulators of MamK dynamics.

MamK-GFP turnover *in vivo* does not require *mamE*, or *mamQ*.
To characterize other candidates, the ∆mamE∆limE and ∆mamQ∆R9 cells were also analyzed by FRAP. Similar to results from Onur Erbilgin (a previous rotation student in the lab), ∆mamE∆limE mutants were indistinguishable from wild-type in their ability to turnover MamK-GFP by FRAP (40 percent recovery, $T_{1/2}$: 8 ± 4 minutes, Table 7, Figure 20AB). These results were similar to ∆mamQ∆R9 cells that displayed 50 percent recovery and a $T_{1/2}$ of 16 ± 8 minutes (Table 7, Figure 20CD).

The *mamAB* reduction results in turnover of MamK-GFP.
As *mamAB* cells still displayed MamK-GFP recovery (Figure 16), construction of a more minimal mutant generated a strain containing only 6 magnetosome genes total (*mamHIEJKL*, Figure 17B). This strain was then transformed with MamK-GFP and FRAP experiments were carried out. The results demonstrated that recovery could occur in this background (57 percent compared to 50 percent in wild-type, Table 7). The pattern of recovery in these cells was different than the wild-type background. Rather than holding at the 50 percent recovery threshold and or increasing, cells experiencing recovery in the *mamHIEJKL* stain would often dip back below the 50 percent point. The average $T_{1/2}$ was slower than in wild-type cells (17 ± 8 minutes, Table 7, Figure 21AB). Because recovery in the *mamHIEJKL* strain occurred, FRAP on remaining double deletions ∆mamO∆R9, ∆mamR∆R9 and ∆mamB∆R9 were not performed.

A fast recovering mutant, MamK-R85A/D86A, does not require MamJ or LimJ to recover.
Previous results indicated that MamK-GFP might only need *mamJ* or *limJ* in order to recover via FRAP. It is unclear whether this is because of a complete lack in the ability of MamK-GFP to recover, or whether the recovery has slowed down in the ∆mamJ∆limJ background. To test whether recovery rates could affect this genetic requirement, a point mutation that had significantly faster rates of recovery was analyzed in the ∆mamJ∆limJ background. MamK-R85A/D86A-GFP did have faster rates of recovery in the ∆mamJ∆limJ strain, with 80 percent of cells recovering and $T_{1/2}$ of 4 ± 2 minutes (Table 7, Figure 22 AB). This recovery speed could potentially be indicative of rapid depolymerization events, as noted in right angle light scattering experiments with MamK-R85A/D86A (Ozyamak, unpublished work)

N-terminally tagged GFP-MamK has fast turnover and lacks genetic requirements.
To further characterize differences that could impact MamK's ability to turnover, an N terminal fusion to MamK was created and analyzed by microscopy and FRAP. GFP-MamK in cells did appear as filaments (Figure 23A), and upon FRAP analysis, their

recovery was drastically different from MamK-GFP. As opposed to the longer recovery rates, GFP-MamK cells had a higher proportion of recovering cells (100 percent, Table 7) and faster rates of recovery ($T_{1/2}$: 3 ± 3 minutes) in the wild-type AMB-1 background. Additionally, as MamK-GFP cells required components from the MAI to recover, GFP-MamK expressing cells did not need the MAI for recovery. GFP-MamK in the MAI deletion strain experienced recovery (60 percent, Table 7) and faster rates of recovery as well ($T_{1/2} = 4 \pm 2$ minutes, Table 7). (Figure 23B). Additionally, work by Han Teng Wong, a rotation student in the lab, showed that GFP-MamK could recover in *E. coli* cells with similar characteristics as in AMB-1 (data not shown). These results highlight the effect that tagging location plays in altering the behavior of a protein.

DISCUSSION

Microscopy using fluorescently labeled proteins is a powerful tool to study *in vivo* protein behavior. In our lab, we used Fluorescence Recovery After Photobleaching (FRAP) to study dynamics and turnover of MamK filaments. Previous studies in our group had determined a requirement of magnetosome genes *mamJ* and *limJ* in the recovery of MamK (*36*). By doing this in various genetic backgrounds of AMB-1, I aimed to identify additional components required for MamK turnover.

Because potential interacting proteins also contain redundancy inside and outside of the *mamAB* region of the MAI, double deletion strains were analyzed (Figure 17A). In summation, the only double deletion strain of the ones tested that displayed varying FRAP recovery of MamK-GFP was the Δ*mamH*ΔR12 double deletion. Upon further characterization, it was determined that the culture condition affected the cell morphology, resulting in elongated cells. The elongation of cells correlated with a significant decrease in the ability of MamK-GFP to turnover. This was ameliorated by changing the media back to original media conditions, where Δ*mamH*ΔR12 cells became more wild-type in their cell lengths and MamK-GFP turnover frequencies. I speculate that the elongation of Δ*mamH*ΔR12 cells could limit the amount of MamK-GFP in the cytoplasm and account for the decrease in turnover rate. Nonetheless, more research is needed to determine the cause of this phenotypic change, as pleiotropic affects may be taking place under certain culture conditions.

The reduction of the *mamAB* strain to a strain only containing six magnetosome genes (*mamHIEJKL*, Figure 17B) still resulted in MamK-GFP turnover. This is interesting as the only redundant genes in this group are *mamH* and *mamE* (Figure 17A). These results would implicate by process of elimination that *mamH* and/or *mamE* could be the potential additional factor. However, because of results indicating no need for *mamE* in MamK-GFP turnover, this can rule out *mamE* as a necessary factor. On the other hand, *mamH* was found to affect MamK-GFP turnover under the culture conditions tested. Given this, we could conclude that either 1) loss of *mamH* is not as severe as loss of *mamJ* or *limJ* or 2) *mamH* is not involved. Alternatively, if neither *mamE* nor *mamH* are involved in MamK-GFP turnover, this would imply that the *mamHIEJKL* strain is supported in turnover due to the increase of endogenous MamK. Experiments should be conducted where levels of MamK are elevated in the MAI deletion to test whether this is all that is needed for facilitating turnover of MamK-GFP.

Results also suggest that tagging of MamK affects turnover capability. The MamK-GFP fusion turns over at slower rates and less frequently. It can be noted that this rate of turnover is rather slow compared to other bacterial actins studied. In some cases, turnover on the order of seconds for AlfA (*98*) and a few minutes for the MreB-related protein Mbl (*99*) have been observed. The MamK-GFP fusion, for example, could have its behavior impacted in that it recovers slower than endogenous MamK. In this scenario, the technique to observe MamK-GFP, FRAP, is at the limit of detecting turnover. By only catching the faster recovering filaments, this could account for the 50 percent recovery frequencies. Additionally, attempts were made to increase the amount of MamJ

in this system to see if turnover could be enhanced. This was unsuccessful however as overexpression of MamJ was toxic to AMB-1 cells (data not shown). In contrast, the N-terminal fusion of MamK, GFP-MamK, had increased rates and frequencies of turnover. Additionally, the genetic requirement for turnover is not observed with this fusion, where GFP-MamK AMB-1 cells lacking the entire MAI and *E. coli* both displayed recovery. It is worth noting that GFP-MamK turning over faster could also be an artifact, or altered from endogenous MamK. MamK has charged and hydrophobic residues at its N terminus, a feature that could implicate its interaction with the magnetosome membrane. If this is the case, the GFP-MamK fusion could be impacted in its behavior due it its disassociation with magnetosomes. To test this further, an assay to assess the complementation of MamK fusions on magnetosome alignment is absolutely necessary. Additionally, finding a sandwich fusion that complements the *mamK* deletion would be very useful in determining the affect of tagging on MamK's behavior.

Research from the Schüler lab has demonstrated that linker lengths affect MamK's filament morphology and behavior (*39*). It is possible that this has impacted our current characterization of MamK in AMB-1. Additional experiments are needed to determine which combination of linker and fusion location best resembles endogenous MamK *in vivo*, again necessitating a high throughput method for complementation.

Point mutations of MamK demonstrated different recovery capabilities in FRAP. The MamK-R85A/D86A mutant of MamK was chosen to study by FRAP due to previous work that determined faster recovery (Draper, unpublished). FRAP of MamK-R85A/D86A-GFP in Δ*mamJ*Δ*limJ* deletion cells determined that these genes are not required for turnover of the mutant protein. Interestingly, MamK-R85A/D86A filaments do not have a propensity to bundle under high KCl conditions, as assessed by TEM and right angle light scattering experiments (Ozyamak and Kollman, unpublished data). These results potentially link FRAP behavior to an inability to bundle *in vivo* Perhaps, in this scenario, MamK filaments that don't bundle are more prone to depolymerization and turnover.

Finally, it is worth noting that FRAP recovery, though indicative of the movement of MamK proteins in the cell, does not provide a molecular mechanism for how it aligns magnetosomes in AMB-1. For example, recovery could be the result of a combination of mechanisms including filament sliding, polymerization/depolymerization, and *de novo* filament formation could all account for the behavior we are observing. Additionally, an analysis of MamK point mutants has found that MamK recovery rates and frequencies did not correlate with alignment of magnetosome chains in AMB-1 (Draper, unpublished work). Additional research using higher resolution methods, such as PALM/STORM and single particle tracking studies are needed to provide more data to how this protein behaves *in vivo*.
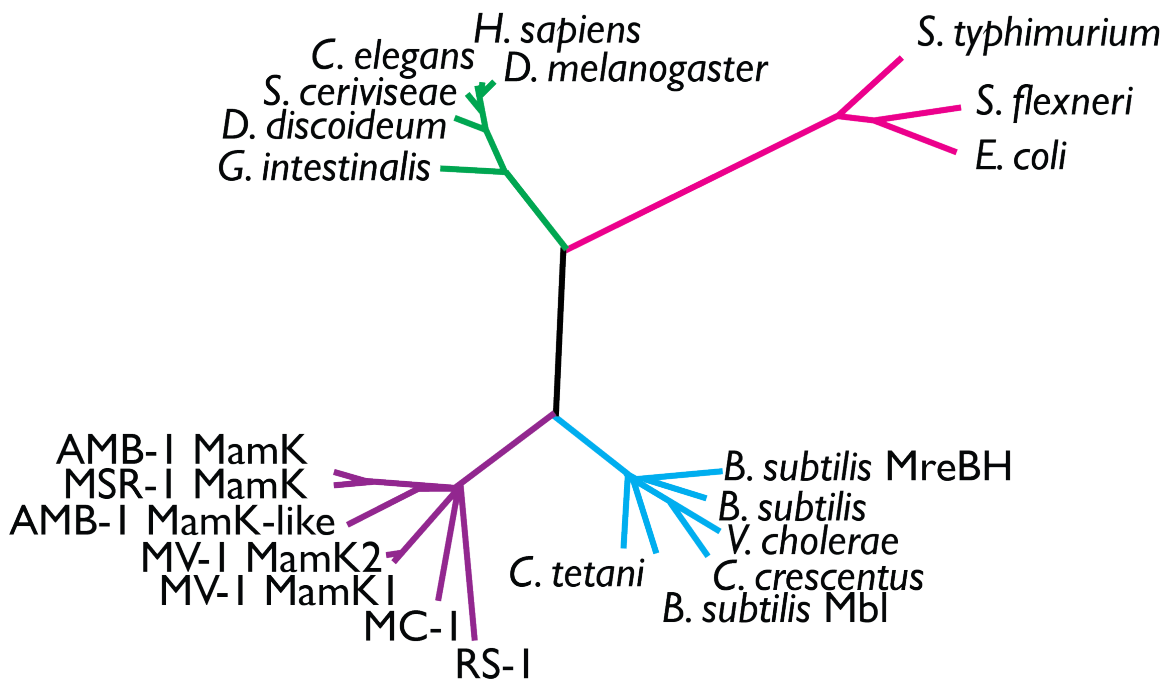
Figure 15. Actin superfamily of selected representative organisms accession numbers: MamK family (purple lines): *Magnetospirillum magneticum* AMB-1: YP_420328.1, *Magnetospirillum gryphiswaldense* MSR-1: CAM78025.1, AMB-1 MamK-like: ACU87671, *Magnetovibrio blakemorei* MV-1 MamK1: CAV30816.1, *Magnetovibrio blakemorei* MV-1 MamK2: CAV30798.1, *Desulfovibrio magneticus* RS-1: YP_002955471.1

MreB family (blue lines): *Bacillus subtilis* MreBH: P39763.1, *Bacillus subtilis:* NP_390681.2, *Vibrio cholera*: AAF93588, *Caulobacter crescentus*: NP_420354.1, *Bacillus subtilis* Mbl: AAA67878.1, *C. tetani*: NP_781022

ParM family (pink lines): *Salmonella typhimurium*: NP_058228.1, *Shigella. flexneri*: AAL72301, *Escherichia coli*: P11904.1

Eukaryotic Actin (green lines): *Giardia intestinalis*: AAA99305.1, *D. discoideum*: YP_644247.1, *Saccharomyces cereviseae*: NP_116614.1, *C. elegans* Act5: NP_499809.1, *Homo sapiens* Gamma-actin: NP_001605.1, *Drosophila melanogaster* Actin 5C: NP_001014725.1

	Dynamic?	% recovery	$t_{1/2m}$(minutes)
WT	✓	47	11±6
ΔMAI	✗	0	N/A
mamAB	✓	56	8±5
Δ*mamAB*	✓	TBD	TBD
Δ*mamJ*	✓	20	13±9
Δ*limJ*	✓	35	12±8
Δ*mamJ*Δ*limJ*	✗	0	N/A
Δ*mamJ*Δ*limJ* + *mamJ* / *limJ*	✓	13/47	8±4 / 6±4
ΔMAI + *mamJ* or *limJ*	✗	0	N/A

Figure 16. Previous FRAP data. Blue boxes represent the Magnetosome Island (MAI), green boxes represent direct repeat (DR) regions where homologous recombination results in loss of the MAI. A ✓ indicates observed recovery of MamK-GFP filaments in a subset of cells analyzed; ✗ indicates no recovery observed in any cell observed.
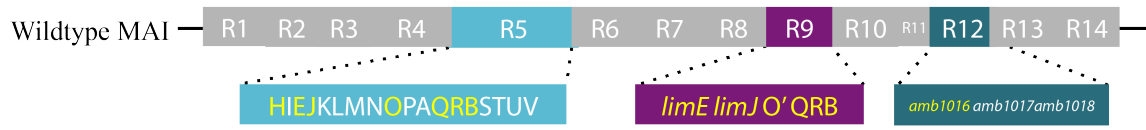
Figure 17. Two approaches to identify a minimal gene set for MamK-GFP FRAP dynamics. A) The wild-type magnetosome island (MAI) was sectioned into 14 regions to probe magnetosome function (work in (*29*)). Redundant genes are highlighted in yellow. Double deletions of redundant genes were made: Δ*mamH*ΔR12 (containing *amb1016*), Δ*mamE*Δ*limE*, Δ*mamJ*Δ*limJ*, Δ*mamO*ΔR9, Δ*mamQ*ΔR9, Δ*mamR*ΔR9, and Δ*mamB*ΔR9 B) A strain only containing the *mamAB*(R5) region was further reduced to make the *mamHIEJKL* strain (this work).

A

B

ΔmamHΔR12　　　　　　　ΔmamHΔR12

MG HEPES, pH 7.2　　　　　MG, pH 6.9
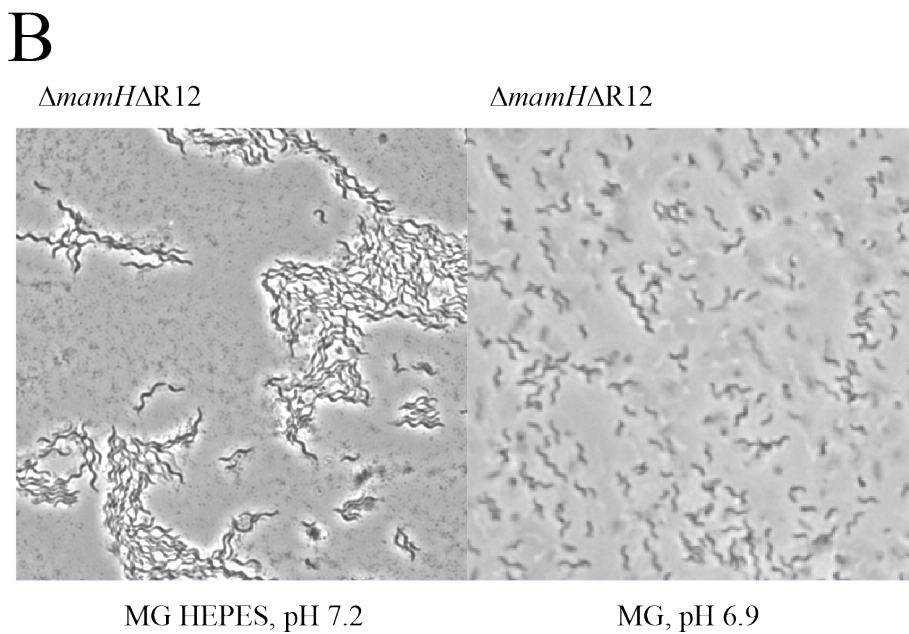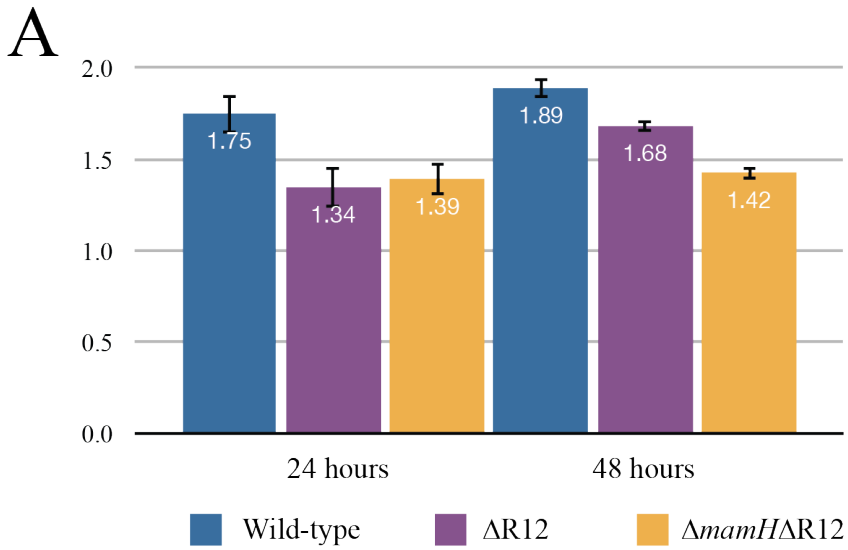
Figure 18. Cell morphology in the Δ*mamHΔR12* background is dependent on media used. A) C_{mag} measurements taken at 24 and 48 hours post inoculation. Wild-type, R12 and HR12 genetic backgrounds. B) Phase contrast images of HR12 cells in different media conditions (i): MG HEPES, pH 7.2 and (ii): MG, pH 6.9.

A

ΔmamHΔR12 cells in MG HEPES, pH 7.2

| Pre-bleach | Bleach | 15 minutes | 30 minutes |

B

C

ΔmamHΔR12 cells in MG, pH 6.9

| Pre-bleach | Bleach | 15 minutes | 30 minutes |

D
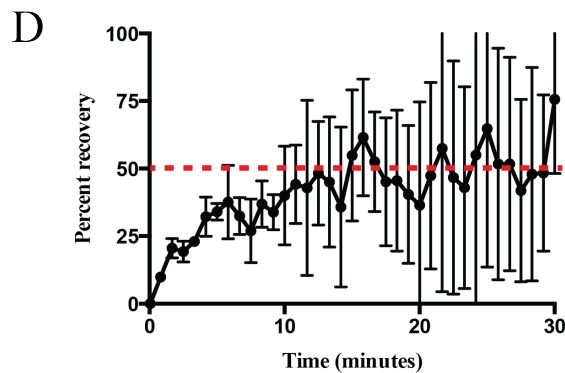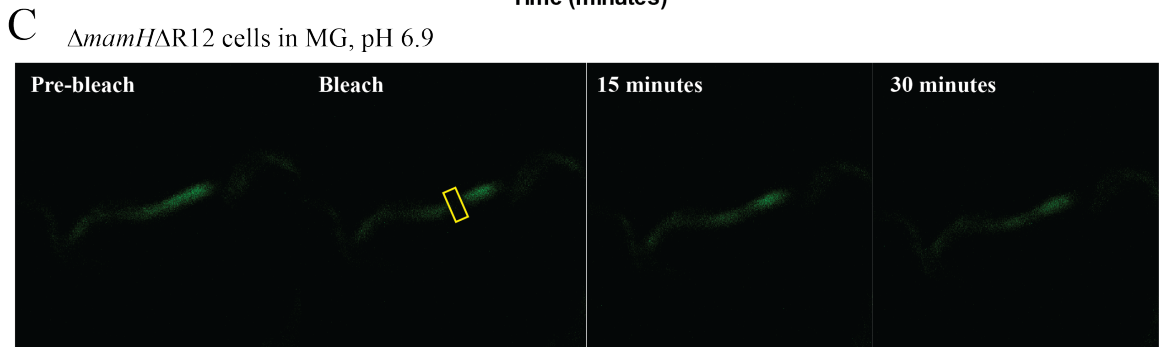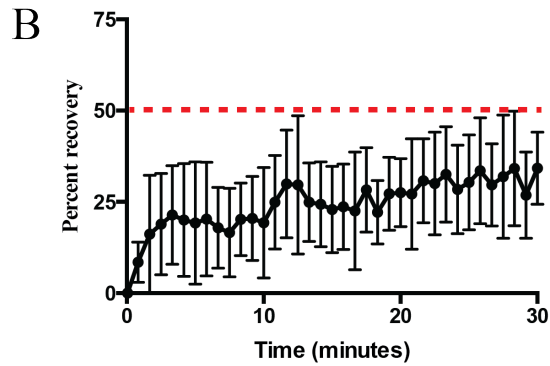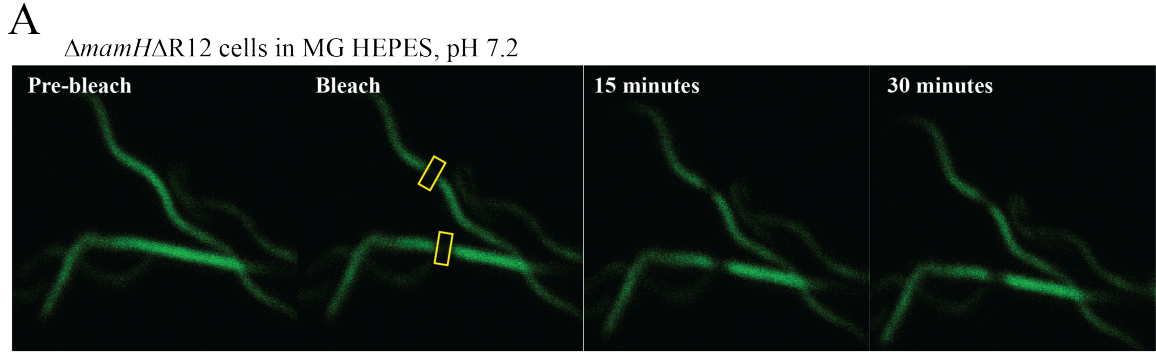
Figure 19. FRAP turnover in ΔmamHΔR12 background is dependent on media used. A) Representative FRAP run of ΔmamHΔR12 cells in HEPES buffered MG, pH 7.2. B) Recovery graphs of ΔmamHΔR12 in HEPES buffered MG, pH 7.2. (n = 10) C) Representative FRAP run of ΔmamHΔR12 cells in MG, pH 6.9. D) Recovery graphs of ΔmamHΔR12 in MG, pH 6.9 (n = 4). Only cells experiencing recovery were included in D.
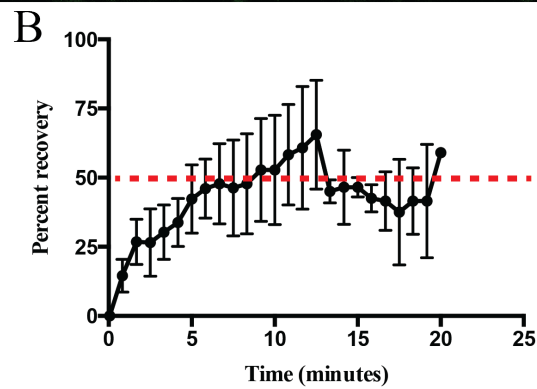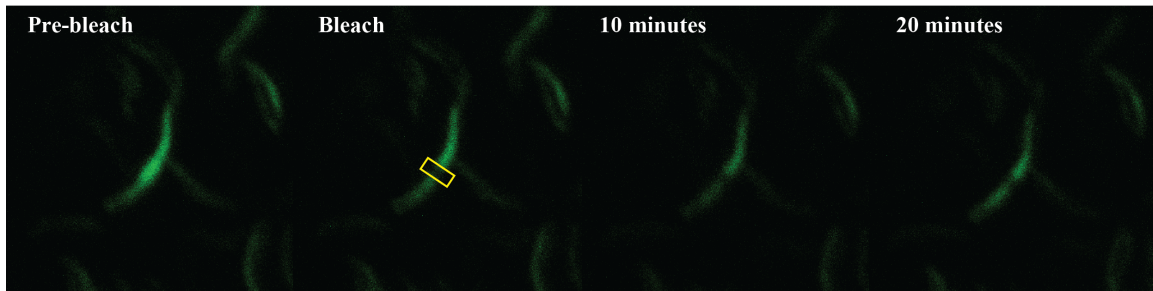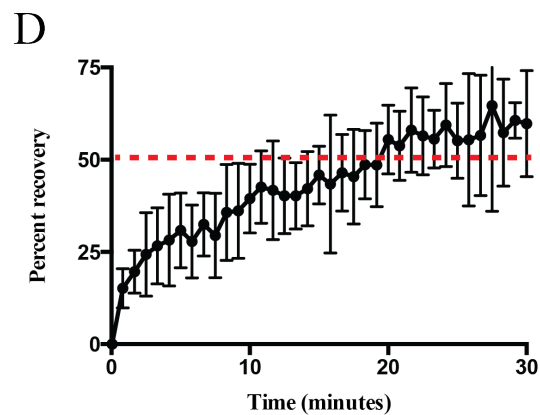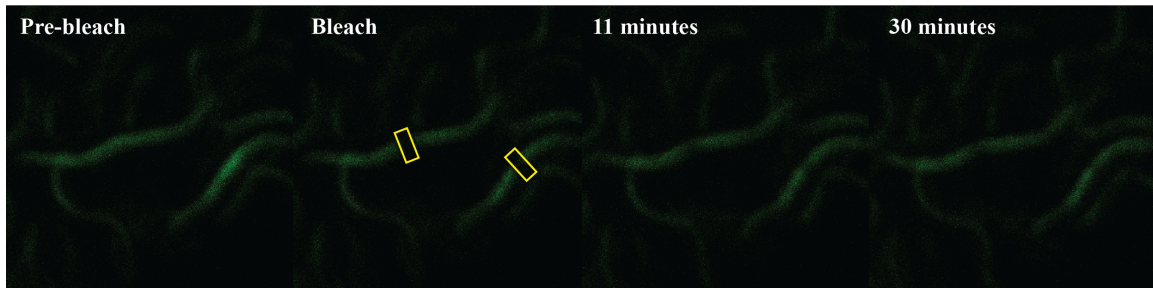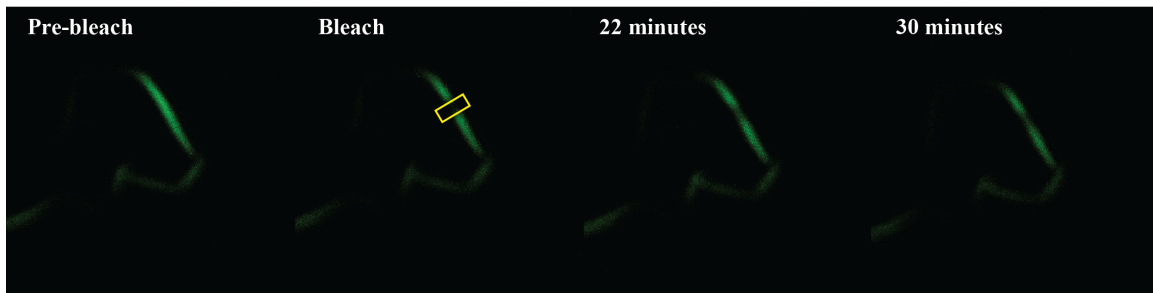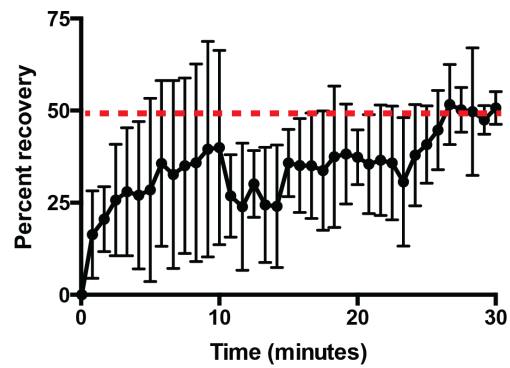
Figure 20. MamE and MamQ are not needed for proper MamK-GFP FRAP turnover. A) Representative FRAP run of Δ*mamE*Δ*limE* cells B) Recovery graphs of Δ*mamE*Δ*limE* (n = 4). C) Representative FRAP run of Δ*mamQ*ΔR9 cells. D) Recovery graphs of Δ*mamQ*ΔR9 (n = 6). Only recovering cells were depicted in these data sets.
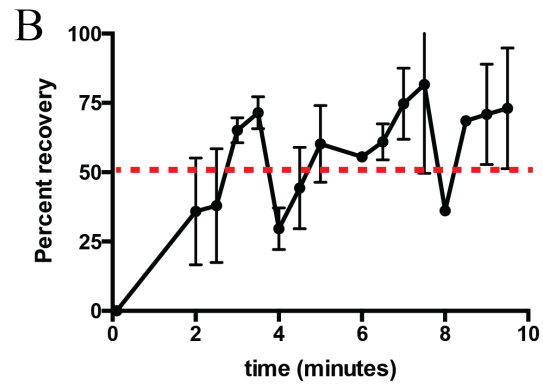
A   *mamHIEJKL*

B

Figure 21. *mamHIEJKL* are sufficient for MamK-GFP FRAP turnover. A) Representative FRAP run of *mamHIEJKL* cells B) Recovery graphs of *mamHIEJKL* (n = 5) cells. Only cells experiencing recovery were included in this dataset.
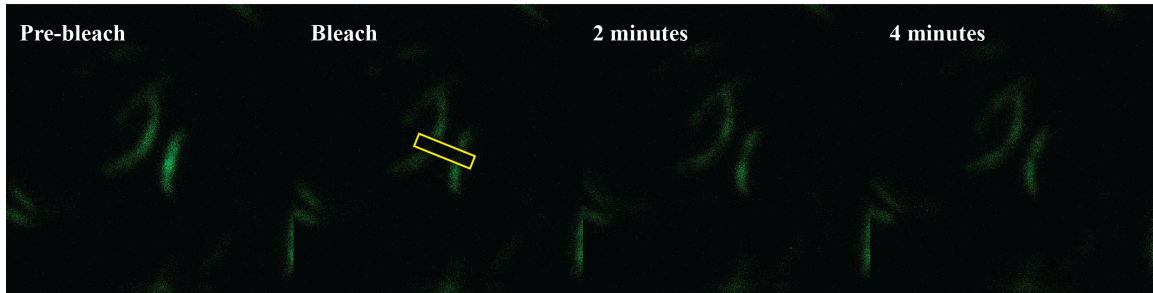
Figure 22. FRAP of MamK-R85A/D86A displays faster turnover rates and no requirement for MamJ or LimJ. A) Representative FRAP run of MamK-R85A/D86A-GFP in Δ*mamJ*Δ*limJ* cells B) Recovery graphs of Δ*mamJ*Δ*limJ* (n = 6) cells. Only cells experiencing recovery were included in this dataset.
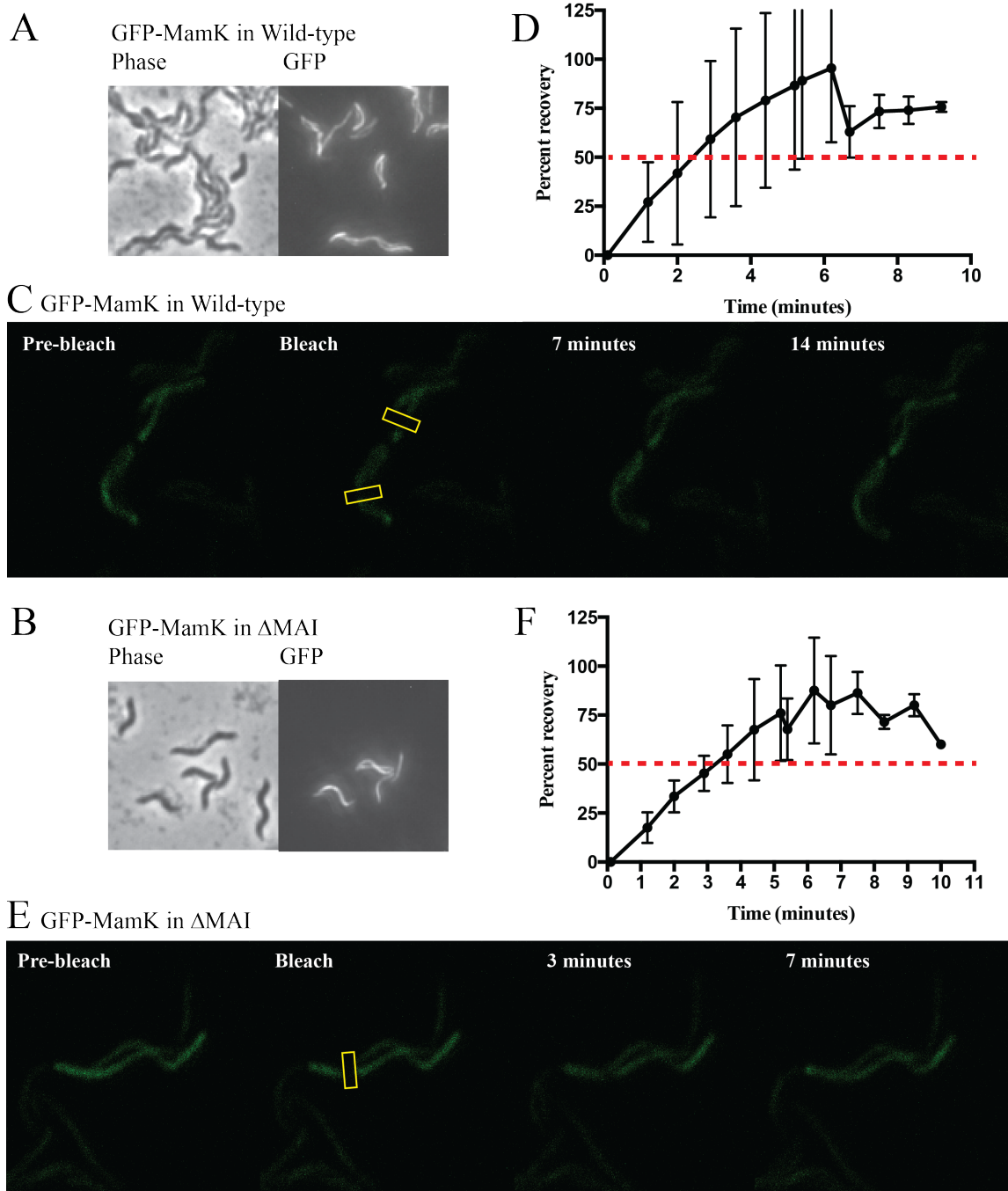
Figure 23. FRAP of GFP-MamK. GFP-MamK filaments in representative cells from A) wild-type and B) ΔMAI genetic backgrounds. C) Representative FRAP run of GFP-MamK in wild-type cells D) Recovery graphs of wild-type (n = 6) cells. E) Representative FRAP run of GFP-MamK in ΔMAI cells F) Recovery graphs of ΔMAI (n = 4) cells. Only cells experiencing recovery were included in these datasets.

Table 6. MamK-GFP recovery results between instruments

	Genetic Background	
	Wild-type	$\Delta mamJ\Delta limJ$
Zeiss 510 (Draper *et al* 2011)		
Percent recovery	47	0
$T_{1/2}$ (minutes)	11 ± 6	N/A
Total # of cells	34	25
Zeiss 710 (this work)		
Percent recovery	50	0
$T_{1/2}$ (minutes)	14 ± 6	N/A
Total # of cells	32	12

Table 7. FRAP on Zeiss 710

Genetic background	MamK variant	% recovery	$T_{1/2}$(minutes)	Total # of cells
Wild-type	MamK-GFP	50	14 ± 6	32
$\Delta mamH\Delta$R12[i]	MamK-GFP	6	N/A	16
$\Delta mamH\Delta$R12[ii]	MamK-GFP	44	12 ± 4	10
$\Delta mamE\Delta limE$	MamK-GFP	40	8 ± 4	10
$\Delta mamQ\Delta$R9	MamK-GFP	50	16 ± 8	16
mamHIEJKL	MamK-GFP	57	17 ± 8	14
$\Delta mamJ\Delta limJ$	MamK-R85A/D86A	80	4 ± 2	10*
Wild-type	GFP-MamK	100	3 ± 3	9
ΔMAI	GFP-MamK	60	4 ± 2	10*

[i]: MG Media buffered with HEPES, pH7.2
[ii]: MG Media, pH 6.9
*: Because of faster overall recovery rates, experiments were stopped earlier than normal (10 minutes rather than 30 minutes), which could account for some runs not experiencing recovery. Longer experimental timeframes are recommended for future experiments.

CHAPTER 4

The investigation of MamK and MamJ interacting proteins by bacterial two-hybrid and immunoprecipitation in *Magnetospirillum magneticum* AMB-1 (unpublished data)

INTRODUCTION

The bacterial actin field is fairly nascent compared to the field of eukaryotic actin, which has had many decades dedicated to its study. The initiation of studying these proteins is due in part to recent technological advances, as bioinformatics approaches identified the bacterial actins as having similar modular domains to actin (*75*). Additionally, many years of biochemical characterization of actin has identified numerous interacting proteins that are required for its regulation and function (*100-102*). To date, over 100 actin interactors that regulate processes such as nucleation, branching, capping, and severing have been identified. This staggering level of complexity has not been observed in bacterial actin families inspiring us to identify and investigate whether our model bacterial actin, MamK, has interacting proteins associated with it.

These interacting proteins could serve different functions in AMB-1 to align magnetosome chains. For example, interactors that regulate the polymerization and/ or depolymerization of MamK filaments could regulate filament dynamics and turnover *in vivo*. Evidence in our lab indicates that cell viability is linked to MamK turnover, as ATPase mutants are lethal in AMB-1 cells and result in a cell-chaining defect. Regulating the filament could be required during chain partition and cell division. Alternatively, MamK interacting proteins may be needed to physically attach the filaments to magnetosomes. To identify these proteins in AMB-1, we sought to use a combination of *in vitro* and *ex vivo* approaches.

To isolate MamK from AMB-1 cell lysates, a tagged form (MamK-M2) was used allowing the use of FLAG-conjugated resin for immunoprecipitation (IP) experiments. Much time was spent to isolate MamK in a soluble form before IP experiments could be performed. Despite the successful isolation of MamK-M2 from cell lysates, IP experiments and subsequent mass spectrometry did not identify a strong candidate interacting protein.

For the *ex vivo* approach, a bacterial two hybrid assay relying on the reconstitution of adenylate cyclase was used. Since most magnetosome genes encode predicted transmembrane proteins, the bacterial two-hybrid strategy is beneficial compared to a yeast two-hybrid, which requires the protein candidates to be soluble and nuclear-localized to detect interaction. Bacterial two-hybrid experiments were also unable to find interacting proteins in the *mamAB* region of the magnetosome island. More effort will be needed in the future to find MamK interacting proteins.

MATERIALS & METHODS

Cell cultures.
AMB-1 cells (wild-type, Δ*mamK*, and ΔMAI transformed with plasmids pAK 392: MamK-M2 or pAK786: MamK-gsgs-TEV-gsgs-SNAP) were grown in 1.5 ml microcentrifuge tubes with MG liquid media supplemented with 1X Ferric Malate (100X: 3 mM, Fe 9 mM Malate), 1X vitamins (100X: Biotin 2 mg/L, Folic acid 2 mg/L, Pyridoxine hydrochloride 10 mg/L, Vitamin B1 hydrochloride 5 mg/L, (-)-Riboflavin 5 mg/L, Nicotinic acid 5 mg/L, Calcium pantothenate 5 mg/L, Vitamin B12 0.1 mg/L, 4-Aminobenzoic acid 5 mg/L, and (±)-α-Lipoic acid 5 mg/L), and Kanamycin [10 ug/ml]$_{final}$ (referred to as MG Kanamycin), for 4-5 days at 30° C before inoculating into 50 ml falcon tube cultures (with MG Kanamycin). After 2 days at 30° C The 50 ml cultures were used to inoculate 1L bottles containing MG (no Kanamycin) flushed with N$_2$ and grown for 2-3 days in the 10% O$_2$ incubator at 30° C.

1L cultures were pelleted by centrifugation at 6,000 rpm for 10 minutes at 4° C (Sorvall Superspeed RC2-B). Supernatant was discarded and cells were resuspended in 40 ml (4 X 10 ml) of 1X DPBS (no Mg^{2+}/Ca^{2+}) (unless concentrated by resuspending in a single 10 ml aliquot). After resuspension, cells were pelleted by spinning at 8,000 X g for 10 minutes at 4° C (Sorvall Legend Mach 1.6R). Supernatant was discarded and samples were worked with immediately or were flash frozen in liquid N$_2$ before storing at -80° C.

Cell lysis and protein purification.
To lyse cells, two different methods were attempted: 1) Enzymatic via lysozyme and 2) mechanical via French Press. For enzymatic lysis: 900 μl of Sample Buffer A2 (10 mM Tris-HCl pH 8.0, 50 mM KCl, 1 mM EDTA) was added to cell pellet. Afterwards, protease inhibitors (1 μl of 1 mg/ml Leupeptin [1 μg/ml]$_{final}$, 1 μl of 1 mg/ml Pepstatin A [1 μg/ml]$_{final}$, and 10 μl of 100 mM PMSF [1 mM]$_{final}$) were added. Pellet was resuspended by pipetting up and down, and three freeze (Liquid N$_2$) thaw (ice) cycles were applied with resuspension in between each cycle. Next, 20 μl of 50 mg/ml lysozyme [1 mg/ml final] was added. The cells were allowed to lyse at room temperature for 15 minutes on a rotating carousel (Labquake shaker rotisserie). Next, 4 ml of buffer 3.1 (20 mM HEPES-KOH pH7.5, 50 mM KCl, 50 μM MgCl$_2$, 1 mM EDTA, 10% glycerol) was added. Prep was then sonicated 2 times 10 seconds each at 70% duty, output 3 (Branson Sonifier 250). Lysate was then centrifuged at 10,000 X g for 15 minutes at 4° C (Sorvall Legend Mach 1.6R). For French press protocol: 900 μl of Sample Buffer A2 (10 mM Tris-HCl pH 8.0, 50 mM KCl, 1 mM EDTA) was added to cell pellet. Afterwards, protease inhibitors (1 μl of 1 mg/ml Leupeptin [1 μg/ml]$_{final}$, 1 μl of 1 mg/ml Pepstatin A [1 μg/ml]$_{final}$, and 10 μl of 100 mM PMSF [1 mM]$_{final}$) were added. Pellet was resuspended by pipetting up and down. Next, 4 ml of buffer 3.1 (20 mM HEPES-KOH pH7.5, 50 mM KCl, 50 μM MgCl$_2$, 1 mM EDTA, 10% glycerol) was added before samples were subjected to two rounds of French Press disruption (1100 psi). Total lysate samples were taken at this time and mixed with SDS loading buffer. Lysate was then centrifuged at 10,000 X g for 15 minutes at 4° C (Sorvall Legend Mach 1.6R). Pellet and supernatant fractions were then taken at this time.

MamK pull down experiments.

To equilibrate resin, 80 µl Anti Flag M2 affinity gel (Sigma) was washed with 1 ml of Buffer B3.1 (20 mM HEPES-KOH pH7.5, 50 mM KCl, 50 µM $MgCl_2$, 1 mM EDTA, 10% glycerol) in eppendorf tubes by centrifugation at 6000 rpm for 1.5 min (Denville 2600 brushless microcentrifuge). Next, 1 ml of cell supernatant fraction of cell lysate was added to resin and incubated in the cold room overnight on a rotating carousel (Labquake shaker rotisserie). The next day, samples were spun at 6000 rpm for 1.5 min 4° C and the flowthrough was collected. The samples were then washed three times with 1 ml each of buffer B3.1 with spinning at 6000 rpm for 1 minute. Wash buffer was collected after each step. Samples were then brought back to room temperature and 100 µl of 0.1 M glycine, pH 3.5 was added and incubated for 5-10 minutes each elution. This was repeated for a total of three elution fractions.

Immunoprecipitation preparation and Mass Spectrometry.

50 µl of sample was transferred to a low adhesion eppendorf tube. 10 µl of 50 mM ammonium bicarbonate (NH_4HCO_3) and 25 µl of Rapigest SF (Waters) were added. Samples were vortexed and incubated at 80° C for 15 minutes. Next, 2.5 µl of 100 mM DTT was added, the sample(s) were vortexed and incubated at 60° C for 30 minutes. Sample(s) were allowed to cool to room temperature before 2.5 µl of 300 mM iodoacetomide was added. Sample(s) were then vortexed and incubated in the dark at room temperature for 30 minutes. Next, 2.5 µl of trypsin (Promega) was added, the sample(s) were vortexed, and incubated overnight at 37° C. The following morning, 10 µl of 5% TFA (Thermo Fisher Scientific) was added, sample(s) were vortexed and incubated at 37° C for 90 minutes. Sample(s) were then spun at 14000 rpm for 30 minutes at 4° C before 100 µl was transferred to a total recovery vial (Waters). Sample(s) were then stored at 4° C before transport to Mass Spectrometry facility (QB3). Sample(s) were analyzed using a Thermo Dionex UltiMate3000 RSLCnano liquid chromatograph that was connected in-line with an LTQ Orbitrap XL mass spectrometer equipped with a nanoelectrospray ionization source.

Bacterial Two-hybrid.

Bacterial two-hybrid (BACTH) assays were conducted employing a previously established plasmid and reporter strain system (*103*). This system works due to the ability of the catalytic domain of *Bordatella pertussis* adenylate cyclase (CyaA) to be split into two fragments, T18 and T25 (*104*). The T18 and T25 fragments of CyaA can then be fused to proteins of interest to assess their interaction. Heterodimerization of the fusion proteins results in cAMP synthesis. Cyclic AMP binds to the catabolite activator protein CAP, resulting in the transcription of numerous genes, including genes involved in lactose/maltose metabolism and high β-galactosidease activity (*104*).

To create fusion proteins for BACTH analysis, the *mamK* was fused to the N and C terminus of the T18 plasmid resulting in plasmids pAK327 and pAK327, respectively (Sepehr Keyhani in Komeili lab, pervious work). The bait plasmids were also made by fusing T25 to *mamK* on the N and C terminus to make plasmids pAK324 and pAK325, respectively (Sepehr Keyhani in Komeili Lab, previous work). For the prey proteins, gene sequences for *mamAB* genes were amplified from AMB-1 gDNA using primer sets

specified in Table 8 and ligated into T18 plasmids through XbaI and KpnI restriction sites. Special consideration had to be taken to ensure that the constructs were in frame as the T18 and T25 plasmids did not result in fragments that were kept in frame after restriction digest. Plasmids were co-transformed into the bacterial reporter strain DHM1 (*103*). Cells were selected on LB agar plates containing Kanamycin (50 µg/ml) and Carbenicillin (100 µg/ml). Colonies from these plates were then grown up in 5 ml of LB media overnight at 30°C before serial 1:10 dilutions were made and plated on LB plates containing Kanamycin, Carbenicillin, and X-Gal. The formation of blue colonies on these plates indicates the interaction of candidate proteins. Plasmids made for these experiments are listed in Table 9.

RESULTS

MamK-M2 solubility is affected by conditions used to isolate protein.
We envisioned that two classes of proteins could interact with MamK, cytoplasmic and membrane bound proteins. With our methodology, the supernatant fraction of our cell lysate would contain a mixture of these protein types. We focused on the supernatant fraction of MamK to minimize working on protein aggregates that may be present in the pellet fraction of the isolation. To get a soluble, supernatant form of MamK, multiple buffer conditions and lysis protocols were tested. The first set of approaches was unsuccessful in isolating soluble MamK, as the MamK was only appearing in the pellet fraction of cell preparations (Figure 24A). After troubleshooting, it was determined that heating the sample during lysozyme treatment resulted in dramatic insolubility of MamK. Additionally, lysis under room temperature conditions with lysozyme resulted in a higher proportion of soluble MamK (Figure 24B). The French Press method resulted in the highest amount of soluble MamK, as detected by Western blotting, remaining in the supernatant fraction of the cell lysate (Figure 24C). For this reason, French press was used for further experiments.

MamK-M2 can be identified in affinity purification / mass spectrometry experiments.
After performing the pull down and sample preparation, western blots and silver staining were performed to verify the presence of MamK in the elution fraction of the pull down. Indeed, MamK-M2, but not untagged MamK, was present in the elution fraction (Figure 25AB). This was also confirmed by silver stain of a protein gel (Figure 25C). Mass spectrometry was performed on the elution fraction in MamK-M2 tagged lysates, using untagged MamK as a negative control. Untagged MamK preparation only resulted in one protein found, GroEL, an abundant cellular chaperone. The MamK-M2 tagged experiment resulted in identifying 5 proteins with 2 peptides or more detected (Table 10). One of the proteins identified was MamK, proof of the pull down experiment working. The four remaining proteins were identified as highly abundant proteins in AMB-1 cells (via communication with Pat Browne, David Hershey, and Ertan Ozyamak).

MamK does not interact with *mamAB* proteins by Bacterial two-hybrid.
In AMB-1, MamK is encoded from a region of the magnetosome island with 17 other magnetosome genes. Given that these genes are located in the same region, we reasoned that they could potentially interact with each other. Because many of the proteins encoded in this region are membrane proteins, a bacterial two-hybrid assay that reconstitutes the adelylate cyclase catalytic domain was used (*103*). We know from previous work that MamK interacts with itself in a yeast two-hybrid (*105*) as well as a bacterial two-hybrid system (unpublished work). As a positive control, MamK paired with itself showed a strong interaction (Figure 26). As a negative control, pairings between empty vector constructs did not result in interaction and growth (Figure 26). Pairings between other *mamAB* region genes did not result in interaction (Figure 26, Table 11).

<u>MamJ does not interact with itself or with *mamAB* proteins by Bacterial two-hybrid.</u>
Because of the chain alignment defect observed previously in cells (*36*, *60*, *97*), MamJ
was a logical candidate to search for interacting proteins in the *mamAB* region. Pairings
between MamJ and other *mamAB* region-encoded proteins (including MamK) did not
result in detectable interactions (Table 12, Figure 27). Additionally, MamJ did not
interact with itself under these conditions (Table 12, Figure 27).

DISCUSSION

To identify MamK interacting proteins, two separate approaches were undertaken. The first approach used an *in vitro* affinity purification method and mass spectrometry to identify interacting proteins. The second approach relied on a bacterial two-hybrid assay to address the same question. Both approaches were unsuccessful in identifying interacting proteins.

It took multiple trials to ensure MamK's solubility for affinity purification experiments. Heating AMB-1 cells during lysozyme treatment proved to be the step that rendered MamK insoluble, as lysozyme treatment at room temperature resulted in a higher proportion of soluble MamK. Ultimately, I used French press for downstream experiments.

It could be possible that MamK may not have strongly interacting proteins associated with it. Though the French press method resulted in soluble MamK isolation, and was subsequently used for immunoprecipitation experiments, the shearing forces of this method could be too disruptive to MamK's interaction with other proteins. Preparation of lysates using a room temperature lysozyme treatment may be a better alternative for future affinity purification experiments.

To attempt these experiments in the future, increasing the culture volume and concentrating the proteins is recommended. Initial attempts were made without success, however, with more troubleshooting, increasing the concentration of MamK in the reaction volume could be successful. As opposed to shotgun mass spectrometry of the elution, a more effective strategy would be to isolate individual candidate protein bands from a Commassie-stained gel for mass spectrometry identification. This would potentially avoid detection of the bulk of false positive signals from abundant cellular proteins.
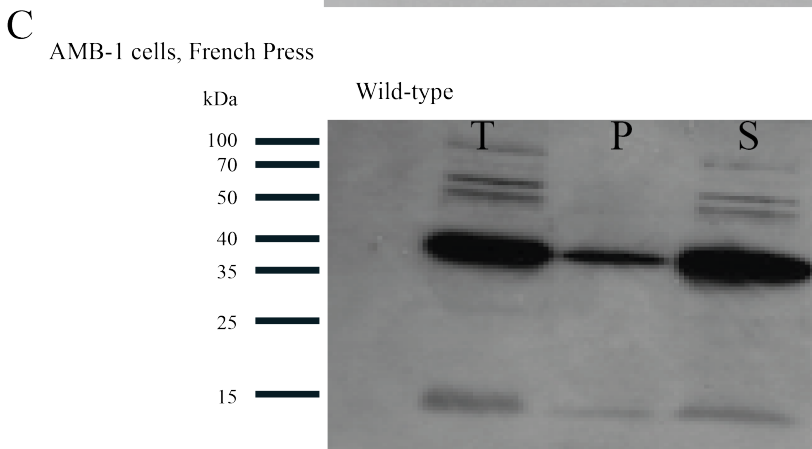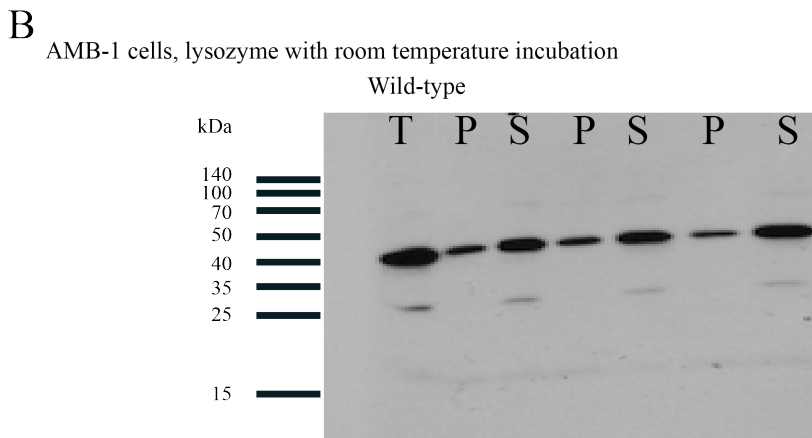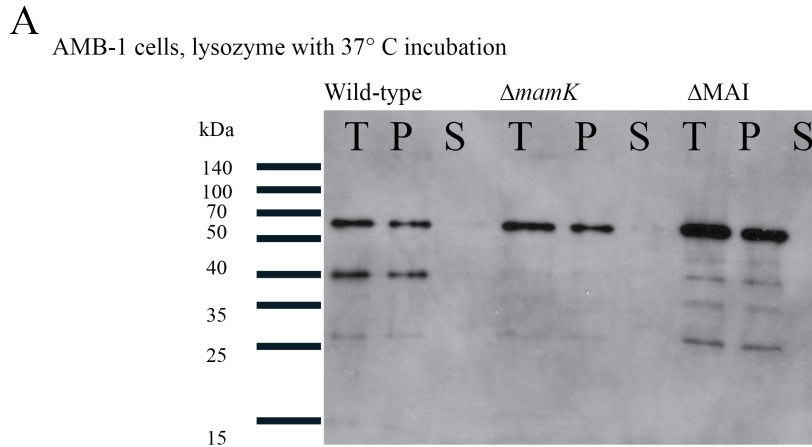
Bacterial two hybrid experiments were not successful in identifying MamK or MamJ interacting proteins. This experiment was limited in that it relies on each fusion protein remaining intact but we know from our experience that magnetosome proteins are processed *in vivo*. Additionally, we only tested genes from the *mamAB* region, which biases our search and excludes potential candidates from the rest of the genome. To get around these issues in the future, generating a prey library is a suitable approach. By shearing the *mamAB* region to generate a prey library, interacting domains of candidate proteins would remain fused to the T18 protein. Also, by expanding the prey library to the entire AMB-1 genome, candidates outside of the *mamAB* region can be identified as well.

Finally, rather than having weak interaction with magnetosome proteins, it is possible that MamK does not have interacting proteins to mediate attachment to the magnetosome membrane. In this case, MamK could interact with lipids in isolation. This is supported by the observation that the N-terminus of MamK contains both charged and hydrophobic amino acids. Liposome flotation assays would be a great way to assess whether MamK

can interact with lipid vesicles without the need for accessory proteins. Alternatively, if MamK does not interact with the lipid vesicles on its own, and, if future experiments determine that there is an interacting protein in the magnetosome membrane, mixing purified candidate protein(s) with liposomes would test this hypothesis and identify a minimal set of proteins for MamK/magnetosome interaction.

A

AMB-1 cells, lysozyme with 37° C incubation

B

AMB-1 cells, lysozyme with room temperature incubation

C

AMB-1 cells, French Press

Figure 24. MamK purification and solubility. A) Initial trials with lysis protocols with heating (37 C) resulted in insoluble MamK B) Room temperature lysozyme treatment resulted in a higher proportion of soluble MamK. C) French press without lysozyme treatment resulted in the highest proportion of soluble MamK.
(T = Total cell lysate, P = Pellet fraction, S = Supernatant fraction)
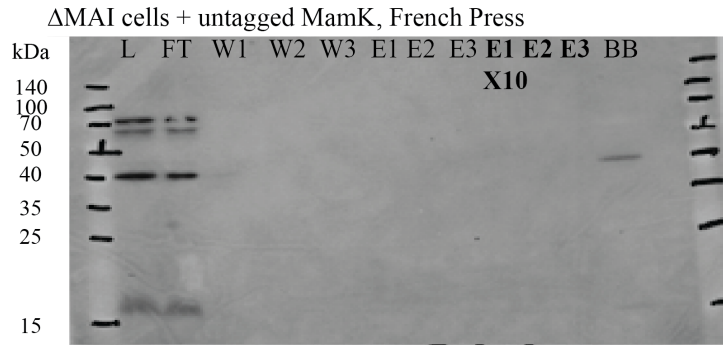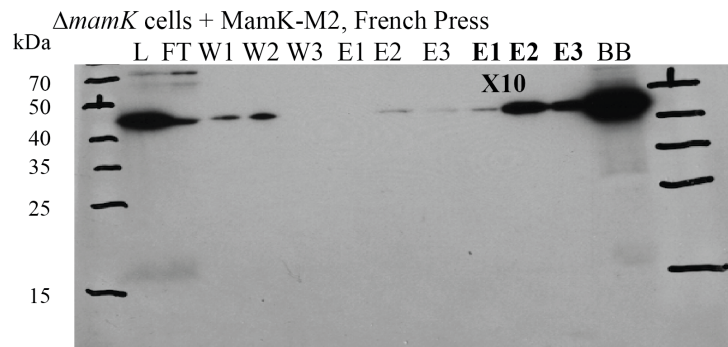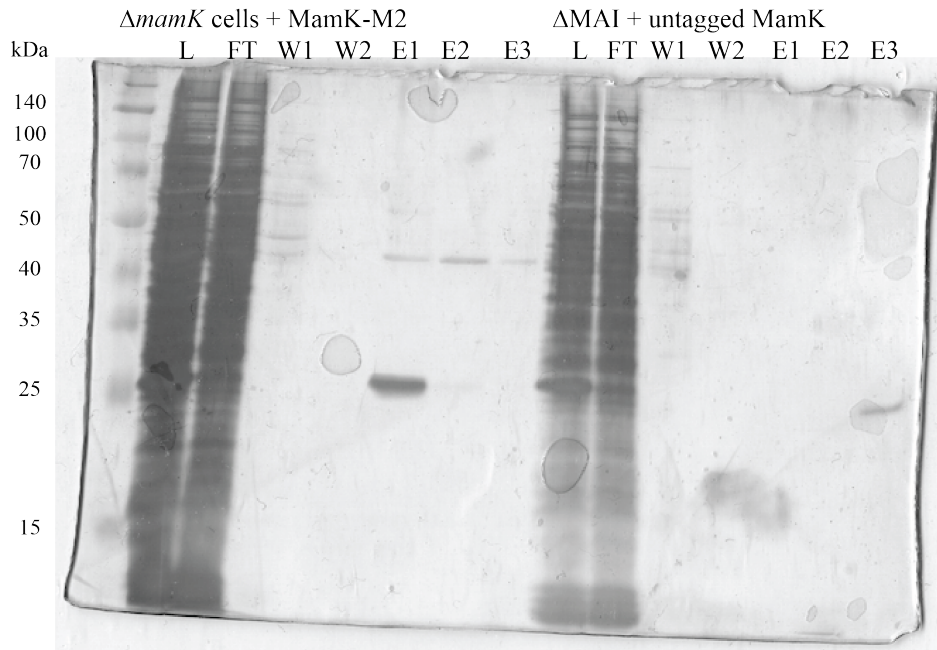
Figure 25. MamK-M2 can be isolated by immunoprecipitation. A) αMamK Western blot of ΔMAI cells expressing untagged MamK from a plasmid (pAK742). B) αMamK Western blot of ΔmamK cells expressing MamK-M2 from a plasmid (pAK392). C) Silver stain of samples from A & B. (MamK ~ 42 kDa)

Combination #:

1: pAK320 (empty)   10: pAK874 (MamM-T18)   19: pAK855 (T18-MamU)
2: pAK326 (MamK-T18)   11: pAK868 (MamN-T18)   20: pAK860 (T18-MamP)
3: pAK865 (MamA-T18)   12: pAK873 (MamP-T18)   21: pAK863 (T18-MamA)
4: pAK872 (MamQ-T18)   13: pAK851 (T18-MamI)   22: pAK861 (T18-MamQ)
5: pAK866 (MamB-T18)   14: pAK854 (T18-MamL)   23: pAK852 (T18-MamR)
6: pAK867 (MamS-T18)   15: pAK859 (T18-MamM)   24: pAK853 (T18-MamB)
7: pAK869 (MamU-T18)   16: pAK857 (T18-MamN)   25: pAK864 (T18-MamS)
8: pAK870 (MamI-T18)   17: pAK858 (T18-MamO)
9: pAK816 (MamJ-T18)   18: pAK862 (T18-MamH)

Figure 26. MamK BACTH.

Combination #:

26 25   6 5   4   3   2   1   26   + 12 11 10 9   8   7
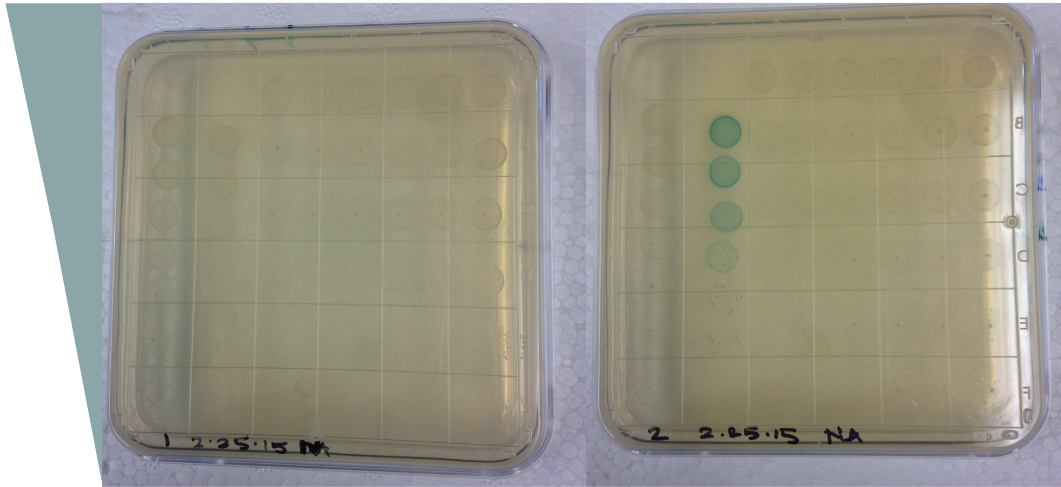
26 -   18 17 16 15 14 13   26 -   24 23 22 21 20 19

1: pAK320 (empty)   10: pAK874 (MamM-T18) 19: pAK855 (T18-MamU)
2: pAK326 (MamK-T18)   11: pAK868 (MamN-T18) 20: pAK860 (T18-MamP)
3: pAK865 (MamA-T18)   12: pAK873 (MamP-T18) 21: pAK863 (T18-MamA)
4: pAK872 (MamQ-T18)   13: pAK851 (T18-MamI) 22: pAK861 (T18-MamQ)
5: pAK866 (MamB-T18)   14: pAK854 (T18-MamL) 23: pAK852 (T18-MamR)
6: pAK867 (MamS-T18)   15: pAK859 (T18-MamM) 24: pAK853 (T18-MamB)
7: pAK869 (MamU-T18)   16: pAK857 (T18-MamN) 25: pAK864 (T18-MamS)
8: pAK870 (MamI-T18)   17: pAK858 (T18-MamO) 26: pAK325 (MamK-T25)
9: pAK818 (T25-MamJ)   18: pAK862 (T18-MamH)   & pAK816 (MamJ-T18)

Figure 27. MamJ BACTH.

Table 8. Primers used to generate *mamAB* BACTH vectors

Primer name		Sequence
NA207	*mamH*_XbaI_C_F	acacacaTCTAGAcgtgtctcgagtggaagcggc
NA208	*mamH*_KpnI_R	acacacaGGTACCctacgccaccccgtcgtcccc
NA209	*mamH*_XbaI_F	acacacaTCTAGAgtgtctcgagtggaagcggc
NA211	*mamI*_XbaI_C_F	acacacaTCTAGAcatgccaagcgtgattttcgg
NA212	*mamI*_KpnI_R	acacacaGGTACCtcaaccatcgatgtcagggtc
NA213	*mamI*_XbaI_F	acacacaTCTAGAatgccaagcgtgattttcgga
NA215	*mamE*_XbaI_C_F	acacacaTCTAGAcatggccatgttcaatggtgac
NA216	*mamE*_KpnI_R	acacacaGGTACCtcaaaggacaatccagaactc
NA217	*mamE*_XbaI_F	acacacaTCTAGAatggccatgttcaatggtgac
NA219	*mamL*_XbaI_C_F	acacacaTCTAGAcatggtaagattgatcggatc
NA220	*mamL*_KpnI_R	acacacaGGTACCtcagcgcttgatgacgatgct
NA221	*mamL*_XbaI_F	acacacaTCTAGAatggtaagattgatcggatcg
NA223	*mamM*_XbaI_C_F	acacacaTCTAGAcatgaggaagagcggttgcacg
NA224	*mamM*_KpnI_R	acacacaGGTACCctagttatccaccttcgacaa
NA225	*mamM*_XbaI_F	acacacaTCTAGAatgaggaagagcggttgcacg
NA227	*mamN*_XbaI_C_F	acacacaTCTAGAcatgatcggacttctcaccct
NA228	*mamN*_KpnI_R	acacacaGGTACCtcatcccacgagaaccgcgat
NA229	*mamN*_XbaI_F	acacacaTCTAGAatgatcggacttctcaccctt
NA231	*mamO*_XbaI_C_F	acacacaTCTAGAcatgattgaagtcggcgagac
NA232	*mamO*_KpnI_R	acacacaGGTACCtcacaccgaggtcagcatctt
NA233	*mamO*_XbaI_F	acacacaTCTAGAatgattgaagtcggcgagacc
NA235	*mamP*_XbaI_C_F	acacacaTCTAGAcatgaatagcaaggtggcgct
NA236	*mamP*_KpnI_R	acacacaGGTACCtcactttatgacgtggcaggc
NA237	*mamP*_XbaI_F	acacacaTCTAGAatgaatagcaaggtggcgctt
NA239	*mamA*_XbaI_C_F	acacacaTCTAGActtggagaacactatgtctag
NA240	*mamA*_KpnI_R	acacacaGGTACCtcagaccgaggcccccttcgtc
NA241	*mamA*_XbaI_F	acacacaTCTAGAttggagaacactatgtctagc
NA243	*mamQ*_XbaI_C_F	acacacaTCTAGAcatggcattaggcgacgcgaa
NA244	*mamQ*_KpnI_R	acacacaGGTACCtcatttcttgatgtcctgcgc
NA245	*mamQ*_XbaI_F	acacacaTCTAGAatggcattaggcgacgcgaat
NA247	*mamR*_XbaI_C_F	acacacaTCTAGAcatgatctggacggcggtgat
NA248	*mamR*_KpnI_R	acacacaGGTACCtcatcggttcatgtaatccac
NA249	*mamR*_XbaI_F	acacacaTCTAGAatgatctggacggcggtgatc
NA251	*mamB*_XbaI_C_F	acacacaTCTAGAcatgaccctgttcaagggggt
NA252	*mamB*_KpnI_R	acacacaGGTACCtcaggccccgtgccgcggcggc
NA253	*mamB*_XbaI_F	acacacaTCTAGAatgaccctgttcaaggggggtc
NA255	*mamS*_XbaI_C_F	acacacaTCTAGAcatggacatccggccagagcg
NA256	*mamS*_KpnI_R	acacacaGGTACCtcactgcaccaccatccacag

NA257	*mamS*_XbaI_F	acacacaTCTAGAatggacatccggccagagcgt
NA259	*mamT*_XbaI_C_F	acacacaTCTAGAcatggaggcgccgcggcgcggc
NA260	*mamT*_KpnI_R	acacacaGGTACCtcataattgccatctcatgcc
NA261	*mamT*_XbaI_F	acacacaTCTAGAatggaggcgccgcggcgcggc
NA263	*mamU*_XbaI_C_F	acacacaTCTAGAcatgcgcatcgcggcgatcat
NA264	*mamU*_KpnI_R	acacacaGGTACCttatttgggcaccagcatggg
NA265	*mamU*_XbaI_F	acacacaTCTAGAatgcgcatcgcggcgatcatc
NA267	*mamV*_XbaI_C_F	acacacaTCTAGAcatgctgggaaggccgatgaa
NA268	*mamV*_KpnI_R	acacacaGGTACCtcagccgccattgcggctgtg
NA269	*mamV*_XbaI_F	acacacaTCTAGAatgctgggaaggccgatgaaa
NA271	*mamH*_KpnI_NOSTOP_gc_R	acacacaGGTACCgccgccacccccgtcgtccct
NA272	*mamI*_KpnI_NOSTOP_gc_R	acacacaGGTACCgcaccatcgatgtcagggtct
NA273	*mamE*_KpnI_NOSTOP_gc_R	acacacaGGTACCgcaaggacaatccagaactct
NA274	*mamJ*_KpnI_NOSTOP_gc_R	acacacaGGTACCgctttttcttgcccaccgtatc
NA275	*mamL*_KpnI_NOSTOP_gc_R	acacacaGGTACCgcgcgcttgatgacgatgctctt
NA276	*mamM*_KpnI_NOSTOP_gc_R	acacacaGGTACCgcgttatccaccttcgacaacat
NA277	*mamN*_KpnI_NOSTOP_gc_R	acacacaGGTACCgctcccacgagaaccgcgatata
NA278	*mamO*_KpnI_NOSTOP_gc_R	acacacaGGTACCgccaccgaggtcagcatcttgag
NA279	*mamP*_KpnI_NOSTOP_gc_R	acacacaGGTACCgcctttatgacgtggcaggcttc
NA280	*mamA*_KpnI_NOSTOP_gc_R	acacacaGGTACCgcgaccgaggccccttcgtcaag
NA281	*mamQ*_KpnI_NOSTOP_gc_R	acacacaGGTACCgctttcttgatgtcctgcgcatg
NA282	*mamR*_KpnI_NOSTOP_gc_R	acacacaGGTACCgctcggttcatgtaatccacaag
NA283	*mamB*_KpnI_NOSTOP_gc_R	acacacaGGTACCgcggcccgtgccgcggcggcggg
NA284	*mamS*_KpnI_NOSTOP_gc_R	acacacaGGTACCgcctgcaccaccatccacagtgc
NA285	*mamT*_KpnI_NOSTOP_gc_R	acacacaGGTACCgctaattgccatctcatgccgcc
NA286	*mamU*_KpnI_NOSTOP_gc_R	acacacaGGTACCgctttgggcaccagcatgggtag
NA287	*mamV*_KpnI_NOSTOP_gc_R	acacacaGGTACCgcgccgccattgcggctgtggcc

Table 9. Prey plasmids made for *mamAB* BACTH

Plasmid name	*mamAB* gene	resulting fusion	source
pAK 324	*mamK*	T25-MamK	Sepehr Keyhani, Komeili Lab
pAK 325	*mamK*	MamK-T25	Sepehr Keyhani, Komeili Lab
pAK326	*mamK*	MamK-T18	Sepehr Keyhani, Komeili Lab
pAK327	*mamK*	T18-MamK	Sepehr Keyhani, Komeili Lab
pAK862	*mamH*	T18-MamH	this work
pAK851	*mamI*	T18-MamI	this work
pAK870	*mamI*	MamI-T18	this work
pAK816	*mamJ*	MamJ-T18	this work
pAK854	*mamL*	T18-MamL	this work
pAK859	*mamM*	T18-MamM	this work
pAK874	*mamM*	MamM-T18	this work
pAK857	*mamN*	T18-MamN	this work
pAK868	*mamN*	MamN-T18	this work
pAK858	*mamO*	T18-MamO	this work
pAK860	*mamP*	T18-MamP	this work
pAK873	*mamP*	MamP-T18	this work
pAK863	*mamA*	T18-MamA	this work
pAK865	*mamA*	MamA-T18	this work
pAK861	*mamQ*	T18-MamQ	this work
pAK872	*mamQ*	MamQ-T18	this work
pAK852	*mamR*	T18-MamR	this work
pAK853	*mamB*	T18-MamB	this work
pAK866	*mamB*	MamB-T18	this work
pAK864	*mamS*	T18-MamS	this work
pAK867	*mamS*	MamS-T18	this work
pAK855	*mamU*	T18-MamU	this work
pAK869	*mamU*	MamU-T18	this work

Table 10. Mass spectrometry results

MamK-M2

Accession	protein	peptides
VIMSS1101124	amb0203 Chaperonin GroEL	9
VIMSS1100946	amb0025 Hypothetical PE-PGRS protein	4
VIMSS1105066	amb4141 F0F1-type ATP synthase	3
VIMSS1100934	amb0013 Nitrogen regulatory protein PII	2
VIMSS1101888	**amb0965 Actin-like ATPase (MamK)**	2
VIMSS1100935	amb0014 Ammonia permease	1
VIMSS1102522	amb1599 Dehydrogenase	1
VIMSS1103246	amb2321 Pyruvate/2-oxoglutarate dehydrogenase	1
VIMSS1103544	amb2619 Uncharacterized protein	1
VIMSS1103708	amb2783 NADH ubiquinone oxidoreductase	1
VIMSS1103718	amb2793 FKBP-type peptidyl-prolyl isomerase	1
VIMSS1103963	amb3038 Ribosomal protein L31	1
VIMSS1104135	amb3210 Outer membrane protein	1
VIMSS1104346	amb3421 hypothetical protein	1
VIMSS1104496	amb3571 hypothetical protein	1
VIMSS1105064	amb4139 F0F1-type ATP synthase, beta subunit	1
VIMSS1105365	amb4440 Molecular chaperone	1
VIMSS1105377	amb4452 Nuclease precursor	1

MamK untagged (negative control)

Accession	protein	peptides
VIMSS1101124	amb0203 Chaperonin GroEL	1

Table 11. BACTH results for MamK (pAK325 / MamK-T25)

Plasmid name	*mamAB* gene	resulting fusion	interaction
pAK320	empty vector	T18	-
pAK326	*mamK*	MamK-T18	+
pAK327	*mamK*	T18-MamK	+
pAK862	*mamH*	T18-MamH	-
pAK851	*mamI*	T18-MamI	-
pAK870	*mamI*	MamI-T18	-
pAK816	*mamJ*	MamJ-T18	-
pAK854	*mamL*	T18-MamL	-
pAK859	*mamM*	T18-MamM	-
pAK874	*mamM*	MamM-T18	-
pAK857	*mamN*	T18-MamN	-
pAK868	*mamN*	MamN-T18	-
pAK858	*mamO*	T18-MamO	-
pAK860	*mamP*	T18-MamP	-
pAK873	*mamP*	MamP-T18	-
pAK863	*mamA*	T18-MamA	-
pAK865	*mamA*	MamA-T18	-
pAK861	*mamQ*	T18-MamQ	-
pAK872	*mamQ*	MamQ-T18	-
pAK852	*mamR*	T18-MamR	-
pAK853	*mamB*	T18-MamB	-
pAK866	*mamB*	MamB-T18	-
pAK864	*mamS*	T18-MamS	-
pAK867	*mamS*	MamS-T18	-
pAK855	*mamU*	T18-MamU	-
pAK869	*mamU*	MamU-T18	-

Table 12. BACTH results for MamJ (pAK818 / MamJ-T25)

Plasmid name	*mamAB* gene	resulting fusion	interaction
pAK320	empty vector	T18	-
pAK326	*mamK*	MamK-T18	-
pAK327	*mamK*	T18-MamK	-
pAK862	*mamH*	T18-MamH	-
pAK851	*mamI*	T18-MamI	-
pAK870	*mamI*	MamI-T18	-
pAK816	*mamJ*	MamJ-T18	-
pAK854	*mamL*	T18-MamL	-
pAK859	*mamM*	T18-MamM	-
pAK874	*mamM*	MamM-T18	-
pAK857	*mamN*	T18-MamN	-
pAK868	*mamN*	MamN-T18	-
pAK858	*mamO*	T18-MamO	-
pAK860	*mamP*	T18-MamP	-
pAK873	*mamP*	MamP-T18	-
pAK863	*mamA*	T18-MamA	-
pAK865	*mamA*	MamA-T18	-
pAK861	*mamQ*	T18-MamQ	-
pAK872	*mamQ*	MamQ-T18	-
pAK852	*mamR*	T18-MamR	-
pAK853	*mamB*	T18-MamB	-
pAK866	*mamB*	MamB-T18	-
pAK864	*mamS*	T18-MamS	-
pAK867	*mamS*	MamS-T18	-
pAK855	*mamU*	T18-MamU	-
pAK869	*mamU*	MamU-T18	-

CHAPTER 5

Conclusions and implications for future research in MamK behavior in
Magnetospirillum magneticum AMB-1

This work sought to characterize the alignment of magnetosomes by MamK by studying the protein's behavior *in vivo* and by identifying interacting protein partners. To identify interacting proteins, three main approaches were performed. First, a candidate approach was taken by assessing whether a gene from the Magnetosome Islet, MamK-like, had an effect on magnetosome alignment. Second, experiments using the foundation of previously established research in the lab were used to identify additional genetic requirements for MamK-GFP turnover in Fluorescence Recovery After Photobleaching (FRAP) assays. Third, *in vitro* and *ex vivo* approaches were undertaken to try to identify additional interacting proteins. The results and conclusions of each section will be summarized, followed by recommendations for future experiments.

Studying turnover frequency and rates in FRAP assays in various genetic backgrounds provided some insight into MamK's behavior in AMB-1. Previous results were confirmed, where MamJ or LimJ were still required for MamK-GFP turnover in the new microscope setup. Though previous work implicated that other factors from the *mamAB* region of the MAI are needed (in addition to *mamJ* or *limJ*) for MamK-GFP dynamics, my work on this project did not conclusively identify an additional necessary factor.

Initially, my work did identify a candidate in MamH, as cells in the Δ*mamH*ΔR12 genetic background had reduced turnover frequencies. These results were not entirely conclusive, as the turnover frequencies varied under different culture conditions tested. There was a correlation between cell length and MamK-GFP recovery, as longer cells were less prone to FRAP turnover. This could be due to a decrease in available MamK-GFP protein levels in a larger cytoplasmic environment. Future research into this phenotype would require testing media conditions to ensure recapitulation of cell length changes.

Additionally, I identified that a *mamHIEJKL* strain was sufficient for MamK-GFP turnover. Because the two redundant genes in this minimal strain, *mamH* and *mamE*, were not needed for MamK-GFP recovery in the double deletion experiments, I concluded that these are probably not required for sufficiency of MamK-GFP turnover. Rather, having additional endogenous MamK in the cell could be attributing to the turnover observed. The next experiment to test this hypothesis would be to express MamK in the ΔMAI strain (preferably by incorporating it into the chromosome) in addition to MamK-GFP and MamJ or LimJ on a plasmid to see whether this restores recovery. I would recommend incorporating MamK onto the chromosome due to previous observations where protein levels decrease in bicistronic plasmids, with the

assumption that a tricistronic plasmid would have even less expression of the third gene. Alternatively, a plasmid with multiple promoters could be used in place of a tricistronic plasmid or chromosomal incorporation.

My results also demonstrate the differences in protein behavior based on the location of a GFP tag. It is possible that the MamK-GFP fusion is delayed in its turnover capability. Given that FRAP runs are taken on the order of 30 minutes; it is possible that we are reaching the limit for detecting recovery in this case. For future work with this project, I would recommend first finding the fusion that complements the *mamK* deletion background. Currently, the lab has only one method to assess complementation, GFP-MamI localization quantification. To test multiple fusion proteins (as I would recommend testing linkers, N/C terminal, and sandwich fusions), multiple vectors will need to be constructed that contain both the MamK fusion protein and MamI fused to a second fluorophore. After such a fusion is identified, I would recommend an alternative method to FRAP. FRAP recovery does not seem to correlate with GFP-MamI/magnetosome alignment (Draper, unpublished work). This may indicate that MamK turnover is not a property required for magnetosome alignment; rather it could be needed to allow for proper cell division by clearing away from the cell division machinery. Also, FRAP recovery does not have a detectable directionality in our case, such as treadmilling, which could provide insight into its recovery mechanism. Using a different approach, such as single particle tracking for example, could be useful to gain a better understanding for MamK's *in vivo* behavior.

The candidate approach proved to be the most successful of the three approaches, as MamK-like was not only an interacting protein of MamK, but was itself also involved with magnetosome alignment. These findings were exciting as they were the first set of experiments that proved a gene from the Magnetosome Islet served any function. The magnetosome alignment defect in cells lacking *mamK-like* was not as severe as cells lacking *mamK*, potentially indicating a more pronounced role for MamK in AMB-1. However, this phenotype is consistent with MamK-like levels being less in the cell (as transcript levels indicate).

Due to its higher level of ATPase activity, as measured by phosphate release, it can be assumed that monomers of MamK-like promote depolymerizing events more than MamK monomers do *in vivo*. This is supported by FRAP experiments in which the Δ*mamK* background has a higher proportion of MamK-like to MamK (in the form of MamK-GFP, Figure 11A) and a more erratic pattern of recovery. The Δ*mamK* strain percent recovery values have a much wider variance over each time point, in stark contrast to the other three genetic backgrounds tested (Figure 11F). At a higher concentration of MamK-like than MamK, one would predict that cofilaments of these two proteins would be less stable and prone to depolymerization. Support for this model could come from *in vitro* experiments in which varying ratios of the two proteins affected depolymerization/polymerization dynamics.

For future work in this project, I would recommend *in vitro* isolation and characterization of MamK-like and of the combination of MamK and MamK-like. It would be interesting

not only to assess MamK-like's polymerization properties *in vitro*, but also determine whether MamK and MamK-like form copolymers. Formation of copolymers can be investigated by mixing the two proteins at levels below their respective critical concentrations. Right angle light scattering and TEM can then be used to detect the presence of copolymers of MamK and MamK-like.

Experiments that isolated MamK were unable to find an interacting factor. This is contradictory to previous work by others (*41*) and by our lab that have resulted in numerous interacting proteins identified. It is worth noting that these sets of experiments were not carried to completion given my graduation timeframe, therefore it is difficult to conclude that MamK does not have interacting factors associated with it. MamK-like, for instance, was not identified by this method. More work will obviously need to be done to identify factors *in vitro*. This would include increasing protein preparation volumes and concentrating samples. Additionally, I recommend liposome flotation assays to assess whether MamK is sufficient to interact with membranes in isolation. If MamK is sufficient to interact with membrane vesicles, perhaps it does not require additional proteins to attach itself to the magnetosome membrane.

In closing, my efforts were successful in providing more information about the mechanisms of magnetosome alignment in AMB-1. This work, the first of its kind that demonstrated the influence of an islet gene, identified homologous proteins that behave in concert to align magnetosomes. This phenomenon is not entirely unique to AMB-1, as many other magnetotactic bacteria have multiple copies of MamK. These results indicate that this organism, either by horizontal gene transfer or by duplication, has acquired an additional copy of a similar gene. By copolymerizing monomers with distinct biochemical properties, a related interacting protein can serve a regulatory function in the cell.

REFERENCES

1. J. Spitzer, B. Poolman, How crowded is the prokaryotic cytoplasm? *FEBS Letters* **587**, 2094–2098 (2013).

2. D. Murat, M. Byrne, A. Komeili, Cell biology of prokaryotic organelles. *Cold Spring Harb Perspect Biol* **2**, a000422 (2010).

3. C. A. Kerfeld, S. Heinhorst, G. C. Cannon, Bacterial microcompartments. *Annu. Rev. Microbiol.* **64**, 391–408 (2010).

4. G. T. Oostergetel, H. van Amerongen, E. J. Boekema, The chlorosome: a prototype for efficient light harvesting in photosynthesis. *Photosyn. Res.* **104**, 245–255 (2010).

5. U. C. Vothknecht, P. Westhoff, Biogenesis and origin of thylakoid membranes. *Biochim. Biophys. Acta* **1541**, 91–101 (2001).

6. J. Errington, Regulation of endospore formation in Bacillus subtilis. *Nat. Rev. Microbiol.* **1**, 117–126 (2003).

7. S. Schlimpert *et al.*, General protein diffusion barriers create compartments within bacterial cells. *Cell* **151**, 1270–1282 (2012).

8. Y. Diekmann, J. B. Pereira-Leal, Evolution of intracellular compartmentalization. *Biochem. J.* **449**, 319–331 (2013).

9. D. Higgins, J. Dworkin, Recent progress in Bacillus subtilis sporulation. *FEMS Microbiol. Rev.* **36**, 131–148 (2012).

10. A. Abanes-De Mello, Y.-L. Sun, S. Aung, K. Pogliano, A cytoskeleton-like role for the bacterial cell wall during engulfment of the Bacillus subtilis forespore. *Genes Dev.* **16**, 3253–3264 (2002).

11. D. H. Broder, K. Pogliano, Forespore engulfment mediated by a ratchet-like mechanism. *Cell* **126**, 917–928 (2006).

12. P. Meyer, J. Gutierrez, K. Pogliano, J. Dworkin, Cell wall synthesis is necessary for membrane dynamics during sporulation of Bacillus subtilis. *Mol. Microbiol.* **76**, 956–970 (2010).

13. M. D. Sharp, K. Pogliano, An in vivo membrane fusion assay implicates SpoIIIE in the final stages of engulfment during Bacillus subtilis sporulation. *Proc. Natl. Acad. Sci. U.S.A.* **96**, 14553–14558 (1999).

14. M. D. Sharp, K. Pogliano, The membrane domain of SpoIIIE is required for membrane fusion during Bacillus subtilis sporulation. *J. Bacteriol.* **185**,

2005–2008 (2003).

15. T. Doan *et al.*, FisB mediates membrane fission during sporulation in Bacillus subtilis. *Genes Dev.* **27**, 322–334 (2013).

16. F. Kawai *et al.*, Cardiolipin domains in Bacillus subtilis marburg membranes. *J. Bacteriol.* **186**, 1475–1483 (2004).

17. K. Matsumoto, J. Kusaka, A. Nishibori, H. Hara, Lipid domains in bacterial membranes. *Mol. Microbiol.* **61**, 1110–1117 (2006).

18. A. B. Abecasis *et al.*, A genomic signature and the identification of new sporulation genes. *J. Bacteriol.* **195**, 2101–2115 (2013).

19. N. Ruiz, D. Kahne, T. J. Silhavy, Transport of lipopolysaccharide across the cell envelope: the long road of discovery. *Nat. Rev. Microbiol.* **7**, 677–683 (2009).

20. N. Ruiz, D. Kahne, T. J. Silhavy, Transport of lipopolysaccharide across the cell envelope: the long road of discovery. *Nat. Rev. Microbiol.* **7**, 677–683 (2009).

21. N. W. Rigel, T. J. Silhavy, Making a beta-barrel: assembly of outer membrane proteins in Gram-negative bacteria. *Curr. Opin. Microbiol.* **15**, 189–193 (2012).

22. S. Okuda, E. Freinkman, D. Kahne, Cytoplasmic ATP hydrolysis powers transport of lipopolysaccharide across the periplasm in E. coli. *Science* **338**, 1214–1217 (2012).

23. E. I. Tocheva *et al.*, Peptidoglycan remodeling and conversion of an inner membrane into an outer membrane during sporulation. *Cell* **146**, 799–812 (2011).

24. P. T. McKenney, A. Driks, P. Eichenberger, The Bacillus subtilis endospore: assembly and functions of the multilayered coat. *Nat. Rev. Microbiol.* **11**, 33–44 (2013).

25. E. I. Tocheva *et al.*, Peptidoglycan transformations during Bacillus subtilis sporulation. *Mol. Microbiol.* **88**, 673–686 (2013).

26. R. G. Endres, Intracellular chemical gradients: morphing principle in bacteria. *BMC Biophys* **5**, 18 (2012).

27. F. Caudron, Y. Barral, Septins and the lateral compartmentalization of eukaryotic membranes. *Dev. Cell* **16**, 493–506 (2009).

28. A. Komeili, Molecular mechanisms of compartmentalization and

biomineralization in magnetotactic bacteria. *FEMS Microbiol. Rev.* **36**, 232–255 (2012).

29.   D. Murat, A. Quinlan, H. Vali, A. Komeili, Comprehensive genetic dissection of the magnetosome gene island reveals the step-wise assembly of a prokaryotic organelle. *Proc. Natl. Acad. Sci. U.S.A.* **107**, 5593–5598 (2010).

30.   A. Lohsse *et al.*, Functional analysis of the magnetosome island in Magnetospirillum gryphiswaldense: the mamAB operon is sufficient for magnetite biomineralization. *PLoS ONE* **6**, e25561 (2011).

31.   A. Quinlan, D. Murat, H. Vali, A. Komeili, The HtrA/DegP family protease MamE is a bifunctional protein with roles in magnetosome protein localization and magnetite biomineralization. *Mol. Microbiol.* **80**, 1075–1087 (2011).

32.   R. Uebe *et al.*, The cation diffusion facilitator proteins MamB and MamM of Magnetospirillum gryphiswaldense have distinct and complex functions, and are involved in magnetite biomineralization and magnetosome membrane assembly. *Mol. Microbiol.* (2011), doi:10.1111/j.1365-2958.2011.07863.x.

33.   A. Komeili, Z. Li, D. K. Newman, G. J. Jensen, Magnetosomes are cell membrane invaginations organized by the actin-like protein MamK. *Science* **311**, 242–245 (2006).

34.   D. Murat *et al.*, The magnetosome membrane protein, MmsF, is a major regulator of magnetite biomineralization in Magnetospirillum magneticum AMB-1. *Mol. Microbiol.* **85**, 684–699 (2012).

35.   R. B. Frankel, D. A. Bazylinski, M. S. Johnson, B. L. Taylor, Magneto-aerotaxis in marine coccoid bacteria. *Biophys. J.* **73**, 994–1000 (1997).

36.   O. Draper *et al.*, MamK, a bacterial actin, forms dynamic filaments in vivo that are regulated by the acidic proteins MamJ and LimJ. *Mol. Microbiol.* **82**, 342–354 (2011).

37.   E. Ozyamak, J. Kollman, D. A. Agard, A. Komeili, The bacterial actin MamK: in vitro assembly behavior and filament architecture. *J. Biol. Chem.* **288**, 4265–4277 (2013).

38.   S. Sonkaria *et al.*, Insight into the assembly properties and functional organisation of the magnetotactic bacterial actin-like homolog, MamK. *PLoS ONE* **7**, e34189 (2012).

39.   E. Katzmann, A. Scheffel, M. Gruska, J. M. Plitzko, D. Schüler, Loss of the actin-like protein MamK has pleiotropic effects on magnetosome formation and chain assembly in Magnetospirillum gryphiswaldense. *Mol. Microbiol.*

77, 208–224 (2010).

40.   E. Katzmann *et al.*, Magnetosome chains are recruited to cellular division sites and split by asymmetric septation. *Mol. Microbiol.* **82**, 1316–1329 (2011).

41.   N. Philippe, L.-F. Wu, An MCP-like protein interacts with the MamK cytoskeleton and is involved in magnetotaxis in Magnetospirillum magneticum AMB-1. *J. Mol. Biol.* **400**, 309–322 (2010).

42.   S. Sakaguchi, A. Taoka, Y. Fukumori, Analysis of magnetotactic behavior by swimming assay. *Biosci. Biotechnol. Biochem.* **77**, 940–947 (2013).

43.   D. F. Savage, B. Afonso, A. H. Chen, P. A. Silver, Spatially ordered dynamics of the bacterial carbon fixation machinery. *Science* **327**, 1258–1261 (2010).

44.   M. A. J. Roberts, G. H. Wadhams, K. A. Hadfield, S. Tickner, J. P. Armitage, ParA-like protein uses nonspecific chromosomal DNA binding to partition protein complexes. *Proc. Natl. Acad. Sci. U.S.A.* **109**, 6698–6703 (2012).

45.   S. R. Thompson, G. H. Wadhams, J. P. Armitage, The positioning of cytoplasmic protein clusters in bacteria. *Proc. Natl. Acad. Sci. U.S.A.* **103**, 8209–8214 (2006).

46.   I. H. Jain, V. Vijayan, E. K. O'Shea, Spatial ordering of chromosomes enhances the fidelity of chromosome partitioning in cyanobacteria. *Proc. Natl. Acad. Sci. U.S.A.* **109**, 13638–13643 (2012).

47.   J. Spitzer, B. Poolman, How crowded is the prokaryotic cytoplasm? *FEBS Letters* **587**, 2094–2098 (2015).

48.   D. L. Balkwill, D. Maratea, R. P. Blakemore, Ultrastructure of a magnetotactic spirillum. *J. Bacteriol.* **141**, 1399–1408 (1980).

49.   A. I. Derman *et al.*, Phylogenetic analysis identifies many uncharacterized actin-like proteins (Alps) in bacteria: regulated polymerization, dynamic instability and treadmilling in Alp7A. *Mol. Microbiol.* **73**, 534–552 (2009).

50.   E. Ozyamak, J. M. Kollman, A. Komeili, Bacterial actins and their diversity. *Biochemistry* **52**, 6928–6939 (2013).

51.   L. J. Jones, R. Carballido-López, J. Errington, Control of cell shape in bacteria: helical, actin-like filaments in Bacillus subtilis. *Cell* **104**, 913–922 (2001).

52.   J. Domínguez-Escobar *et al.*, Processive movement of MreB-associated cell

wall biosynthetic complexes in bacteria. *Science* **333**, 225–228 (2011).

53. E. C. Garner *et al.*, Coupled, circumferential motions of the cell wall synthesis machinery and MreB filaments in B. subtilis. *Science* **333**, 222–225 (2011).

54. E. M. F. Mauriello *et al.*, Bacterial motility complexes require the actin-like protein, MreB and the Ras homologue, MglA. *EMBO J.* **29**, 315–326 (2010).

55. R. B. Jensen, K. Gerdes, Partitioning of plasmid R1. The ParM protein exhibits ATPase activity and interacts with the centromere-like ParR-parC complex. *J. Mol. Biol.* **269**, 505–513 (1997).

56. J. Møller-Jensen *et al.*, Bacterial mitosis: ParM of plasmid R1 moves plasmid DNA by an actin-like insertional polymerization mechanism. *Mol. Cell* **12**, 1477–1487 (2003).

57. P. Gayathri *et al.*, A bipolar spindle of antiparallel ParM filaments drives bacterial plasmid segregation. *Science* **338**, 1334–1337 (2012).

58. B. Lara *et al.*, Cell division in cocci: localization and properties of the Streptococcus pneumoniae FtsA protein. *Mol. Microbiol.* **55**, 699–711 (2005).

59. P. Szwedziak, Q. Wang, S. M. Freund, J. Löwe, FtsA forms actin-like protofilaments. *EMBO J.* **31**, 2235–2437 (2012).

60. A. Scheffel *et al.*, An acidic protein aligns magnetosomes along a filamentous structure in magnetotactic bacteria. *Nature* **440**, 110–114 (2006).

61. J.-B. Rioux *et al.*, A second actin-like MamK protein in Magnetospirillum magneticum AMB-1 encoded outside the genomic magnetosome island. *PLoS ONE* **5**, e9151 (2010).

62. E. C. Garner, C. S. Campbell, R. D. Mullins, Dynamic instability in a DNA-segregating prokaryotic actin homolog. *Science* **306**, 1021–1025 (2004).

63. R. Carballido-López *et al.*, Actin homolog MreBH governs cell morphogenesis by localization of the cell wall hydrolase LytE. *Dev. Cell* **11**, 399–409 (2006).

64. Y. Kawai, K. Asai, J. Errington, Partial functional redundancy of MreB isoforms, MreB, Mbl and MreBH, in cell morphogenesis of Bacillus subtilis. *Mol. Microbiol.* **73**, 719–731 (2009).

65. H. J. D. Soufo, P. L. Graumann, Actin-like proteins MreB and Mbl from Bacillus subtilis are required for bipolar positioning of replication origins. *Curr. Biol.* **13**, 1916–1920 (2003).

66.   P. Domínguez-Cuevas, I. Porcelli, R. A. Daniel, J. Errington, Differentiated roles for MreB-actin isologues and autolytic enzymes in Bacillus subtilis morphogenesis. *Mol. Microbiol.* **89**, 1084–1098 (2013).

67.   R. Schiestl, D. Gietz, High efficiency transformation of intact yeast cells using single stranded nucleic acids as a carrier. *Current Genetics*, 1–8 (1989).

68.   T. Durfee, O. Draper, J. Zupan, D. S. Conklin, P. C. Zambryski, New tools for protein linkage mapping and general two-hybrid screening. *Yeast* **15**, 1761–1768 (1999).

69.   R. C. Edgar, MUSCLE: multiple sequence alignment with high accuracy and high throughput. *Nucleic Acids Res.* **32**, 1792–1797 (2004).

70.   J. Schindelin *et al.*, Fiji: an open-source platform for biological-image analysis. *Nat. Methods* **9**, 676–682 (2012).

71.   D. V. Ward, O. Draper, J. R. Zupan, P. C. Zambryski, Peptide linkage mapping of the Agrobacterium tumefaciens vir-encoded type IV secretion system reveals protein subassemblies. *Proc. Natl. Acad. Sci. U.S.A.* **99**, 11493–11500 (2002).

72.   E. A. Rogulin, T. A. Perevyazova, L. A. Zheleznaya, N. I. Matvienko, Plasmid pRARE as a vector for cloning to construct a superproducer of the site-specific nickase N.BspD6I. *Biochemistry Mosc.* **69**, 1123–1127 (2004).

73.   E. Mossessova, C. D. Lima, Ulp1-SUMO crystal structure and genetic analysis reveal conserved interactions and a regulatory element essential for cell growth in yeast. *Mol. Cell* **5**, 865–876 (2000).

74.   P. A. Lanzetta, L. J. Alvarez, P. S. Reinach, O. A. Candia, An improved assay for nanomole amounts of inorganic phosphate. *Anal. Biochem.* **100**, 95–97 (1979).

75.   P. Bork, C. Sander, A. Valencia, An ATPase domain common to prokaryotic cell cycle proteins, sugar kinases, actin, and hsp70 heat shock proteins. *Proc. Natl. Acad. Sci. U.S.A.* **89**, 7290–7294 (1992).

76.   F. van den Ent, L. A. Amos, J. Löwe, Prokaryotic origin of the actin cytoskeleton. *Nature* **413**, 39–44 (2001).

77.   A. Heichlinger *et al.*, The MreB-like protein Mbl of Streptomyces coelicolor A3(2) depends on MreB for proper localization and contributes to spore wall synthesis. *J. Bacteriol.* **193**, 1533–1542 (2011).

78.   C. Jogler *et al.*, Comparative analysis of magnetosome gene clusters in magnetotactic bacteria provides further evidence for horizontal gene transfer.

Environ Microbiol **11**, 1267–1277 (2009).

79.   C. T. Lefèvre *et al.*, Comparative genomic analysis of magnetotactic bacteria from the Deltaproteobacteria provides new insights into magnetite and greigite magnetosome genes required for magnetotaxis. *Environ Microbiol* **15**, 2712–2735 (2013).

80.   A. R. Paredez *et al.*, An actin cytoskeleton with evolutionarily conserved functions in the absence of canonical actin-binding proteins. *Proc. Natl. Acad. Sci. U.S.A.* **108**, 6151–6156 (2011).

81.   F. van den Ent, L. Amos, J. Löwe, Bacterial ancestry of actin and tubulin. *Curr. Opin. Microbiol.* **4**, 634–638 (2001).

82.   Z. Gitai, The new bacterial cell biology: moving parts and subcellular architecture. *Cell* **120**, 577–586 (2005).

83.   J. W. Shaevitz, Z. Gitai, The structure and function of bacterial actin homologs. *Cold Spring Harb Perspect Biol* **2**, a000364 (2010).

84.   R. Carballido-López, The bacterial actin-like cytoskeleton. *Microbiol. Mol. Biol. Rev.* **70**, 888–909 (2006).

85.   K. Gerdes, J. Møller-Jensen, R. Bugge Jensen, Plasmid and chromosome partitioning: surprises from phylogeny. *Mol. Microbiol.* **37**, 455–466 (2000).

86.   R. B. Jensen, M. Dam, K. Gerdes, Partitioning of plasmid R1. The parA operon is autoregulated by ParR and its transcription is highly stimulated by a downstream activating element. *J. Mol. Biol.* **236**, 1299–1309 (1994).

87.   J. Salje, P. Gayathri, J. Löwe, The ParMRC system: molecular mechanisms of plasmid segregation by actin-like filaments. *Nat. Rev. Microbiol.* **8**, 683–692 (2010).

88.   R. B. Jensen, R. Lurz, K. Gerdes, Mechanism of DNA segregation in prokaryotes: replicon pairing by parC of plasmid R1. *Proc. Natl. Acad. Sci. U.S.A.* **95**, 8550–8555 (1998).

89.   E. C. Garner, C. S. Campbell, D. B. Weibel, R. D. Mullins, Reconstitution of DNA segregation driven by assembly of a prokaryotic actin homolog. *Science* **315**, 1270–1274 (2007).

90.   J. K. Polka, J. M. Kollman, R. D. Mullins, Accessory factors promote AlfA-dependent plasmid segregation by regulating filament nucleation, disassembly, and bundling. *Proc. Natl. Acad. Sci. U.S.A.* **111**, 2176–2181 (2014).

91.   M. Wachi *et al.*, Mutant isolation and molecular cloning of mre genes, which

determine cell shape, sensitivity to mecillinam, and amount of penicillin-binding proteins in Escherichia coli. *J. Bacteriol.* **169**, 4935–4940 (1987).

92.   M. Doi *et al.*, Determinations of the DNA sequence of the mreB gene and of the gene products of the mre region that function in formation of the rod shape of Escherichia coli cells. *J. Bacteriol.* **170**, 4619–4624 (1988).

93.   M. Wachi, M. Matsuhashi, Negative control of cell division by mreB, a gene that functions in determining the rod shape of Escherichia coli cells. *J. Bacteriol.* **171**, 3123–3127 (1989).

94.   T. Kruse, J. Bork-Jensen, K. Gerdes, The morphogenetic MreBCD proteins of Escherichia coli form an essential membrane-bound complex. *Mol. Microbiol.* **55**, 78–89 (2005).

95.   M. T. Swulius, G. J. Jensen, The Helical MreB Cytoskeleton in Escherichia coli MC1000/pLE7 Is an Artifact of the N-Terminal Yellow Fluorescent Protein Tag. *J. Bacteriol.* **194**, 6382–6386 (2012).

96.   P. Nurse, K. J. Marians, Purification and characterization of Escherichia coli MreB protein. *J. Biol. Chem.* **288**, 3469–3475 (2013).

97.   A. Scheffel, D. Schüler, The acidic repetitive domain of the Magnetospirillum gryphiswaldense MamJ protein displays hypervariability but is not required for magnetosome chain assembly. *J. Bacteriol.* **189**, 6437–6446 (2007).

98.   E. Becker *et al.*, DNA segregation by the bacterial actin AlfA during Bacillus subtilis growth and development. *EMBO J.* **25**, 5919–5931 (2006).

99.   R. Carballido-López, J. Errington, The bacterial cytoskeleton: in vivo dynamics of the actin-like protein Mbl of Bacillus subtilis. *Dev. Cell* **4**, 19–28 (2003).

100.   S. Craig, T. D. Pollard, Actin-binding proteins. 1–5 (1982).

101.   P. Sheterline, J. Clayton, J. Sparrow, Actin. *Protein Profile* **2**, 1–103 (1995).

102.   C. G. dos Remedios *et al.*, Actin binding proteins: regulation of cytoskeletal microfilaments. *Physiol. Rev.* **83**, 433–473 (2003).

103.   G. Karimova, J. Pidoux, A. Ullmann, D. Ladant, A bacterial two-hybrid system based on a reconstituted signal transduction pathway. *Proc. Natl. Acad. Sci. U.S.A.* **95**, 5752–5756 (1998).

104.   D. Ladant, A. Ullmann, Bordatella pertussis adenylate cyclase: a toxin with multiple talents. *Trends Microbiol.* **7**, 172–176 (1999).

105.   N. Abreu *et al.*, Interplay between two bacterial actin homologs, MamK and MamK-Like, is required for the alignment of magnetosome organelles in Magnetospirillum magneticum AMB-1. *J. Bacteriol.* **196**, 3111–3121 (2014).

Appendix 1. **Detailed FRAP analysis protocol**

1) After acquiring FRAP image file (.lsm) from confocal microscope, open the file in **Fiji**.

2) Draw a large oval shape (background ROI measurement). Ensure that the oval does not contain any fluorescence throughout the entire series of images. (Holding down the ">" and "<" keys enable fast panning through the image stack)
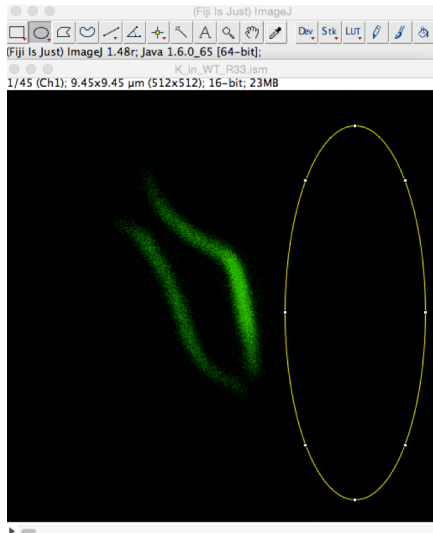

   a. To Measure: Use the "M" button on each image, using the ">" key to advance to next image.
   b. Note: The "results" window will pop up at this time. I always double check to see that the number of measurements I make matches the number of images (45 in this example) after each set of ROIs acquired.

3) Draw with "polygon" tool by clicking along the boundaries of the filament to get the "whole filament" ROI measurement.
   a. Note: use the arrow keys to ensure the polygon follows the filament.

4) Draw with "freehand" tool around the bleached portion of the filament to get the "bleached" ROI measurement.
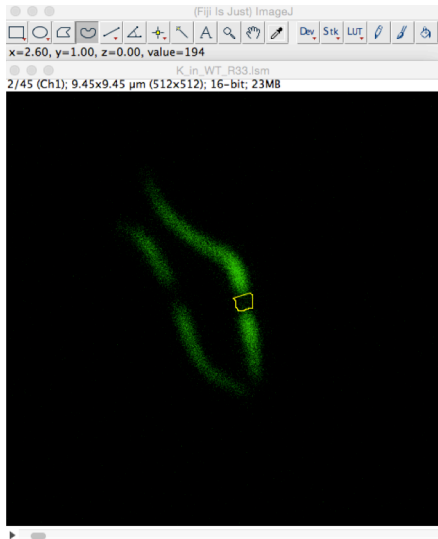
5) Go to "edit," "select all," then copy all of the measurements and paste them into Excel

From Excel:

1) After filling in as illustrated in **A**, Create graph **B** and graph **C**

A

Percent Recovery =
((G3 - G3)/(E3 - G3))*100

Corrected Whole Filament =
Whole Filament ROI - Background ROI

Corrected Bleached =
Bleached ROI - Background ROI

	A	B	C	D	E	F	G	H
1	Time (minute)	Time (seconds)	Background ROI	Whole Filament ROI	Corrected WF	Bleached ROI	Corrected B	Percent Recovery
2	0.0	0	226.509	42512.678	42286.169	49043.064	48816.555	
3	0.1	3.942	217.889	28328.532	28110.643	9620.615	9402.726	0.0
4	0.8	50	221.826	28268.484	28046.658	11733.371	11511.545	11.3
5	1.7	100	229.896	26228.145	25998.249	11594.703	11364.807	11.8
6	2.5	150	224.237	30474.361	30250.124	14178.497	13954.26	21.8
7	3.3	200	201.574	28658.761	28457.187	13206.941	13005.367	18.9
8	4.2	250	210.315	26732.975	26522.66	13402.778	13192.463	22.1
9	5.0	300	211.471	24229.659	24018.188	12719.651	12508.18	21.2
10	5.8	350	215.309	22764.926	22549.617	11687.947	11472.638	15.7
11	6.7	400	262.291	30993.741	30731.45	15346.804	15084.513	26.6
12	7.5	450	250.569	28432.053	28181.484	14242.446	13991.877	24.4
13	8.3	500	251.813	26542.456	26290.643	12862.974	12611.161	19.0
14	9.2	550	230.944	31503.053	31272.109	15477.769	15246.825	26.7
15	10.0	600	235.047	31138.99	30903.943	16024.615	15789.568	29.7
16	10.8	650	247.056	29289.257	29042.201	15143.378	14896.322	28.0
17	11.7	700	249.34	28362.256	28112.916	15481.712	15232.372	31.2
18	12.5	750	235.218	30630.97	30395.752	15890.826	15655.608	29.8
19	13.3	800	226.691	30414.222	30187.531	15918.499	15691.808	30.3
20	14.2	850	237.125	29139.31	28902.185	15877.848	15640.723	32.0
21	15.0	900	239.911	27329.941	27090.03	15459.884	15219.973	32.9
22	15.8	950	242.339	25535.614	25293.275	14645.624	14403.285	31.5
23	16.7	1000	248.701	30270.289	30021.588	17184.664	16935.963	36.5
24	17.5	1050	247.745	29352.159	29104.414	15917.202	15669.457	31.8
25	18.3	1100	231.428	27525.037	27293.609	16318.943	16087.515	37.4
26	19.2	1150	234.701	30803.021	30568.32	19229.662	18994.961	45.3
27	20.0	1200	237.231	28762.107	28524.876	18115.242	17878.011	44.3
28	20.8	1250	278.343	25765.333	25486.99	16467.56	16189.217	42.2
29	21.1	1267	262.172	25154.976	24892.804	15708.068	15445.896	39.0
30	21.3	1275	268.449	30693.328	30424.879	18795.501	18527.052	43.4
31	21.4	1286	254.761	27892.008	27637.247	18199.844	17945.083	46.8
32	21.6	1295	265.331	29021.133	28755.802	18779.998	18514.667	47.1
33	21.7	1304	245.792	29416.963	29171.171	18681.736	18435.944	45.7
34	22.6	1354	229.611	29288.352	29058.741	18850.132	18620.521	46.9
35	23.4	1404	242.801	27068.182	26825.381	17814.912	17572.111	46.9
36	24.2	1454	267.159	28418.495	28151.336	19503.602	19236.443	52.5
37	25.1	1504	268.896	29124.664	28855.768	19480.286	19211.39	50.4

B
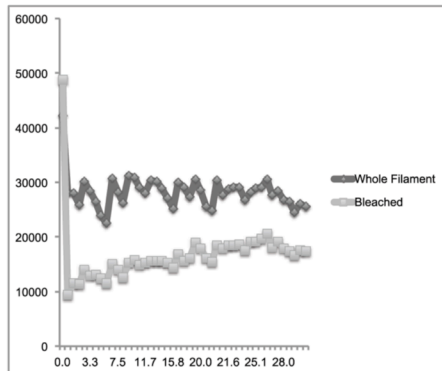
C
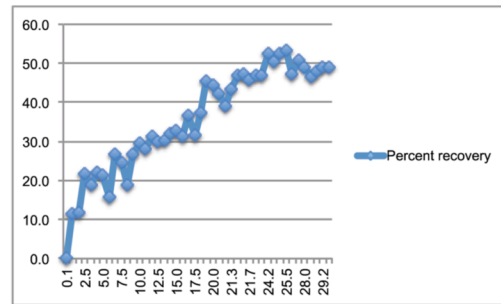
2) **Assess the run.** Any frames with drastic decreases in fluorescence are thrown out of analysis. (In this case, I did not throw out any images.)

    a. Note: As you look at each run, keep in mind that drops in fluorescence can skew the percent recovery, giving a "false positive."

3) After this initial assessment, if percent recovery reaches 50 or higher, I count cell as recovering.

4) **To calculate T$_{1/2}$:**

    a. Find the two time points where the 50 percent is reached

        i. For this case, this occurs between 23.4 (46.9% recovery) and 24.2 (52.5% recovery) minutes

    b. Calculate the slope of the line between these two points

Slope(m) $= (y_1-y_2)/(x_1-x_2)$
$= (52.5-46.9)/(24.2-23.4)$
$= 7$

    c. Use this formula for the point in between:

$y - y_1 = m(x - x_1)$
$50-52.5 = 7 (x - 24.2)$
$-2.5 = 7x-169.4$
$166.9 = 7x$
$23.84 = x$

T$_{1/2}$ for this cell was 23.84 minutes